STUDIES ON HAZARD CHARACTERIZATION FOR PERFORMANCE-BASED STRUCTURAL DESIGN

A Dissertation

by

YUE WANG

Submitted to the Office of Graduate Studies of
Texas A&M University
in partial fulfillment of the requirements for the degree of

DOCTOR OF PHILOSOPHY

May 2010

Major Subject: Civil Engineering

STUDIES ON HAZARD CHARACTERIZATION FOR PERFORMANCE-BASED STRUCTURAL DESIGN

A Dissertation

by

YUE WANG

Submitted to the Office of Graduate Studies of
Texas A&M University
in partial fulfillment of the requirements for the degree of

DOCTOR OF PHILOSOPHY

Approved by:

Co-Chairs of Committee,	David V. Rosowsky
	Jose M. Roesset
Committee Members,	Joseph M. Bracci
	Walter G. Peacock
	Weichiang Pang
Head of Department,	John Niedzwecki

May 2010

Major Subject: Civil Engineering

ABSTRACT

Studies on Hazard Characterization for Performance-Based Structural Design.

(May 2010)

Yue Wang, B.S., Beijing Polytechnic University;

M.S., Tsinghua University

Co-Chairs of Advisory Committee: Dr. David V. Rosowsky
Dr. Jose M. Roesset

Performance-based engineering (PBE) requires advances in hazard characterization, structural modeling, and nonlinear analysis techniques to fully and efficiently develop the fragility expressions and other tools forming the basis for risk-based design procedures. This research examined and extended the state-of-the-art in hazard characterization (wind and surge) and risk-based design procedures (seismic).

State-of-the-art hurricane models (including wind field, tracking and decay models) and event-based simulation techniques were used to characterize the hurricane wind hazard along the Texas coast. A total of 10,000 years of synthetic hurricane wind speed records were generated for each zip-code in Texas and were used to statistically characterize the *N*-year maximum hurricane wind speed distribution for each zip-code location and develop design non-exceedance probability contours for both coastal and inland areas.

Actual recorded wind and surge data, the hurricane wind field model, hurricane size parameters, and a measure of storm kinetic energy were used to develop wind-surge

and wind-surge-energy models, which can be used to characterize the wind-surge hazard at a level of accuracy suitable for PBE applications. These models provide a powerful tool to quickly and inexpensively estimate surge depths at coastal locations in advance of a hurricane landfall. They also were used to create surge hazard maps that provide storm surge height non-exceedance probability contours for the Texas coast.

The simulation tools, wind field models, and statistical analyses, make it possible to characterize the risk-consistent hurricane events considering both hurricane intensity and size. The proposed methodology for event-based hurricane hazard characterization, when coupled with a hurricane damage model, can also be used for regional loss estimation and other spatial impact analyses.

In considering seismic hazard, a risk-consistent framework for displacement-based seismic design of engineered multistory woodframe structures was developed. Specifically, a database of probability-based scale factors which can be used in a direct displacement design (DDD) procedure for woodframe buildings was created using nonlinear time-history analyses with suitably scaled ground motions records. The resulting DDD procedure results in more risk-consistent designs and therefore advances the state-of-the-art in displacement-based seismic design of woodframe structures.

DEDICATION

To my family and friends

ACKNOWLEDGMENTS

I would like to thank my research supervisor and committee chair, Dr. David Rosowsky, for his patient guidance and support throughout the course of this research. It has been a pleasant time for me to work under his guidance and knowledge. His passion and skill made my academic training experience at Texas A&M University a unique one.

Great thanks also are extended to my committee co-chair, Dr. Jose Roesset and committee members Dr. Joseph Bracci and Dr. Walter Peacock, for their help and suggestions related to my studies. Special gratitude is given to my committee member Dr. Weichiang Pang for his instruction and inspiration to help me set up my research work and finish it in the end.

Thanks also go to my friends and colleagues at Texas A&M University for their support and helping me accomplish my goals. Especially, I am grateful to my former officemates, Ms. Qindan Huang and Dr. Jinquan Zhong, for helping me with research problems. Also, I gratefully acknowledge the financial support for this research provided by the National Science Foundation (NSF) and the Network for Earthquake Engineering Simulation (NEES).

Finally, thanks to my mother and father for their affection and encouragement throughout my life.

TABLE OF CONTENTS

CHAPTER Page

LIST OF FIGURES

Page

Page

Page

LIST OF TABLES

CHAPTER I

INTRODUCTION

Background

Modern structural engineering design practice includes consideration of various hazards including earthquake, hurricane, flood, snow and fire. Among these hazards, earthquakes and hurricanes are the most deadly and costly. Following recent high-profile earthquakes and hurricanes in the United States, many individuals were displaced from their homes and many structures suffered significant (and costly) damage. Both the economic and societal impacts (costs) were enormous. Hurricane Katrina in 2005 had a catastrophic impact on the Louisiana coast and caused over $30B in property losses. The Northridge earthquake in 1994 caused extensive structural and lifeline infrastructure damage and approximately $20B in property losses. Although there were relatively few structural collapses, economic losses were unacceptably large. In response to these excessive losses (costs), performance-based engineering (PBE) concepts have evolved and are beginning to be accepted by the structural engineering community. The implementation of performance-based engineering for residential construction, for example, will enhance durability (and reduce maintenance costs) of the nation's housing inventory, and will facilitate reductions in risk of death, injury, and property damage from extreme natural hazards such as earthquakes and hurricanes (Rosowsky and Ellingwood, 2002).

This dissertation follows the style of American Society of Civil Engineering Journal.

Performance-based design (PBD) is a multi-tiered approach that considers a range of different risk-based performance objectives. These are generally expressed in terms of a hazard level (intensity) and a target performance criterion expressed in terms of a structural response. The hazard level is usually described as the probability of exceedance in a certain number of years (e.g., 2%/50 years). In performance-based seismic analysis and design, the performance levels are related to intended performance states (limit states) such as Immediate Occupancy (IO), Life Safety (LS) and Collapse Prevention (CP) with corresponding inter-story drift limits (ASCE 41, 2006). The corresponding hazard levels for these limit states are 50%/50 years, 10%/50 years and 2%/50 years, respectively while the drift limits are material (or structural system) dependent. In the case of earthquakes, the hazard levels are characterized in a consistent probabilistic manner in terms of a single hazard metric (e.g., PGA). Performance-based engineering ensures that a properly designed structure should satisfy the intended performance requirements when subjected to an event intensity corresponding to a specific hazard level. Therefore the characterization of hazard in a probabilistic manner is fundamental to PBE.

Objectives and Scope of Study Work

This overall objective of this research was to advance the state-of-the-art in hazard characterization and its role in performance-based engineering of structures subjected to natural hazards. The current state-of-the-art is different for different hazards. Some fields (e.g., seismic design) are far more mature and associated performance-based procedures are becoming widely adopted in structural engineering practice. These

differences are reflected in the starting points for each of the studies comprising this research.

Progress in performance-based engineering (which is taken to include design, analysis, and assessment/evaluation) requires advances in hazard characterization, structural modeling, and nonlinear analysis techniques to fully and efficiently develop the fragility expressions and other tools forming the basis for risk-based design procedures. The studies in this research address elements of hazard characterization (wind and surge) and risk-based design procedures (seismic). These are introduced in the following sections.

Study 1: Characterizing the combined wind-surge hazard

Strong winds and storm surge induced by large hurricanes can cause coastal flooding and extensive damage. However, neither the wind load provisions in ASCE 7 (2005) nor the flood action provisions in ASCE 24 (2005) address the combined wind-surge hazard. Therefore, there is a need for risk-consistent design criteria for coastal structures subjected to hurricane wind and surge loads built in at-risk coastal zones. Following similar concepts as used for seismic hazard, hurricane hazard levels also can be probabilistically expressed in terms of an appropriate metric (e.g., maximum gust wind speed or maximum surge height). In this study, the Texas coast is selected as the study region. A total of 10,000 years of synthetic hurricane wind speed records were generated for each zip-code in Texas using state-of-the-art hurricane wind-field and tracking models. The synthetic hurricane wind speed database was used to statistically characterize the *N*-year maximum hurricane wind speed distribution for each zip-code

location and develop design non-exceedance probability contours for both coastal and inland areas.

In order to characterize the hurricane surge hazard, a simplified combined wind-surge model was developed for the Texas coast using the increasingly available surge measurement data rather than existing complex (and computationally very intensive) numerical models. This simplified joint wind-surge model could be then used to create surge hazard maps that provide storm surge height non-exceedance probability contours for the Texas coast. If the model could be validated using historical data or could be compared with results from the SLOSH (Sea, Land, and Overland Surge from Hurricanes) model (Jelesnianski et al., 1992), it could provide a powerful tool to quickly and inexpensively estimate surge depths at coastal locations in advance of a hurricane landfall. This has obvious implications for emergency management including pre-disaster planning and post-disaster response. Additional, more recent, hurricane event data (i.e., Gustav, 2008 and Ike, 2008) were included during the course of this study to improve the simplified wind-surge model. However, the simplified wind-surge model may not be able to properly account for the "direct-hit" situation (e.g., hurricane Ike in 2008 on Galveston, TX) and a modified joint wind-surge model was next developed to take into account the impact of relative position of the most intense part of the hurricane to the location where the surge height is being estimated. A new dependent variable, Ratio of Distance (ROD) from a given location to the hurricane eye to the radius of maximum wind speed, was introduced in this modified joint wind-surge model. A possible joint wind-surge-energy model also was proposed using the Integrated

Kinetic Energy (IKE) associated with the most intense part of hurricane wind field. This has potential for improved predictions of surge height and could be explored in future work.

Study 2: Event-based hazard characterization for hurricanes along the Texas coast

In addition to maximum wind speed or intensity, hurricane storm size (i.e., radius of maximum wind, R_{max}) also plays an important role in describing the hurricane wind field and thus in prediction of the spatial extent of damage. Design criteria for coastal structures consider only maximum hurricane wind speed (i.e., a point-measure of intensity with no explicit spatial descriptor) and therefore are not sufficient for performance-based assessment and loss analysis. Therefore, and in order to create needed information for PBE applications, it may be useful to develop parameter combinations that define "characteristic" risk-consistent hurricane events. Using all of the information (intensity, size and other parameters) needed to describe the 10,000 years of hurricane events developed in the synthetic wind speed database in Study 1, the two key parameters (maximum wind speed at the eye-wall V_{max} and the radius of maximum wind R_{max}) are statistically characterized and the joint distribution of these two variables are determined for the entire Texas coast. A suite of characteristic hazard events (V_{max} and R_{max} combinations) corresponding to defined hazard levels are then identified. The resulting ensemble of risk-consistent hurricane events can be used for performance-based assessment of infrastructure and site-specific loss estimation.

Study 3: Creating a risk-consistent framework for displacement-based seismic design of engineered wood structures

This study extends a recently proposed direct displacement design (DDD) procedure (Pang and Rosowsky, 2009) for midrise engineered woodframe structures, specifically by developing a set of factors for use in the procedure to meet specified performance levels with certain target probabilities. The DDD procedure suggested by Pang and Rosowsky (2009) allows the engineer to estimate the inter-story drift in multistory woodframe structures without having to perform nonlinear dynamic analyses. In order to design for additional performance requirements and for non-exceedance (NE) probabilities other than 50% (median), an adjustment factor C_{NE} is introduced. This factor is developed taking into account the uncertainty in the ground motions and therefore is a key factor for characterizing the risk-consistent hazard level, which must be determined such that the structures designed using this procedure meet performance expectations in terms of both drift limit and NE probability. Nonlinear time history analyses were performed to determine the adjustment factors (C_{NE}) for different target NE probabilities and performance requirements for a portfolio of representative mid-rise woodframe structures. The performance requirements (seismic hazard level/drift limit pairs with corresponding NE probabilities) proposed by the NEESWood project were adopted herein (Pang et al., 2009). Design charts were then developed which could be used by engineers/designers to select the appropriate minimum seismic adjustment factor given the building height and desired non-exceedance probability. In this study, the focus was on design in high hazard regions and only hazard level 3 (2%/50 years with a

target drift limit of 4%) was considered. The Level 3 performance requirement was shown to be the governing requirement for most mid-rise woodframe buildings.

Structure of the Dissertation

This dissertation includes five chapters. Chapter II proposes a combined hurricane wind-surge model and a preliminary wind-surge energy model to characterize the hurricane hazard along the Texas coast. Chapter III suggests a methodology for hazard-specific/risk-consistent hurricane event characterization. Chapter IV introduces a risk-consistent framework for displacement-based seismic design of engineered wood structures. Finally, Chapter V presents conclusions of the studies comprising this dissertation.

CHAPTER II

CHARACTERIZING THE COMBINED HURRICANE WIND-SURGE HAZARD ALONG THE TEXAS COAST

Part I

Development of a Synthetic Hurricane Wind Speed Database for Texas

Introduction

Hurricanes (tropical storms) are among the most deadly hazards threatening the Gulf Coast of the United States and Mexico. Significant improvements have been made in hurricane forecasting, warning and evacuation. Recent research (e.g., Huang et al. 2001; FEMA 2003; Khanduri et al. 2003; Sparks 2003; Watson et al. 2004; Heneka 2008) has focused on hurricane loss estimation and mitigation. Despite significant progress in hurricane hazard mitigation, the losses associated with recent events have been very large, demonstrating the vulnerability that remains in these coastal areas. More accurate hurricane prediction models are needed to better anticipate events, estimate losses and prepare for the storm's impact and recovery. Using the models developed by Vickery et al. (2000a,b), Lee and Rosowsky (2007) developed a framework for the simulation of hurricane events. The availability of historical hurricane records (HURDAT, 2005) has enabled such event-based simulation procedures to be developed in the public sector. This paper uses the simulation framework developed by Lee and Rosowsky to develop a hurricane wind speed database for the state of Texas. Key components for the

framework are the gradient wind-field model (Georgiu, 1985) and the tracking and central pressure models (Vickery et al., 2000a,b). For the purposes of this study, decay model parameters for Texas were specifically developed. These models and their various parameters are described in the following sections.

Georgiu's Gradient Wind Field Model

Consistent with information obtained by aircraft reconnaissance observations, well-formed hurricane gradient wind fields can be represented as a vortex with translational movement. Therefore, the gradient wind speed V_g can be decomposed into a rotational component V_R and a translational component V_T (Figure 1). The rotational component V_R can be described as a function of distance from the hurricane eye (Figure 2). Since the gradient rotational wind speed vortex is assumed to be symmetrical about the hurricane eye, the hurricane can be viewed simply as a rotational vortex moving along its track with some translational speed.

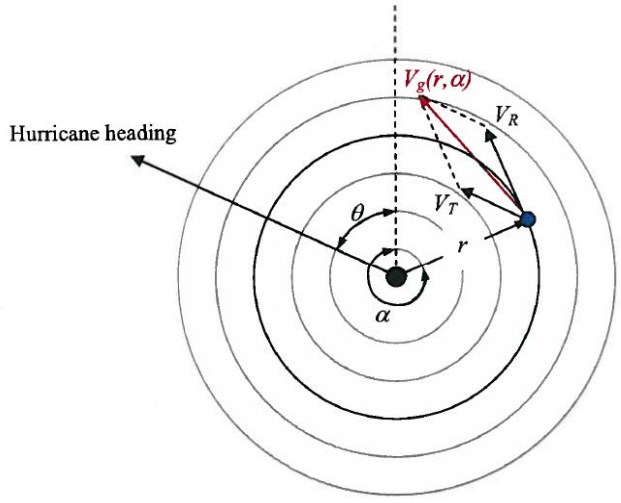

Figure 1: Hurricane gradient wind speed components

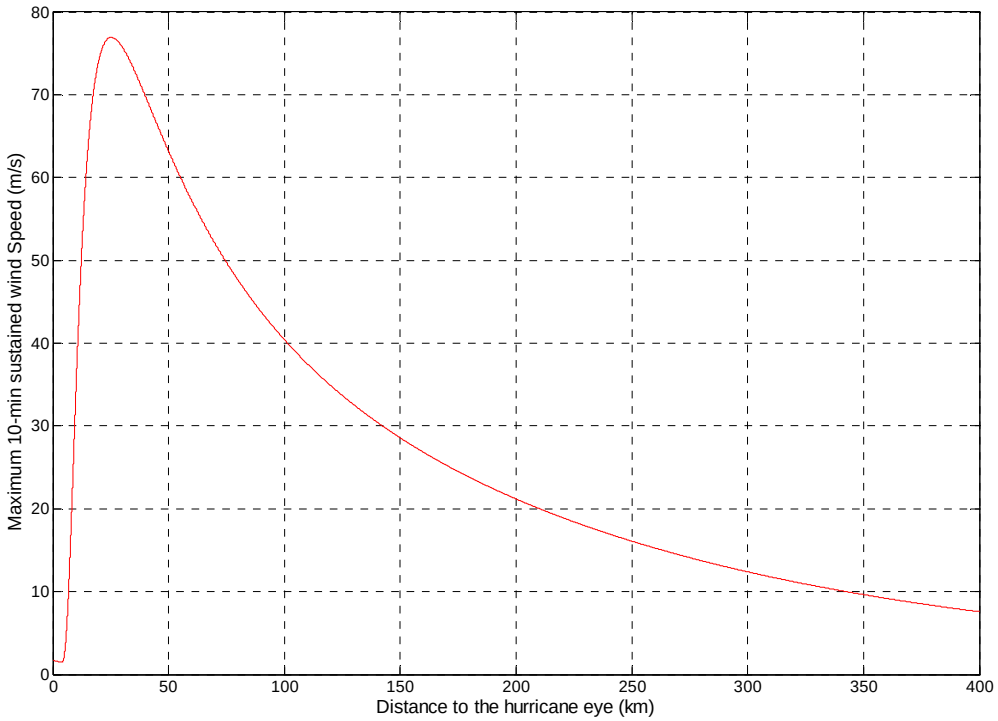

Figure 2: Example of vortex shape of hurricane gradient wind field

Georgiu's model (Georgiu, 1985), used to describe the rotational vortex shape, is defined as:

$$V_g^2(r,\alpha) = \frac{r}{\rho} \cdot \frac{\partial P}{\partial r} + V_g(r,\alpha) \cdot (V_T \sin\alpha - fr) \tag{1}$$

where V_g = gradient wind speed, r = distance from hurricane eye, α = angle from hurricane heading direction (counter-clockwise +), ρ = air density, V_T = translational wind speed, f = coriolis parameter and P = horizontal air pressure. Information needed to statistically characterize these parameters (central pressure, storm track and translational speed) can be obtained from the database of historical hurricane records

(HURDAT, 2005). The horizontal air pressure $P(r)$ at a distance r from the hurricane eye is given by (Vickery et al., 2000b):

$$P(r) = P_c + \Delta p \exp[-(\frac{R_{\max}}{r})^B] \tag{2}$$

where P_c = air pressure at the hurricane eye, Δp = the central pressure deficit (mb) $=1013 - P_c$ (mb), $R_{\max}$ = radius of maximum winds, and B = pressure profile parameter. As suggested by Vickery et al. (2000b), $R_{\max}$ and B are functions of the hurricane eye latitude ψ and central pressure deficit Δp. The best single equation estimates of $R_{\max}$ and B can be written as (Vickery et al., 2000b):

$$\ln R_{\max} = 2.636 - 0.0005086\Delta p^2 + 0.0394899\psi + \varepsilon \tag{3}$$

$$B = 1.38 + 0.00184\Delta p - 0.00309 R_{\max} \tag{4}$$

where the error term ε (in km) is assumed Normal (0, 0.4164) south of 30°N and Normal (0, 0.3778) north of 30°N (Vickery et al., 2000b). As was suggested by Lee and Rosowsky (2007), the error term is assumed herein to be Normal (0, 0.40) at all latitudes.

Once the horizontal air pressure is calculated using Eqs. (2) - (4), the gradient horizontal air pressure $\frac{\partial P}{\partial r}$ can be easily obtained. By substituting Eq. (2) into Eq. (1), the gradient wind speed V_g can be calculated as (Vickery et al., 2000b):

$$V_g = \frac{1}{2}(c\sin\alpha - fr) + \sqrt{\frac{1}{4}(c\sin\alpha - fr)^2 + \frac{B\Delta p}{\rho}(\frac{R_{\max}}{r})^2 \exp[-(\frac{R_{\max}}{r})^2]} \tag{5}$$

Vickery's Empirical Storm Tracking and Central Pressure Model

An empirical tracking model has been developed by Vickery (2000b) to describe the hurricane translational wind speed and heading angle. In this study, the entire Atlantic basin was divided into 5°×5° grid blocks (Figure 3). Each grid block has its own grid-based parameters which are used to determine the translational wind speed and heading angle at next time-step:

$$\begin{cases} \Delta \ln c = a_1 + a_2\psi + a_3\lambda + a_4 \ln c_i + a_5\theta_i + \varepsilon \\ \Delta\theta = b_1 + b_2\psi + b_3\lambda + b_4 c_i + b_5\theta_i + b_6\theta_{i-1} + \varepsilon \end{cases} \tag{6}$$

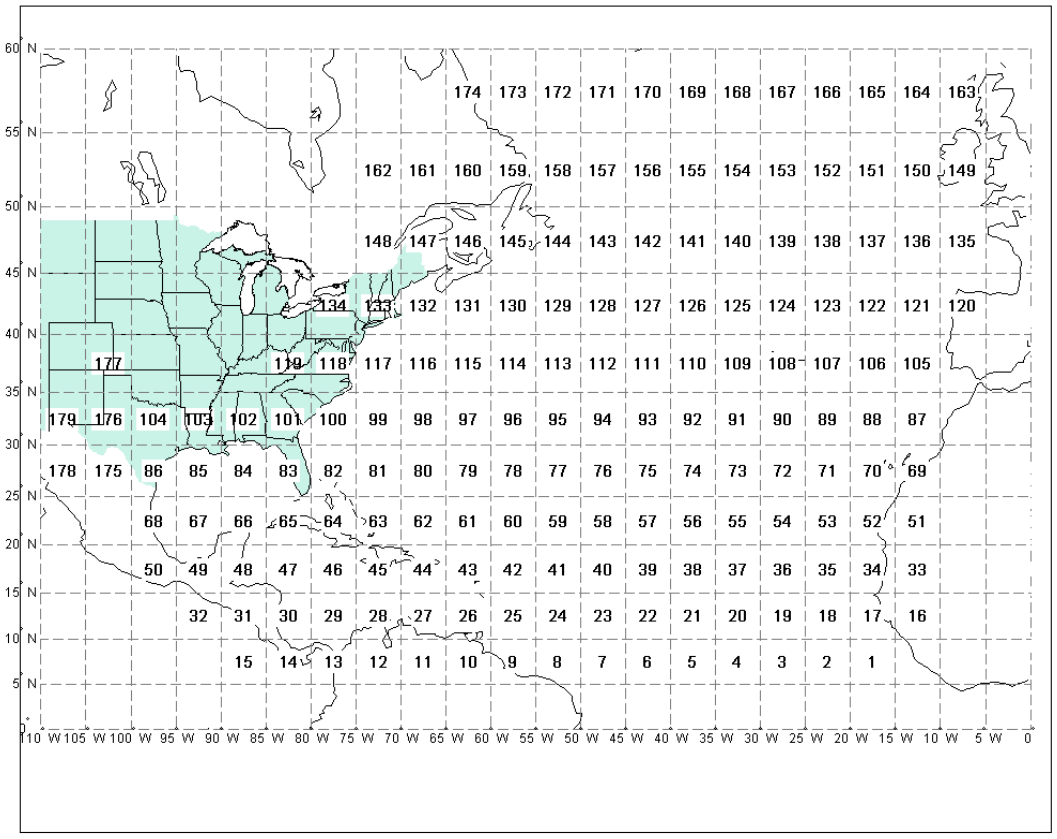

Figure 3: Division of Atlantic basin into 5°×5° grid locations

where c = translational velocity (translational wind speed), θ = heading angle, $a_i (i = 1, 2, ...)$ = grid-based coefficient for translational velocity, $b_i (i = 1, 2, ...)$ = grid-based coefficient for heading angle, ψ and λ = storm latitude and longitude, c_i = translational velocity at previous time-step i, θ_i = heading angle at previous time-step i, θ_{i-1} = heading angle at previous time-step $i-1$, and ε = random error term. The historical HURDAT database contains data at 6-hour intervals describing hurricane eye position, translational velocity, heading angle and central pressure for all hurricanes that have occurred in the Atlantic basin since 1851. Therefore, the coefficient parameters a_i and b_i for each grid can be determined through regression analysis of HURDAT data in each grid location. For those grid locations with little or no hurricane data, the coefficients are assigned the corresponding values from the nearest grid location.

The hurricane central pressure model suggested by Vickery et al. (2000b) was developed based on the relative intensity concept (Darling, 1991). The hurricane eye central pressure P_c can be expressed in terms of relative intensity I, and vice versa. The details of the relationship between hurricane eye central pressure and the relative intensity I can be found in the appendix of Darling's paper (Darling, 1991). In Darling's work, the hurricane eye central pressure is described as a function of environmental conditions such as sea surface temperature so that the relative intensity can be expressed as:

$$\ln(I_{i+1}) = c_0 + c_1 \ln(I_i) + c_2 \ln(I_{i-1}) + c_3 \ln(I_{i-2}) + c_4 T_s + c_5 \Delta T_s + \varepsilon \quad (7)$$

where I_{i+1} = relative intensity at the next time-step $i+1$, I_i, I_{i-1}, I_{i-2} = relative intensity at the previous time-steps i, $i-1$ and $i-2$, c_i = the grid-based coefficient for relative intensity, T_s = sea surface temperature (°K), ΔT_s = difference in sea surface temperatures at time-steps i and $i+1$ (°K), and ε = random error term. Similar to the tracking model coefficients, the coefficient parameters c_i for each grid location can be determined by regression analysis, using the relative intensity values calculated from the HURDAT central pressure data in each grid location. Again, for those grid locations with little or no hurricane data, the coefficients are assigned the corresponding value from the nearest grid location. In cases where the hurricane makes landfall, the central pressure would decay and the relative intensity approach is no longer applicable. Therefore, Eq.(3) only applies when the hurricane eye is over the sea and once the storm makes landfall, the hurricane decay (filling) model proposed by Vickery et al. (1995) is used to describe the central pressure of the hurricane eye. The details of the hurricane decay model are described in the following section.

Decay Model

Once a hurricane makes landfall, its energy decreases due to increased surface friction and the lack of a heat source from the sea. Consequently, both the intensity of the hurricane (i.e., central pressure difference) and the rotational wind speed decrease according to some decay model. A number of decay models have been proposed (Georgiu, 1985; Batts et al., 1980; Ho et al., 1987; Vickery and Twisdale, 1995). The Vickery and Twisdale model is used in the current study. The model takes the form of an exponential decay function:

$$\Delta p(t) = \Delta p_0 \exp(-at) \tag{8}$$

where $\Delta p(t)$ = the central pressure deficit (mb) at time t after landfall, Δp_0 = the central pressure deficit (mb) at landfall, a = site-specific decay parameter (constant), and t = time after landfall. The key decay parameter a for each hurricane can be obtained through analysis of the historical hurricane central pressure data (HURDAT, 2005). The statistical analysis of decay constants for North Carolina, South Carolina and the Florida were performed by Rosowsky et al. (1999). The same procedure was used for Texas and the decay constant was found to follow a lognormal distribution. Eleven hurricane events that made landfall along the Texas coast between 1980 and 2004 were selected to fit the decay rate of Texas. These storm tracks are shown in Figure 4. Figure 5 shows the time history of normalized central pressure deficit of the eleven sample storms after the landfall. This figure plots the mean exponential decay curves along with the one standard deviation bounds. The mean decay constant a for Texas is 0.04, and the standard deviation is 0.032. The corresponding Lognormal parameters λ and ξ are -3.464 and 0.703, respectively.

Gradient-to-Surface Wind Speed Conversion

The surface wind speed at 10 meters height above the ground and an assumed open terrain location can be estimated using conversion factors applied to the wind speed at the gradient level, generally taken as between 500m and 2000m. Gradient-to-surface wind speed conversion factors were proposed by Caton (1975) and later modified by Sparks and Huang (1999). A summary of the gradient-to-surface conversion factors

assumed herein for both 10-min sustained wind speeds and 5-s gust wind speeds are summarized in Table 1 (Lee and Rosowsky, 2007).

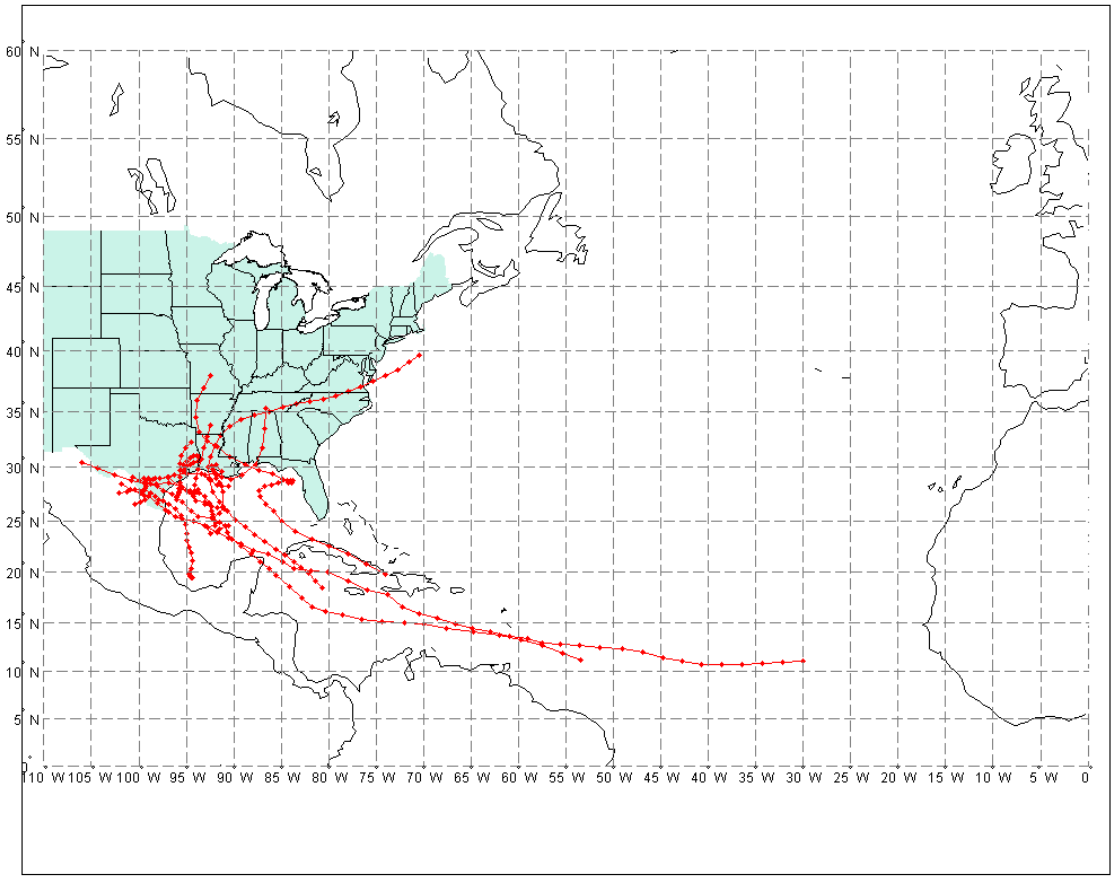

Figure 4: Map showing the tracks of eleven land falling hurricanes along the Texas coast (1980-2004)

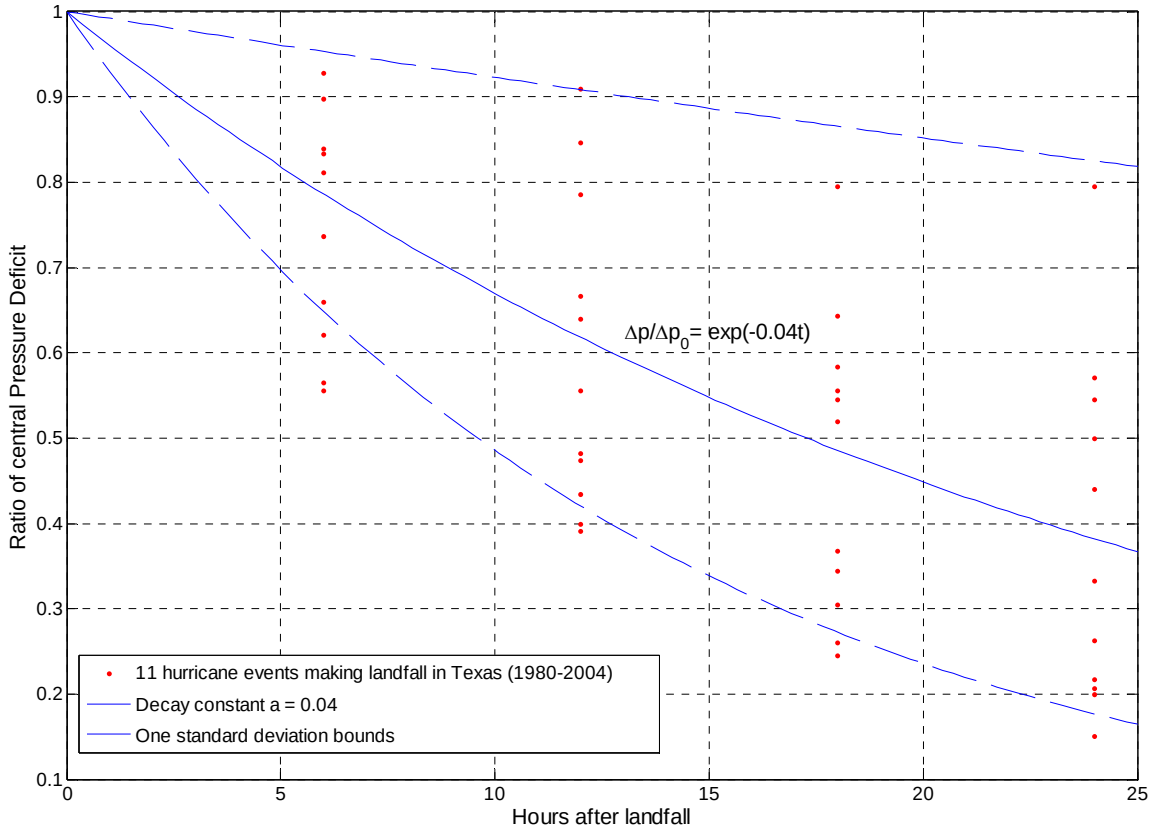

Figure 5: Decay rates of historical hurricanes in Texas

Table 1. Gradient-to-surface wind speed conversion factors (Lee and Rosowsky, 2007)

Location	Wind from ocean		Wind from land	
	Gradient-to-mean	Gradient-to-gust	Gradient-to-mean	Gradient-to-gust
Zone 1[(1)]	0.45	0.72	0.45	0.72
Zone 2[(2)]	0.50	0.80	0.45	0.72
Zone 3[(3)]	0.65	0.90	0.50	0.80
Zone 4[(4)]	0.65	0.90	0.65	0.90

(1) Zone 1 = inland open terrain (airports) more than 10 km from the coast
(2) Zone 2 = airport within 10 km of the coast
(3) Zone 3 = sites adjacent to the sea
(4) Zone 4 = off-shore sites

Simulation Procedure

In order to develop the synthetic hurricane wind speed database, 10,000 years of records were simulated. The occurrence of hurricane events is modeled as a Poisson process with an annual occurrence rate in the Atlantic basin of $\lambda = 8.4$ /year (Lee and Rosowsky, 2007).

The locations of hurricane formation for each event in the HURDAT database are shown in Figure 6. A simulated hurricane starts in the Atlantic basin with parameters based on historical data (i.e. initial location, angle and translational speed). The hurricane then moves along a track defined by the tracking and central pressure model. The hurricane's position at each subsequent 6-hour interval can be determined using Eq. (6), and the parameters derived from information in the HURDAT database. Similarly, the next interval's central pressure can be obtained using Eq. (7). Once the hurricane makes landfall, the central pressure decays according to Eq. (8). Finally the gradient wind speed can be obtained from Eq. (5) and converted to a surface wind speed using the gradient-to-surface wind speed conversion factors in Table 1. If the maximum 10-min surface wind speed at any site is greater than a specified threshold value (15 m/s is used in this study), this value is recorded in the time series for that site. Following this procedure, 10,000 years of simulated hurricane events are generated and the synthetic hurricane wind speed records are developed for every zip-code in Texas.

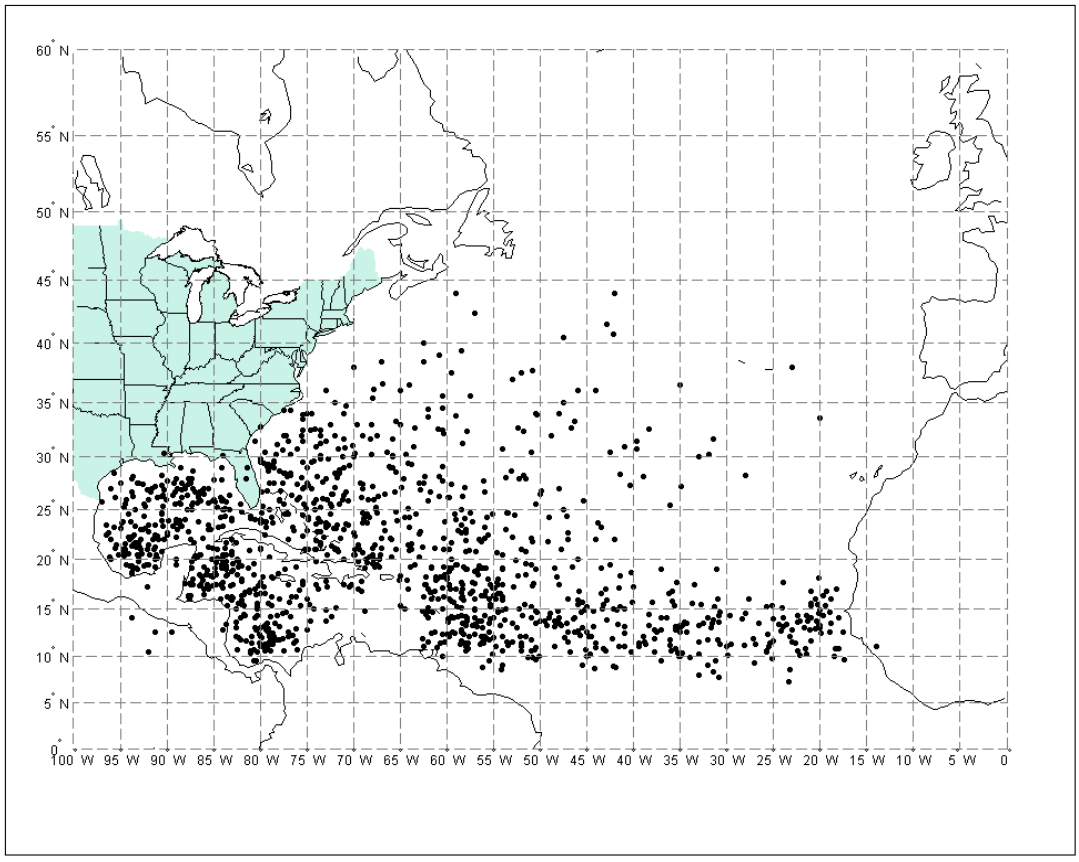

Figure 6: Initial positions of hurricanes in the HURDAT database (2005)

Distribution Fitting

Once the 10,000 years of simulated hurricane events have been generated and the hurricane wind speed time histories have been developed for every location in Texas, the distributions of the N-year maximum wind speed can be fit. For example, to determine the best-fit distribution for the 100-year maximum wind speed for a given location, a total of 100 values of the 100-year wind speed would be used. Three distribution types were considered: Lognormal, Extreme Type-I (ET-I) and Extreme Type-II (ET-II). A MATLAB program (developed previously by Lee and Rosowsky, 2007) can be used to

present the best-fit distribution and to mine and display the synthetic wind speed data. A screen-shot from this MATLAB program is shown in Figure 7 for one location (College Station, TX).

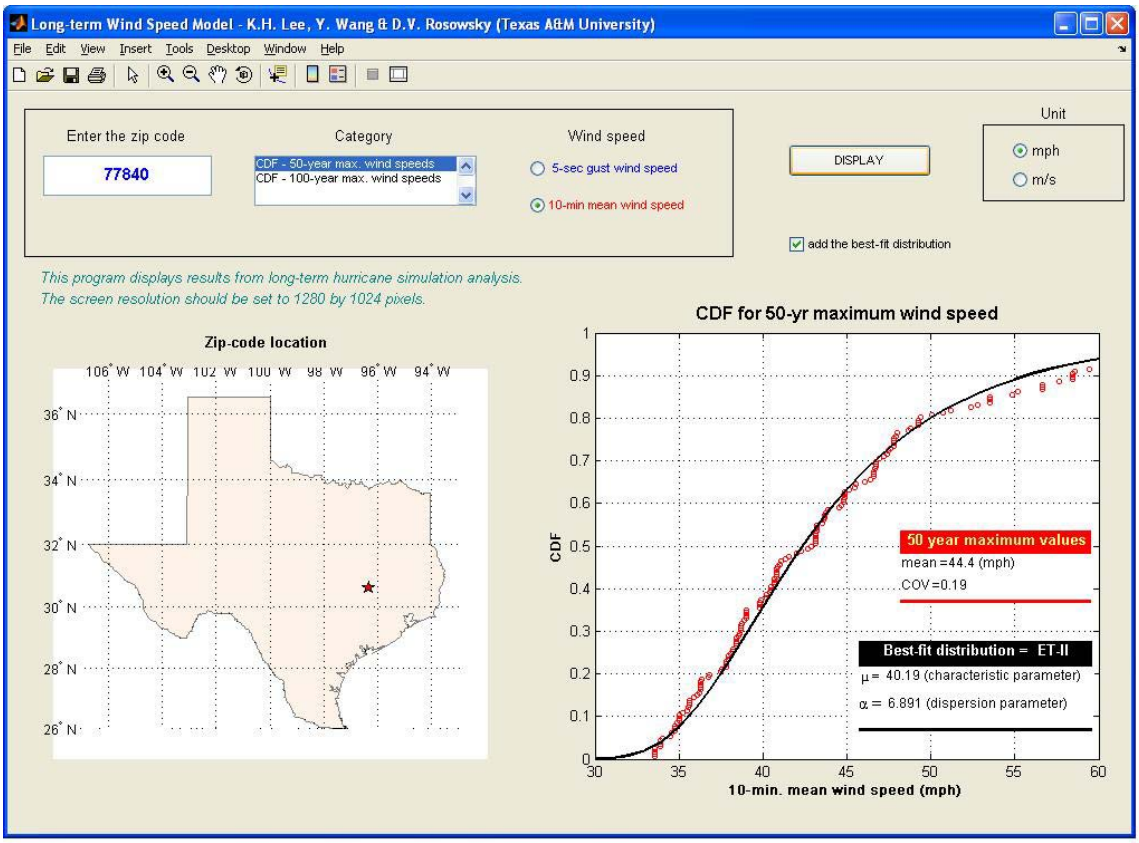

Figure 7: Screen-shot from MATLAB program used to mine and display synthetic wind speed data

Assuming the annual maximum wind speeds are independent, the non-exceedance probability of the *N*-year mean recurrence interval (MRI) wind speed in *m* years can be calculated as $(1-1/N)^m$, using the information of the *m*-year maximum wind speed distribution developed above. The non-exceedance probability of the 50-year

MRI in 50 years is 0.364 and the corresponding 50-year MRI wind speeds at all zip codes were thus determined. The contour map of the 50-year MRI 10-min sustained wind speeds for Texas is shown in Figure 8. Note that in inland locations in Texas, the extreme wind climate may not be characterized by hurricane wind speeds. In these regions, extra-tropical storms, thunderstorms or tornados are expected to control the extreme wind climate. Therefore, the synthetic hurricane wind speed records developed herein can only be used to characterize the wind hazard close to the coast where the extreme wind climate is controlled by tropical storms (hurricanes).

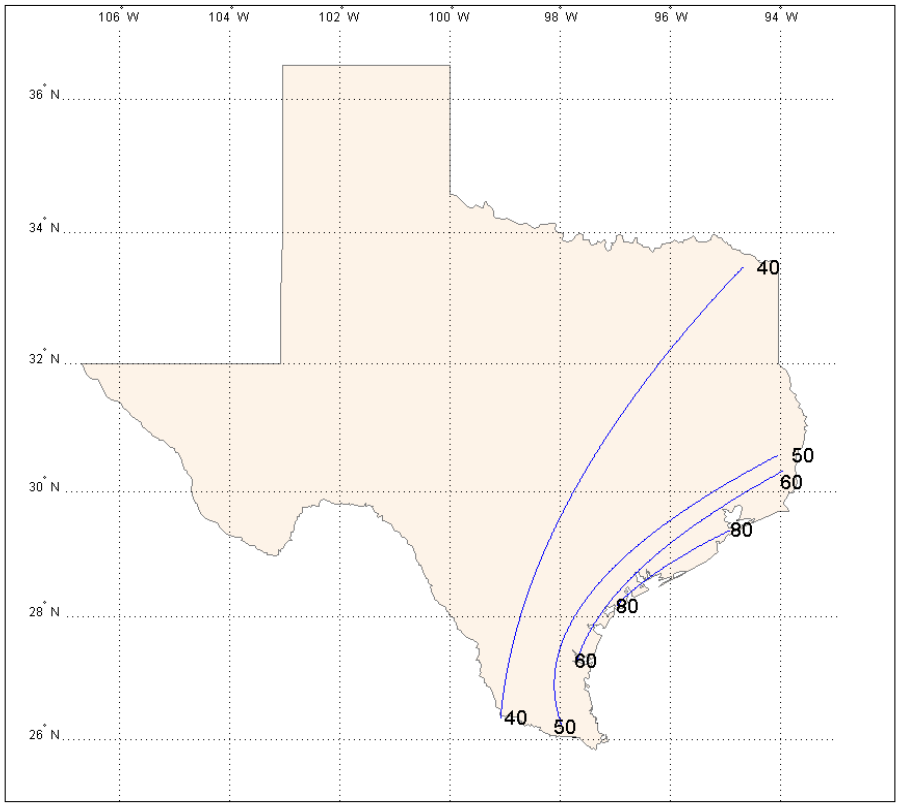

Figure 8: 50-year MRI hurricane (only) wind speed contours for Texas coast (10-min sustained wind speed, mph)

Summary

A total of 10,000 years of synthetic hurricane wind speed records were generated using event-based simulation techniques for every zip-code in Texas. The resulting database includes information on time of hurricane passage, maximum gradient wind speed and maximum surface wind speed (both sustained and gust). The database can be used to statistically characterize the N-year maximum wind speed distribution for a given zip-code location. This information can be used (e.g.) to independently validate the design wind speed maps for Texas, at least close to the coast where the extreme wind climate is controlled by the hurricane hazard. Geographic Information System (GIS) tools also can be used to spatially store and display the wind speed information in the database which, when coupled with a hurricane damage model, could also display expected losses, for example. The simulation framework is modular and thus it is relatively straightforward to include improved wind-field, tracking or other models as well as additional historical data. The simulation framework can be used for near real-time prediction of expected wind conditions using available real-time data (e.g. from the National Hurricane Center). The framework can also be used to investigate possible correlations between hurricane wind speed and other hazards (e.g. surge or coastal flooding). Finally the simulation framework could be used to statistically characterize hurricane parameters (i.e., central pressure, radius of maximum winds or maximum wind speed at eye-wall) and then develop a suite of characteristic hurricane events corresponding to certain hazard levels for use in performance-based engineering applications.

Part II

Modeling the Joint Wind-Surge Hazard due to Hurricanes in the Gulf of Mexico

Introduction

Strong winds and storm surge induced by large hurricanes can cause coastal flooding and extensive damage. Significant advances have been made in the forecasting and modeling of approaching hurricanes, thereby enabling improved prediction of expected strong winds at specific sites. However, storm surge models are far more complex (and thus computationally intensive) and accurate prediction of surge heights is far more difficult. The maximum storm surge height is influenced by both the maximum wind speed and the topography at the site. Advanced numerical models for surge height prediction have been developed using computational fluid dynamics (CFD) and other advanced computational techniques. One example is the SLOSH (Sea, Land, and Overland Surge from Hurricanes) model (Jelesnianski et al., 1992), which is primarily a research tool. Since the model is so computationally intensive, it can not practically be used in real-time over geographically large areas. However results obtained using the SLOSH model have been used to inform other predictive models that can be used more easily in a real-time decision making environment. Another example of a computationally sophisticated model is the ADCIRC (ADvanced CIRCulation) model (Luettich and Westerink, 2004), a finite element model that requires detailed information on local conditions as input, and thus also is very site-specific. While impressive as research tools, models such as SLOSH and ADCIRC are not conducive to real-time

emergency management/response operations. As an alternative to existing numerical models, which are computationally intensive, expensive to run, and require significant amounts of model input, it might be possible to develop a simplified combined wind-surge model that can be used in a real-time predictive mode (with information about expected surface wind speed, for example) with relative confidence and sufficient accuracy for most emergency management purposes.

Estimates of surface wind speed at near-coast locations can be made with some confidence (given the availability of gradient-level wind speed data and current state-of-the-art wind field modeling techniques, including gradient-to-surface conversions over water and over land). However surge height prediction, based largely on complex numerical models (e.g., CFD), has proven more time-consuming, costly, and less accurate. The objective of this study was to determine if a simple wind-surge model could be postulated (and validated in future events), for a portion of the Texas-Louisiana coastline, using widely available data. If the model could be validated, it could provide a powerful tool to quickly and inexpensively estimate surge depths at coastal locations in advance of a hurricane landfall. This has obvious implications for emergency management, pre-disaster planning, and post-disaster response. If such a model proves useful, a framework for additional data collection can be suggested to refine predictions of surge height at critical coastal locations.

Historical Data for Storm Surge and Wind Speed

Storm surge is caused by water that is pushed toward the shore by the force of the winds which, when combined with the normal tide, creates the hurricane storm tide.

Thus, the storm surge can be obtained by subtracting the ambient tide level from the total water height recorded during or after hurricane. CO-OPS (The Center for Operational Oceanographic Products and Services, part of the National Ocean Service (NOS), operated by National Oceanic and Atmospheric Administration (NOAA)) maintains historical water-level data recorded by the NOS observation network. In this study, the storm surge height is taken as the value of water-level above the mean tide level. While historical records are not complete at all measurement sites throughout every hurricane season, complete records at 20 near-shore monitoring stations along the Texas and Louisiana coast are available for 11 historical hurricanes that made landfall along the Texas/ Louisiana coast between 1995 and 2005. These records of the monthly-maximum surge height for each storm in the month the hurricane made landfall were used in this study.

The surface-level wind speeds (1-minute sustained wind speeds at 10m elevation) were measured at surface monitoring stations. The NCDC (National Climatic Data Center) maintains daily maximum surface wind speed data for each monitoring station. In this study, the surge monitoring stations and the wind monitoring stations were assumed to coincide (i.e. be co-located in space) if they were at the same longitude and latitude. For every location of a surge monitoring station at which the NCDC measured surface wind speed data was not recorded (i.e. no co-located surface wind monitoring station), the estimated surface-level wind speed was obtained by simulation. This simulation procedure is described in the part I.

Joint Wind-Surge Model

Data pairs describing peak surface wind speed (1-minute sustained) and surge height for a given location and given hurricane event are developed using (1) measured surge depth information (corrected for tide height) and either (2a) measured surface-level wind speed, where recorded and available, or (2b) estimated surface-level wind speed using state-of-the-art wind field modeling techniques, where surface measurements were not available. Since the latter introduces another source of model error, the two different types of wind-surge data pairs (i.e., measured-measured vs. estimated-measured) were analyzed separately.

The simulated wind speed/measured storm surge data pairs were plotted as shown in Figure 9 (shown for the station located at Galveston Pier 21). Since not all stations have data recorded for each of the 11 hurricanes considered, and in order to consider the effect of (contiguous) areas believed to have similar topography, three "super cells" of clustered stations were created, as shown in Figure 10. The Galveston Bay, TX area defines super cell #1, the TX/LA border area defines super cell #2, and the Grand Isle, LA area defines super cell #3. The wind-surge data pairs of the stations within these "super cells" were then grouped together and analyzed as a cluster. In the same way, the measured wind speed/measured storm surge data pairs were plotted and analyzed. Since only some of the NCDC stations that record surface wind speed coincide with CO-OPS sample stations, there are fewer measured wind speed/measured storm surge data pairs than simulated wind speed/measured storm surge data pairs.

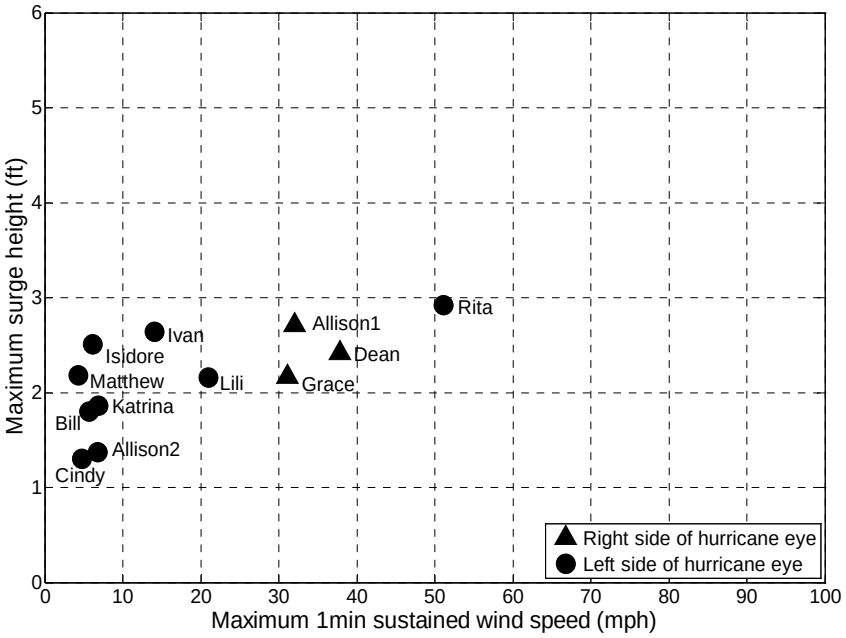

Figure 9: Historical wind speed and surge data for Galveston Pier 21, TX

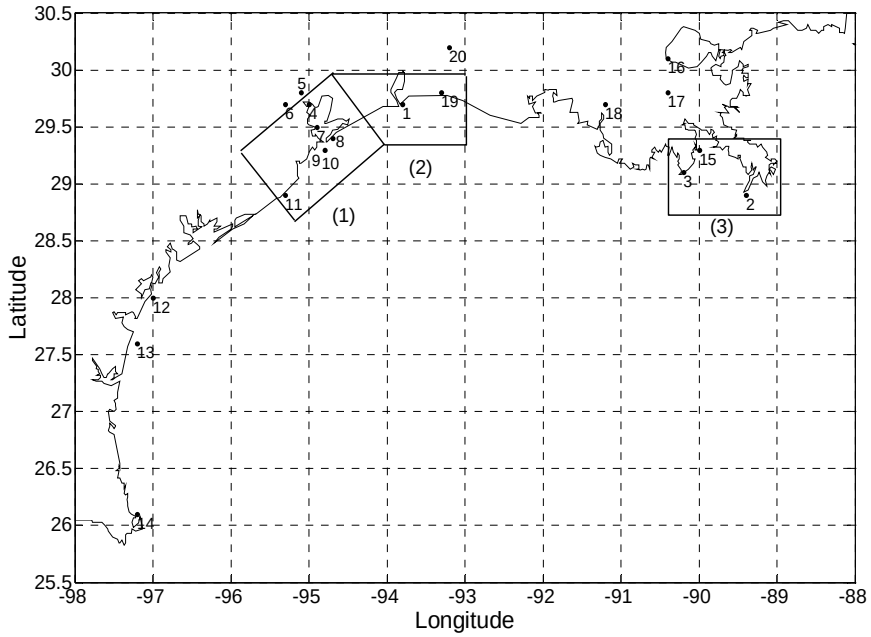

Figure 10: Definition of super cells along TX/LA coastline

The linear regressions (mean ± one standard deviation) of both the simulated wind/measured surge data pairs and measured wind/measured surge data pairs for each of the three super cells are shown in Figures 11 – 13, respectively. Regression lines for the simulated/measured wind speed data pairs are shown separately. To further examine the difference between the resulting two linear models, a multiplier defined as the ratio of measured wind speed to simulated wind speed for the same storm surge data point is considered. In general, the multiplier (in essence a model error term) becomes larger with increasing distance from the hurricane eye as seen in Figure 14. This arises due to: (1) the inherent modeling error in the wind field model, which increases at sites further away from hurricane eye, (2) the difference between the actual landfall time and the time at which the hurricane wind field is simulated, and (3) events other than hurricanes may cause the recorded monthly maximum wind speed (this is rare in this region). The differences between measured wind speed and simulated wind speed for super cells #1-#3 in Figures 11-13 are largely due to the inherent modeling error in the wind field model, which increases at sites further away from hurricane eye. The wind field model is generally more accurate in the range of R_{max}-2*R_{max} and underestimates the wind speed in the tail (lower wind speed) range. For all 11 historical events used to develop the wind-surge model herein, the ROD values in Figure 13 for super cell #3 are less than 10, which is selected as the threshold value for ROD in the modified wind-surge model, and many ROD values in Figure 11 (super cell #1) and 12 (super cell #2) are greater than 10. This may explain why the differences between measured wind speed and simulated wind speed for super cells #3 are smaller than the differences for super cells #1 and #2.

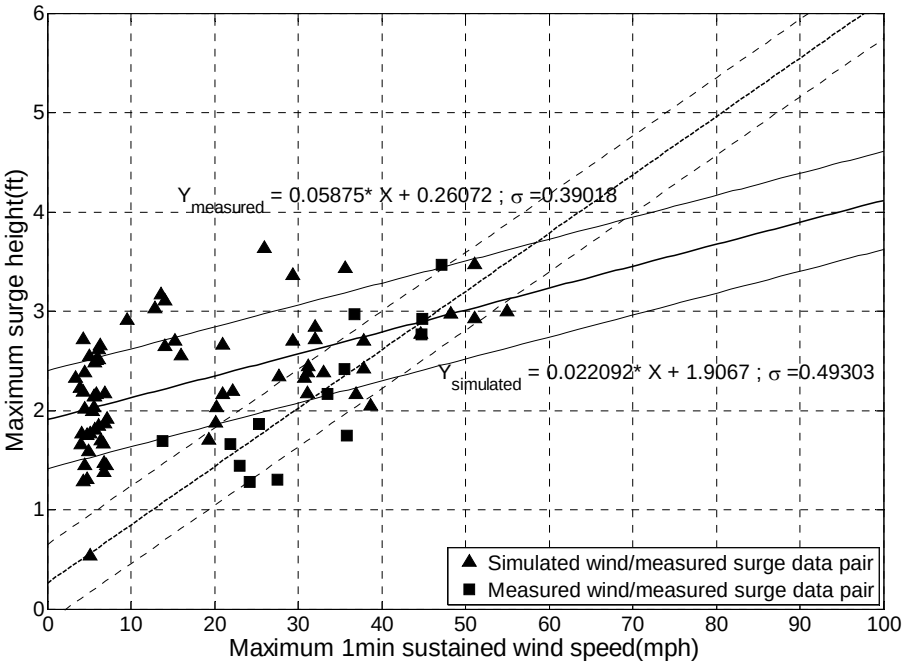

Figure 11: Wind-surge pairs for super cell #1

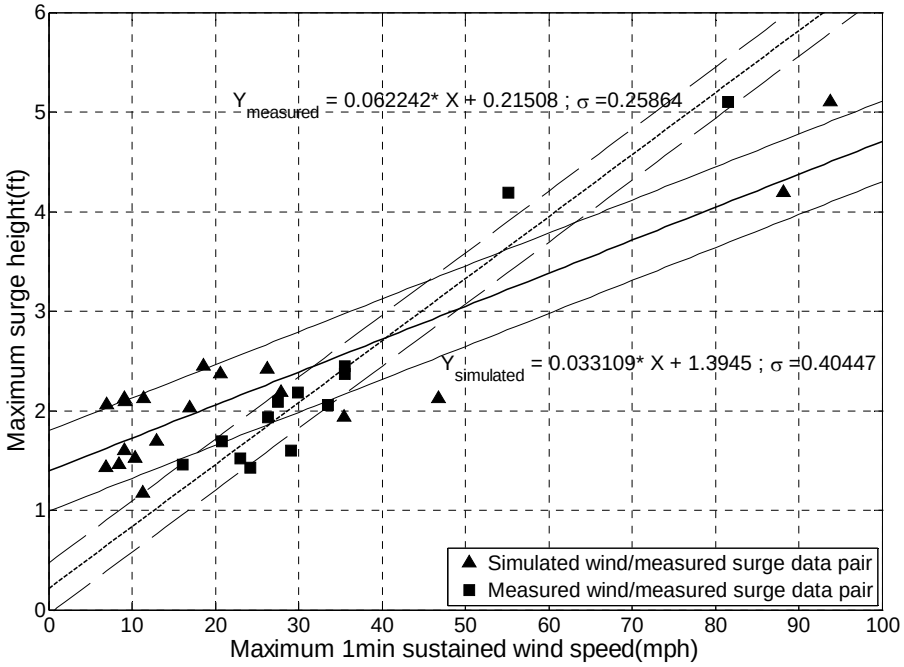

Figure 12: Wind-surge pairs for super cell #2

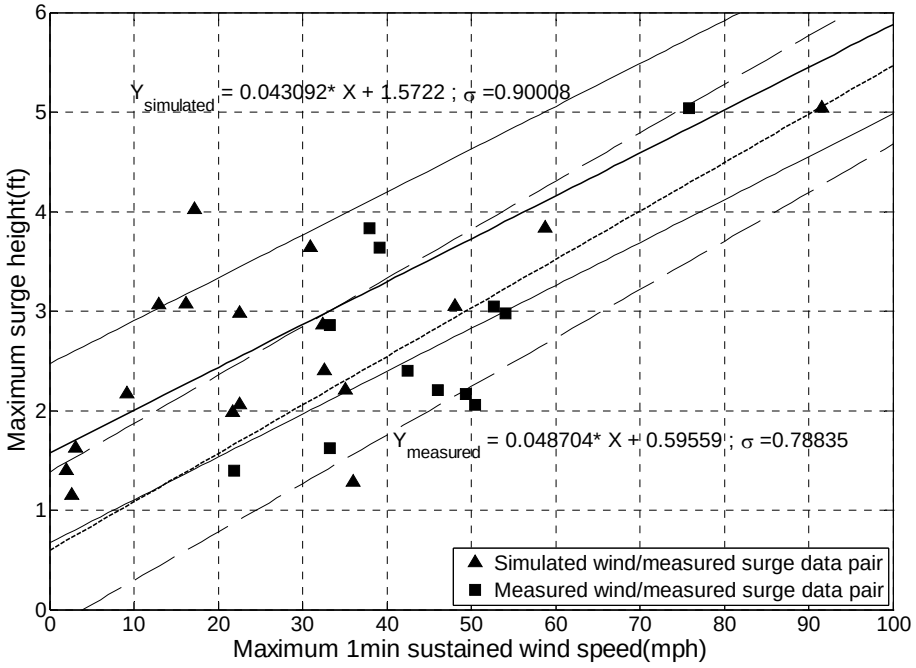

Figure 13: Wind-surge pairs for super cell #3

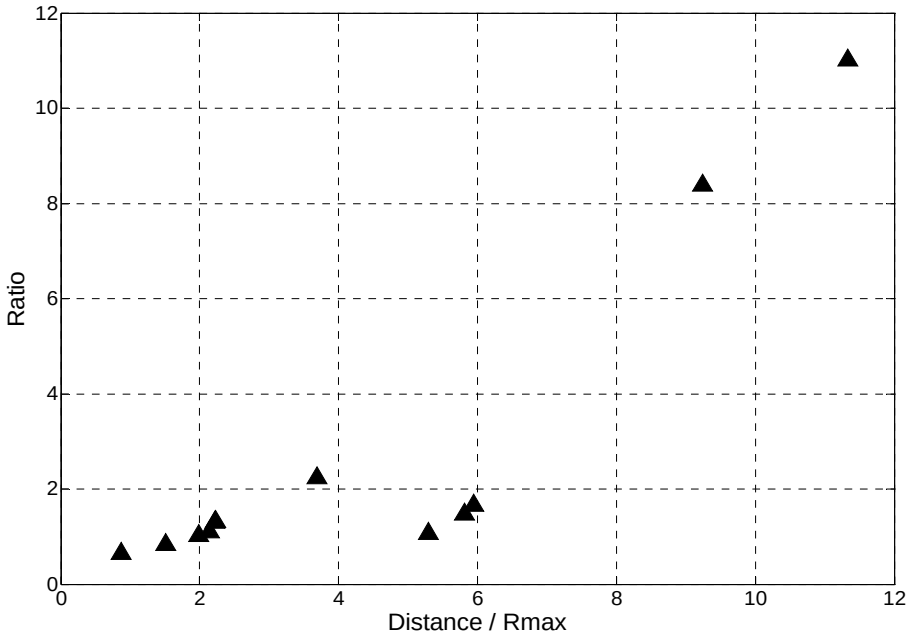

Figure 14: Ratios of measured wind speed to simulated wind speed for super cell #3

An online database product called Probabilistic Hurricane Storm Surge (PHSS), which is based on the SLOSH model, is available to predict the probability that hurricane storm surge will exceed a given height above normal tide levels. The cumulative distribution function (CDF) of storm surge height can thus be determined based on the PHSS results and assuming (e.g.) a Lognormal distribution. Results from four hurricanes (George 1998, Lili 2002, Ivan 2004, Katrina 2005) included in the PHSS database were used to generate Lognormal distributions of maximum storm surge height for each super cell. The maximum simulated surface wind speed during each of the four hurricanes in one super cell was determined by calculating the maximum simulated surface wind speed at each surge monitoring station location in the super cell, and then taking the maximum value. For comparison, the Lognormal distributions based on the linear wind-surge model developed herein, and those based on the SLOSH model results with the corresponding simulated maximum surface wind speeds during each of the four hurricanes, are shown together in Figures 15, 16 and 17 for each super cell, respectively. These models generally compare well.

Recent and future hurricane event data can be used to validate the simplified wind-surge model developed in this study. For example, hurricane Ike occurred in September 2008 and affected a large portion of the Texas coast region. Abundant wind-surge data has been recorded along the affected Texas/LA coast. NOS and other organizations maintain real-time storm surge data from a network of some monitoring stations along TX/LA coast obtained during the passage of hurricane Ike. The National Weather Service (NWS) also maintains hurricane gradient-level wind field data

(measured periodically) as well as surface wind speed data. This model validation was ongoing at the time this paper was prepared.

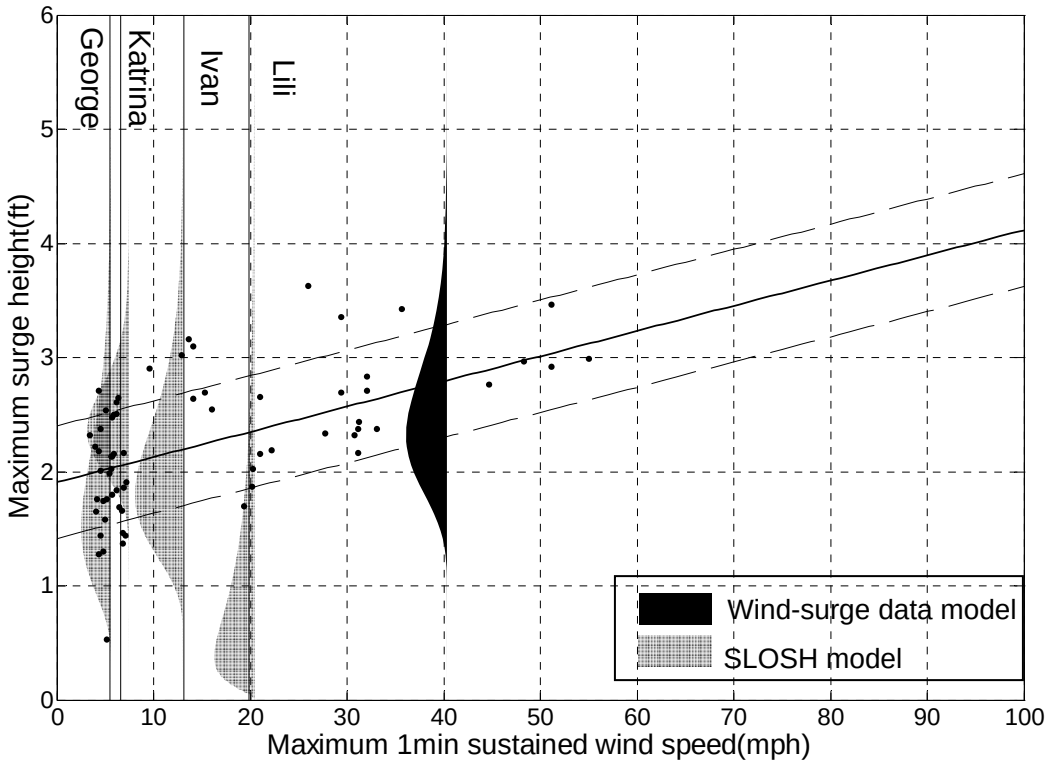

Figure 15: Lognormal fits to wind-surge data for super cell #1

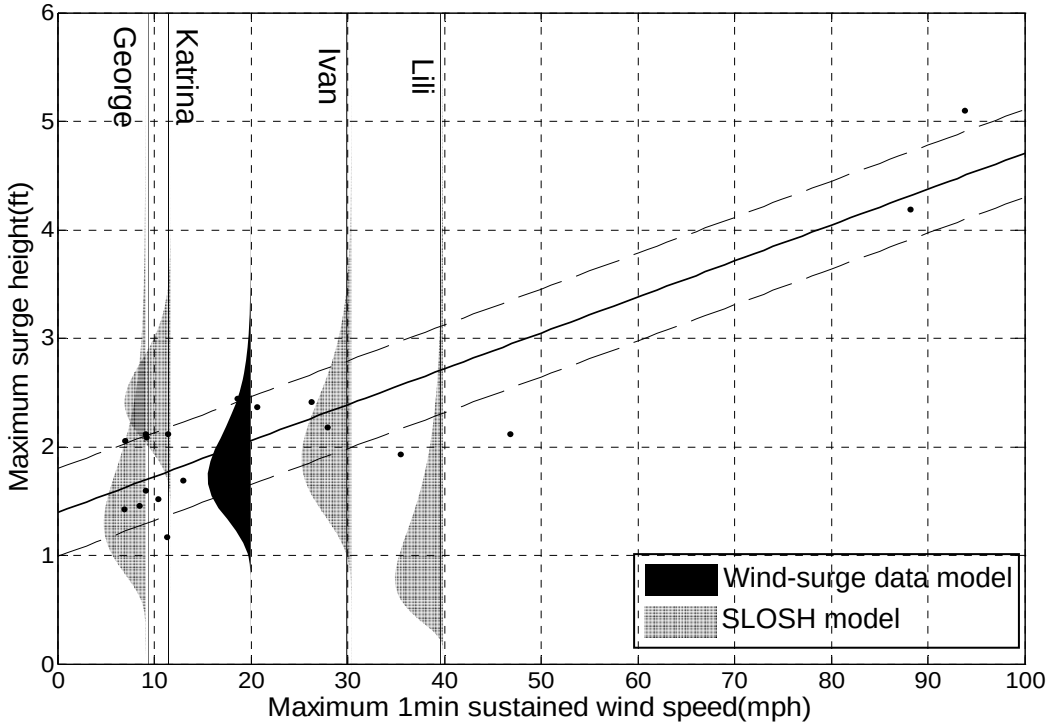

Figure 16: Lognormal fits to wind-surge data for super cell #2

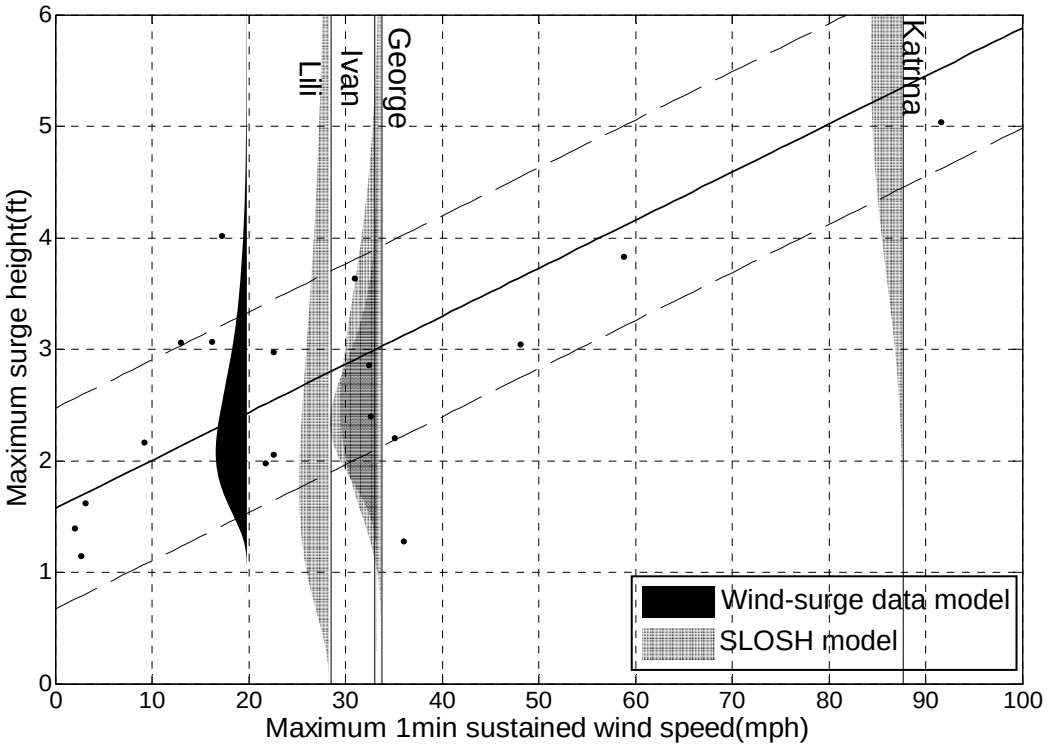

Figure 17: Lognormal fits to wind-surge data for super cell #3

Applications of Simplified Wind-Surge Model

One possible application for the simple linear wind-surge model proposed herein is the rapid prediction of maximum surge height expected to be caused by an approaching hurricane. This has obvious implications for both emergency response and planning. If the surface wind speed is being monitored at a particular location during the hurricane, the maximum expected surge height at this location can be estimated quickly using the linear wind-surge model based on measured wind/measured actual surge data pairs. Alternatively, at locations, at which surface wind speeds are not being recorded, surface wind speeds can be estimated using the wind field model and data made available by the NWS or other sources, and the maximum expected surge height can be estimated using the model based on the simulated wind/measured surge data pairs.

The wind-surge model developed herein can also be used to create surge hazard maps that provide storm surge height non-exceedance probability contours for a particular reference period (e.g., 2% in 50 years, 10% in 100 years, etc.). The non-exceedance probability is defined as:

$$P(S < S_e) = \int P(S < S_e \,|\, V = V_g) \cdot f(V = V_g) \cdot dV \tag{9}$$

where, S = surge height, S_e = surge height value in a particular reference period, V = wind speed value, $f(V = V_g)$ = probability density function (PDF) of wind speeds, and $P(S < S_e \,|\, V = V_g)$ = conditional probability that the surge height is less than a certain value. A statistical characterization of hurricane wind speeds along the Texas coast is presented in part I. Specifically, the 50-year and 100-year maximum tropical wind speed

distributions are presented for each location along the Texas coastline. The conditional probability $P(S < S_e \left| V = V_g \right.)$ is assumed to follow a Lognormal distribution. For a range of surge height values S_e in a particular reference period, the corresponding non-exceedance probabilities at a given location can be calculated by solving Eq. (9) several times. Once these non-exceedance probabilities are obtained, they can be used to describe the CDF of storm surge height at the location. Then, for every location along the Texas coastline, the storm surge height corresponding to a particular non-exceedance probability can be estimated using interpolation. Finally, a design surge height map associated with a particular non-exceedance probability (e.g., 2% in 50 years) can be determined.

Summary

This paper describes a simplified wind-surge model based on archived surface wind speed measurements and storm surge measurements. Given that more surge measurements existed (at more locations and for more events) than ground wind speed measurements, the latter was augmented using results from state-of-the-art wind field models and best estimates of gradient-level wind field parameters obtained just prior to landfall. Linear regression models were developed for both (a) measured wind/measured surge data pairs, and (b) simulated wind/measured surge data pairs. Models were proposed for selected "super cells" (or clusters of coastal locations) along the Texas-Louisiana coastline. It was shown that it was possible to develop these simple regression models for contiguous ("like") regions of the coastline provided the data exist or could be reasonably estimated, and that these models were likely to be sufficiently

accurate for real-time estimates (e.g., of expected surge depth given best predictions of surface wind speed) as a hurricane approaches the coast. Assuming the costs of monitoring stations are modest (i.e., relative to likely post-disaster costs), a strong case can be made to expand the network of surface measurement stations along this vulnerable coastline, providing additional data with which to refine the model's accuracy and expand the coverage area.

Part III

Update on Modeling the Joint Wind-Surge Model and Its Application

Update on Historical Data for Storm Surge and Wind Speed

The previous study considered monthly-maximum surge height records taken at 20 near-shore monitoring stations along the Texas and Louisiana coast. Specially, data were used from 11 historical landfalling hurricanes occurring between 1995 and 2005. Additional, more recent, hurricane event data can be included to improve the simplified wind-surge model developed previously. Hurricane Gustav made landfall in August and September 2008 and affected a large portion of the Louisiana coast. Soon after Gustav, hurricane Ike made landfall at Galveston, TX in September 2008, causing enormous damage to the island. Abundant wind-surge data has been recorded along the affected Texas/LA coast. The National Ocean Service (NOS) and other organizations maintain real-time storm surge data from a network of monitoring stations along the entire US coast and data was recorded along the TX/LA coast during the passage of hurricanes Gustav and Ike.

Data pairs describing peak surface wind speed (1-minute sustained) and surge height for each given location during hurricanes Gustav and Ike were added to the previous wind speed/storm surge data pairs. As before, measured surge depth information (corrected for tide height) and either (a) measured surface-level wind speed, where recorded and available, or (b) estimated surface-level wind speed using state-of-the-art wind-field modeling technique, where surface measurements were not

available, were used and analyzed separately. The simulated wind speed/measured storm surge data pairs were plotted as shown in Figure 18 (shown for the station located at Galveston Pier 21). Compared to the data point for hurricane Rita in Figure 18, the newly added data point for hurricane Ike is an "outlier" from the increasing trend of the simplified wind-surge model based on simple linear regression. One hypothesis is that this is due to the fact that hurricane Ike made a direct hit on the Galveston coast and the kinetic energy associated with this most intense part of storm had a very severe impact on storm surge generation.[1] The simplified wind-surge model may not be able to properly account for this "direct-hit" situation and a modified joint wind-surge model is developed herein.

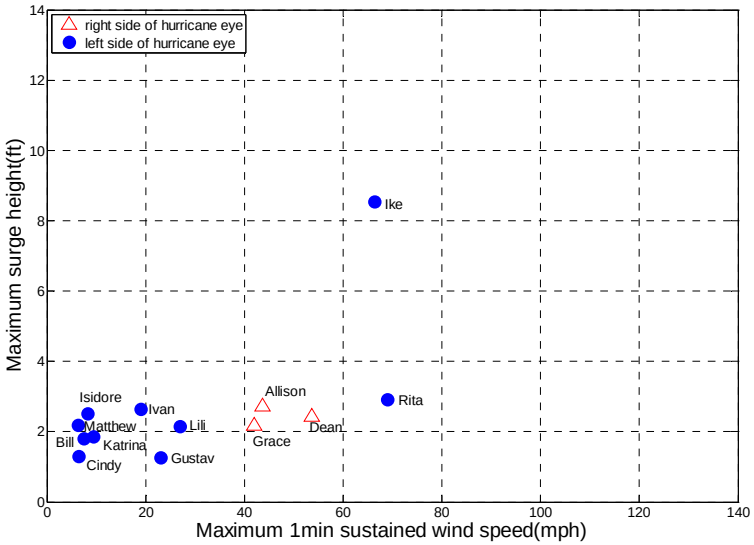

Figure 18: Wind speed and surge data (1995-2008) for Galveston Pier 21, TX, including hurricanes Gustav and Ike (2008)

[1] This hypothesis may warrant further study as it could result in stronger relationships between, e.g., wind energy and surge height.

Modified Joint Wind-Surge Model

As an alternative to the previously proposed simplified wind-surge model, a new dependant-variable (ROD) is introduced. The ROD is defined as the ratio of the distance from a given location to the hurricane eye (R) to the radius of maximum wind speed (R_{max}). This ROD factor (R/R_{max}) therefore takes into account the relative position of the most intense part of the hurricane to the location at which the surge height is being estimated. Unlike the previous simplified joint wind-surge model based only on wind speed/surge height data pairs, the modified joint wind-surge model consists of two correlated sub-models using ROD/maximum wind speed data pairs and maximum surge height/ROD data pairs, respectively. The maximum surge height data are taken from 20 near-shore monitoring stations. The maximum wind speed is the measured surface wind speed or the simulated surface wind speed (where surface measurements were not available). The value of R_{max} of given hurricane event was calculated using the wind-field modeling technique described earlier and this parameter is used to characterize the size of the hurricane wind-field. Consequently, the distance from a given location to the hurricane eye (R) can be calculated knowing its latitude and longitude and therefore the value of ROD can be obtained. Using quantitative analyses on all 20 stations and taking into account the effect of (contiguous) areas believed to have similar topography, three "super cells" of clustered stations were used as before. For example, the data pairs for each of the five stations around Galveston Bay (including data points for hurricanes Gustav and Ike) show similar trends as seen in Figure 18 for the station located at Galveston Pier 21. Therefore, these five stations were grouped

together as a “super-cell” cluster. The updated wind/ROD and ROD/surge data pairs of the stations within these three “super cells” were then grouped together and analyzed as clusters.

Statistical analysis of the wind/ROD pairs and the ROD/surge pairs for the three super cells was performed using nonlinear regression. In order to focus on the region of high wind speed coupled with low ROD, the data points associated with wind speeds of less than 15 mph or ROD values greater than 10 were not included in the analysis. The fitted exponential regression curves (mean ± one standard deviation) of the wind/ROD pairs and the ROD/surge pairs for super cell #2 are shown in Figures 19 and 20. The relationships defined by these two sub-models can be used jointly to estimate the *N*-year maximum surge height or the non-exceedance probability of the *N*-year maximum surge height.

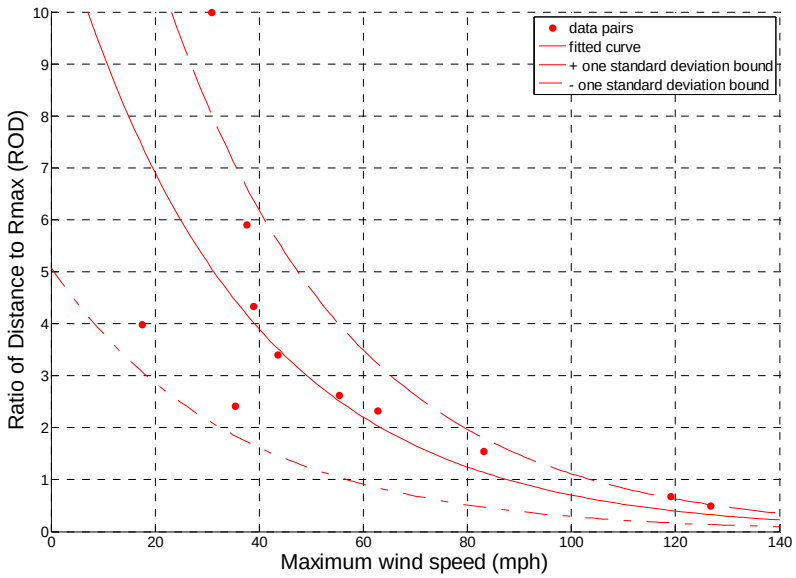

Figure 19: Wind-ROD pairs for super cell #2

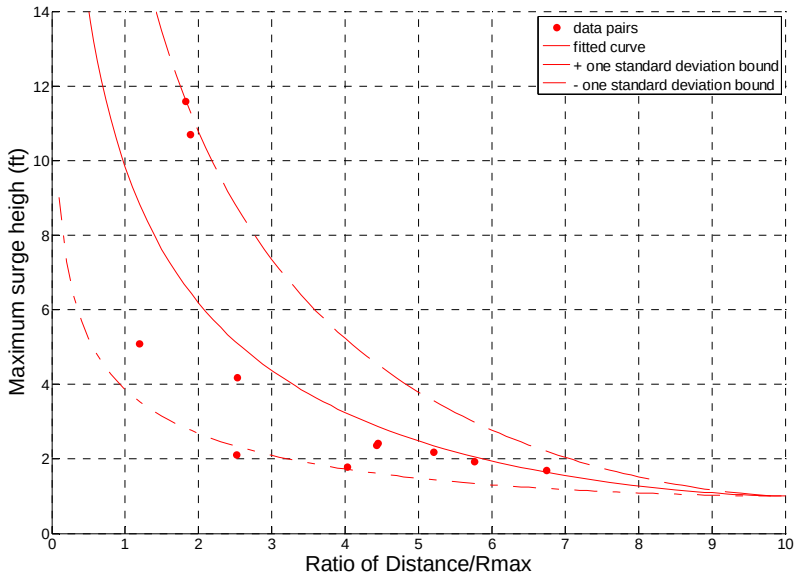

Figure 20: ROD-surge pairs for super cell #2

Applications of Modified Wind-Surge Model

One possible application for the modified wind-surge model proposed herein is the rapid prediction of maximum surge height expected to be caused by an approaching hurricane. This has obvious implications for both emergency response and planning. For each given location, the 10,000 years of simulated hurricane events have been generated and the hurricane wind speed time histories have been developed for every location. For every event, the ROD and maximum surge height can be simulated using the modified two sub-models developed above, and 10,000 years of maximum surge height can be generated. Then the *N*-year maximum surge height for a given location can be developed. For example, a total of 100 point values of the 100-year surge height can be used and then a median surface of the 100-year maximum surge height versus wind speed and ROD can be fitted using a response surface fitting method in MATLAB. The

median-fitted surface of maximum surge height for super cell #2 is shown in Figure 21. If the surface wind speed is being monitored at a particular location during the hurricane or can be estimated using a wind-field model and the ROD value can be calculated using the wind-field model, the next *N*-year maximum expected surge height at this location can be estimated quickly using the median-fitted response surface of the *N*-year maximum surge height for this location.

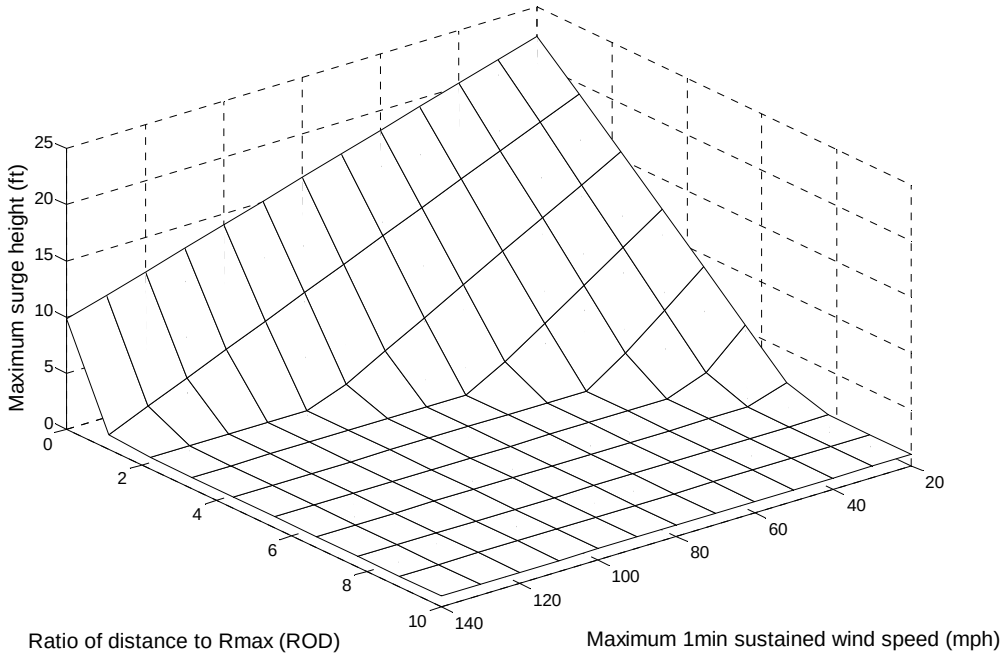

Figure 21: Median-fit response surface of maximum surge height for super cell #2

The wind-surge model developed herein also can be used to characterize the maximum surge height at a given location associated with a certain non-exceedance (NE) probability and reference period (e.g., 2% in 50 years, 10% in 100 years, etc.). Once the *N*-year maximum surge height for a given location is developed using simulation

procedures as described above, the best-fit distribution for the *N*-year maximum surge height can be determined. Three distribution types were considered: Lognormal, Extreme Type-I (ET-I) and Extreme Type-II (ET-II). The Lognormal distribution was found to provide the best-fit (based on regression over the entire distribution) for all three super cells. The NE probabilities of the 50-year and 100-yr maximum surge height for the three super cells are shown in Figures 22, 23 and 24, respectively. Assuming the annual maximum surge heights are independent, the NE probability of the 100-yr maximum surge height can be derived from the NE probability of the 50-year maximum surge height using extreme value theory. The derived NE probability curves of 100-yr maximum surge height also were shown in Figures 22-24 and these compare well with the fitted NE probability curves of 100-yr maximum surge height. This allows one to characterize risk-consistent surge height design values (e.g., 2% in 50 years, 10% in 100 years, etc.) for use in design. The surge heights at two possible target NE probabilities (50% and 80%) for all three super cells are summarized in Table 2. Unlike the wind hazard, which was characterized previously at the zip-code level, the surge hazard is characterized at the much coarser "super cell" level due to the limited available surge data. Therefore, for a given location along the Texas coast, the design value of wind speed would be the value for that zip-code location while the design value of surge height would be the value for the super cell that includes the site. For example, for the location of Galveston Pier 21 (zip code: 77550), the 50-yr MRI hurricane wind speed is 65.2 mph and 50-yr MRI hurricane surge height is 6.5 ft.

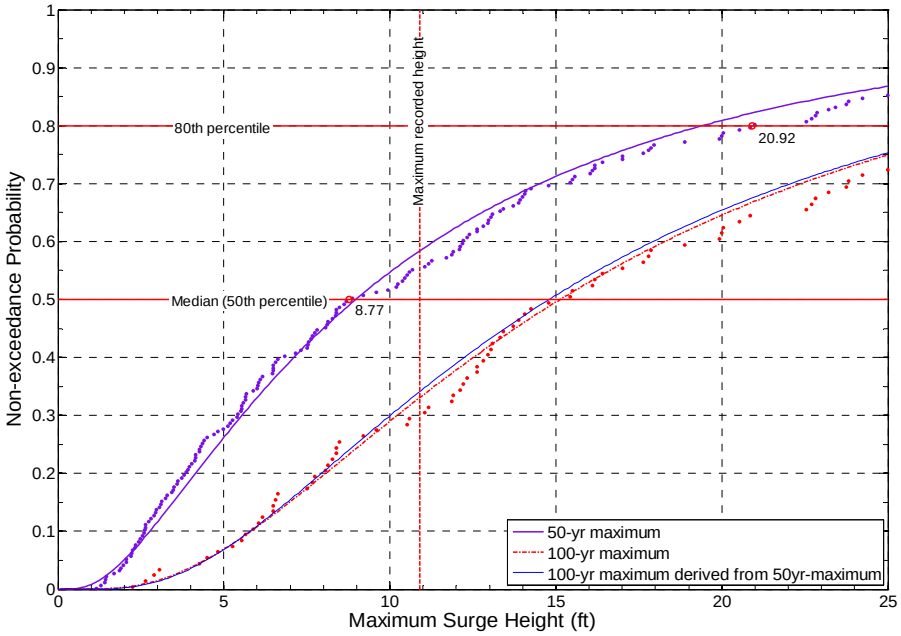

Figure 22: Non-exceedance probability of 50-yr and 100-yr maximum surge height for super cell #1

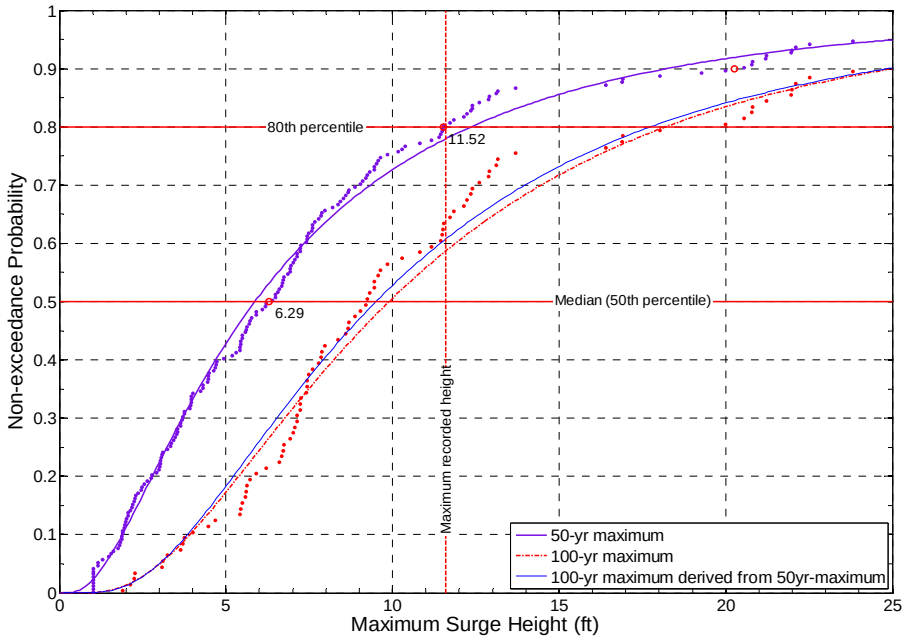

Figure 23: Non-exceedance probability of 50-yr and 100-yr maximum surge height for super cell #2

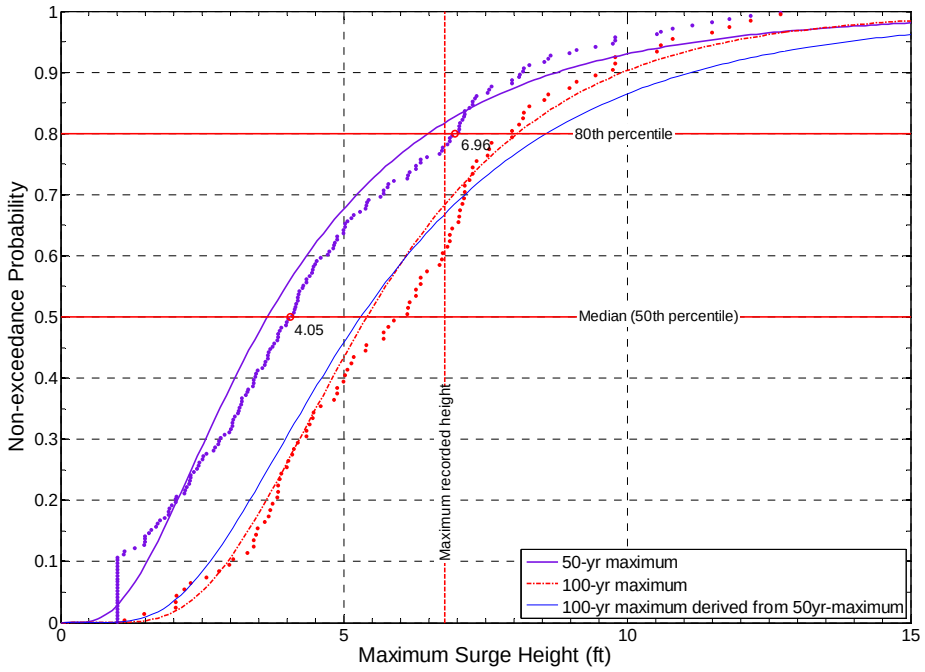

Figure 24: Non-exceedance probability of 50-yr and 100-yr maximum surge height for super cell #3

Table 2: Surge heights at different target non-exceedance probabilities for super cell #1-#3

Hazard Level	Super Cell #1	Super Cell #2	Super Cell #3
Surge height (ft) @ 50% NE probability	9.0	5.9	3.7
Surge height (ft) @ 80% NE probability	19.4	12.4	6.5

Part IV

Preliminary Study on Joint Wind-Surge-Energy Model

Concept of Hurricane Wind Field Energy

Hurricane intensity typically is described in terms of maximum sustained wind speed V_{max} while the "1-5" Saffir-Simpson Hurricane Scale (Simpson, 1974; Saffir, 1975) is most commonly used to express damage potential. Consequently, damage descriptors for hurricane wind and collateral hazards are most commonly related to the maximum wind speed. Some recent studies have suggested that hurricane wind damage is better predicted considering the destructive potential associated with hurricane wind field energy (e.g., Bell et al., 2000; Businger et al., 2001; Emanuel, 2005; Kantha, 2006). Most of these studies focused primarily on maximum hurricane wind speed without taking into account information of the spatial extent of damaging winds. Recognizing the important role that hurricane storm size plays in estimating the spatial extent of damage, Powell and Reinhold (2007) proposed a new method to estimate hurricane wind damage based on Integrated Kinetic Energy (IKE). Specifically, the kinetic energy is integrated over the entire hurricane wind field, thereby directly accounting for the effect of storm size.

As an indicator of the destructive potential associated with wind field energy, the IKE is defined by following equation (Powell and Reinhold, 2007):

$$IKE = \int_V \frac{1}{2} \rho U^2 dV \tag{10}$$

where ρ is the air density = 1 kgm^{-3}, U is the 1-min average surface wind speed and V is the storm domain volume within a certain range above a designated threshold wind speed value. In Powell and Reinhold's calculation, the wind speed and volume elements (dV) are taken from the gridded wind field over a storm-centered 8° latitude domain having grid cells 6km on a side and 1m in the vertical direction. In their calculation, the IKE value for each historical hurricane was estimated from gridded-format operational wind radii listed in graphical products from National Oceanic and Atmospheric Administration (NOAA) Atlantic Oceanographic and Meteorological Laboratory (AOML) Hurricane Wind Analysis System (H*Wind; Powell et al., 1998).

It may be possible to incorporate the hurricane wind field energy concept into the wind-surge model described previously. Using the wind field modeling approach described earlier, the gradient wind speed U is provided explicitly. The volume elements dV are taken from the area elements $dA=rdrd\alpha$ and 1m in the vertical direction (centered at the 3000 meter gradient level). Therefore, the IKE can be expressed in polar coordinates as:

$$IKE = \int_V \frac{1}{2}\rho U^2 dV = \int_0^{360}\int_0^{2\cdot R_{\max}} \frac{1}{2}\cdot\rho\cdot U^2(r,\alpha)\cdot r\cdot dr\cdot d\alpha \qquad (11)$$

where $U(r,\alpha)$ is the gradient-level wind speed expressed as a function of distance r and direction angel α in polar coordinates. The integration range would be 0~2*R_{max} for r and 0~360 degrees for α. The IKE value at each time step (6 hour intervals) for a particular hurricane event can be calculated and used in a proposed wind-surge-energy model as described in the next section.

Joint Wind-Surge-Energy Model

The previous study to develop a simplified wind-surge model utilized monthly-maximum surge height data from 20 near-shore monitoring stations along the Texas and Louisiana coast. Specially, data from 11 hurricanes that made landfall between 1995 and 2005 were considered. Additional data from hurricanes Gustav and Ike, which became available in 2009, also were included.

In the IKE-surge model, the peak surface wind speed (1-minute sustained) in the previous wind-surge model was replaced by the hurricane IKE value. Data pairs describing maximum IKE value and maximum recorded surge height during each of the 13 historical landfalling hurricanes were determined at each monitoring location during the storm. The calculated IKE/measured storm surge data pairs are plotted and shown in Figure 25 (for the station located at Galveston Pier 21, TX). Note that the IKE value is only an indicator of hurricane energy itself and therefore is independent of station location. For comparison, the calculated IKE/measured storm surge data pairs for the station located at SW Pass, LA, also are plotted and shown in Figure 26. Looking at the data pairs plotted in Figure 25, hurricane Ike has the largest IKE value, which means more kinetic energy and thus the largest surge value. However in Figure 26, hurricane Katrina has the largest surge value although it has a lower IKE value (smaller maximum kinetic energy) than hurricane Ike. This demonstrates that, in addition to hurricane intensity and size (maximum kinetic energy), the maximum storm surge height is also related to the relative position of the location of interest to the hurricane eye. The IKE-surge model is very simplistic and does not take into account the relative position of

the location of interest to the strongest part of the storm (the eye-wall region). It would be useful to be able to include this important position information in the model thus enabling better estimates of expected surge height.

As in the previous modified wind-surge model, a new dependant-variable (ratio of distance, ROD) was introduced to create a joint wind-surge energy model, as an improvement to the simpler IKE-surge model. The ROD is defined as the ratio of the distance from a given location to the hurricane eye (R) to the radius of maximum wind speed (R_{max}). This ROD factor (R/R_{max}) therefore accounts for relative position of the recording station to the hurricane eye, the strongest part of the storm. The value of R_{max} is provided by the wind-field model described earlier and provides some indication of the size (spatial extent) of the hurricane wind-field. The distance (R) from a particular location to the hurricane eye can be calculated knowing its latitude and longitude and the value of ROD can therefore be obtained. Three "super cells" of clustered stations (within which coastal topography is assumed to be similar) were defined as before and the updated IKE/ROD/surge data points for the stations within these super cells were then plotted together and analyzed as clusters. The median-fitted surface of maximum surge height versus IKE and ROD for super cells #1, #2 and #3 are shown in Figures 27-29. The IKE/ROD/surge data for each super cell also are shown in these figures.

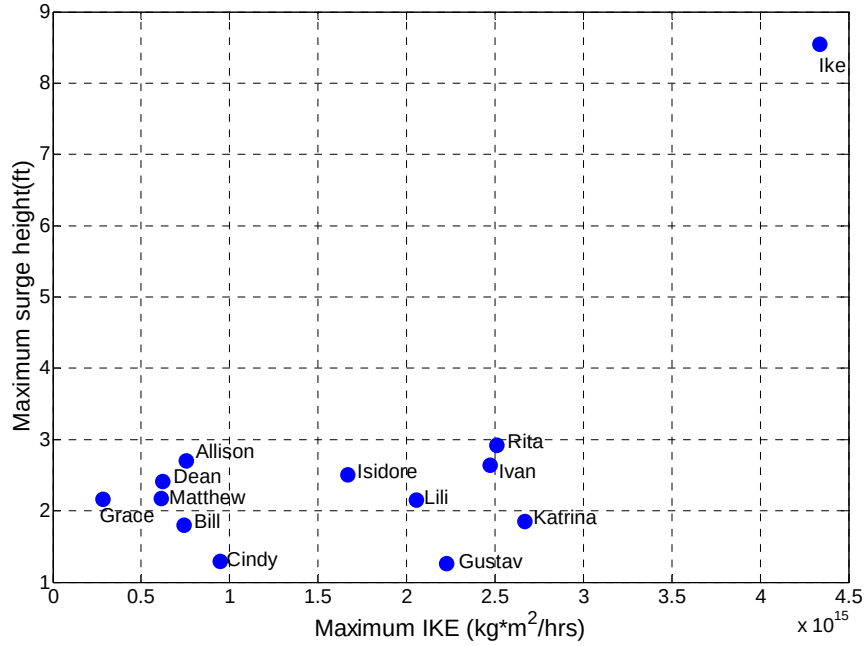

Figure 25: Data pairs of maximum IKE and surge (1995-2008) for Galveston Pier 21, TX

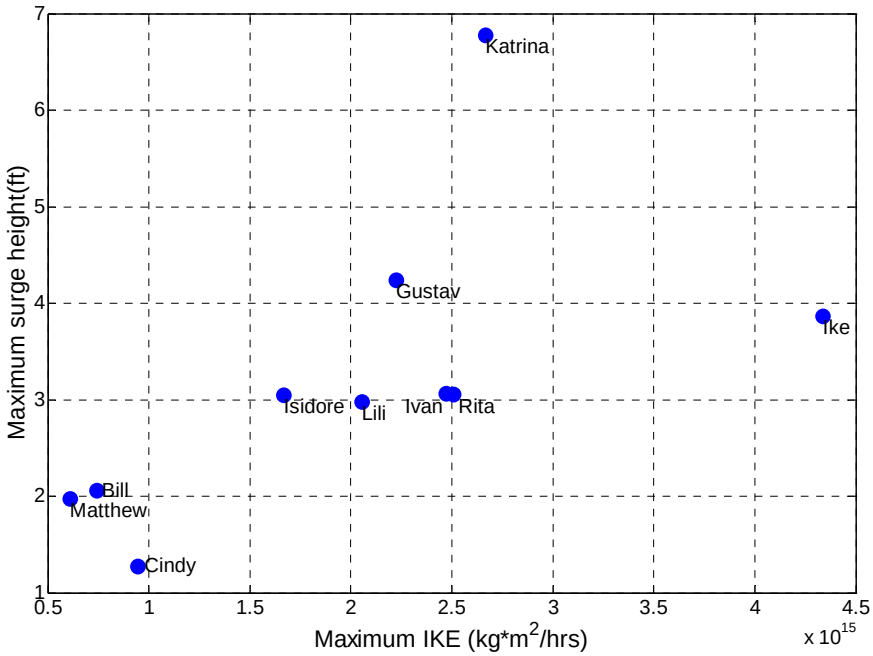

Figure 26: Data pairs of maximum IKE and surge (1995-2008) for SW Pass, LA

One possible application for the joint wind-surge energy model (median-fit) proposed herein is the rapid prediction of maximum surge height expected to be caused by an approaching hurricane. For any given location, if the IKE value of an approaching hurricane can be estimated from available real-time wind field data (e.g., from the National Hurricane Center) or can be calculated using the wind field model, and the ROD value can be determined from the wind field model, the maximum expected surge height at this location can be estimated quickly using the median-fitted response surface of maximum surge height for this location. With additional surge data, it should be possible to statistically characterize the coefficients of the response-surface to generate confidence interval "surfaces" or other statistical bounds on predicted surge values.

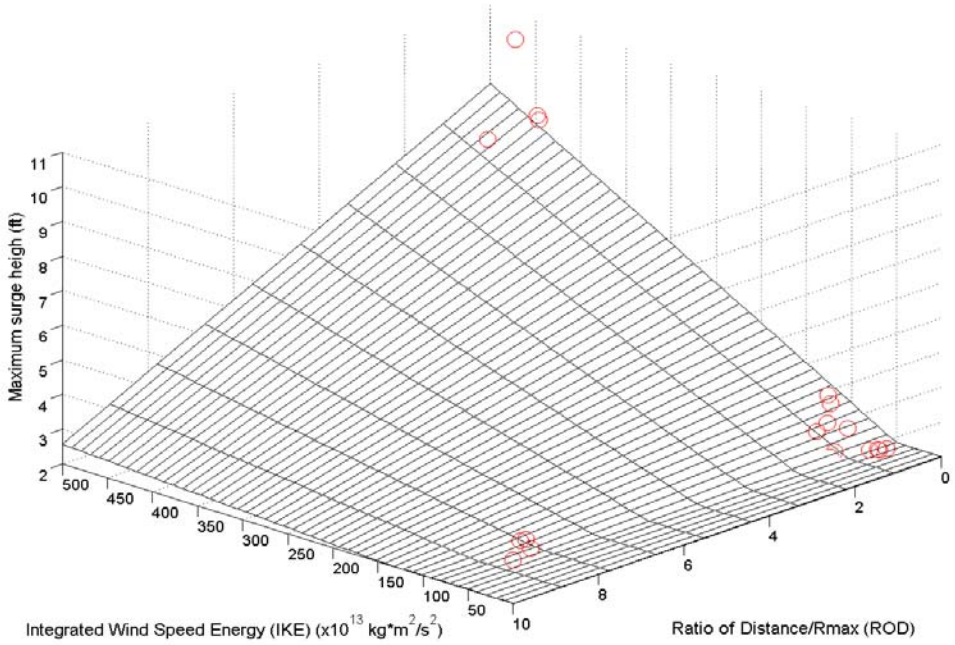

Figure 27: Median-fit response surface of maximum surge height for super cell #1 (Galveston area)

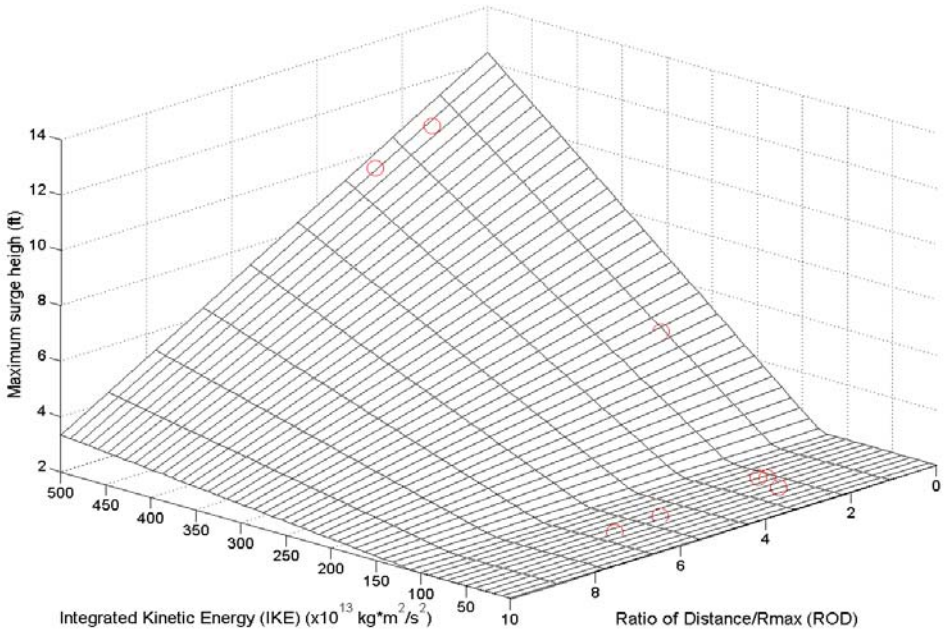

Figure 28: Median-fit response surface of maximum surge height for super cell #2 (TX/LA border area)

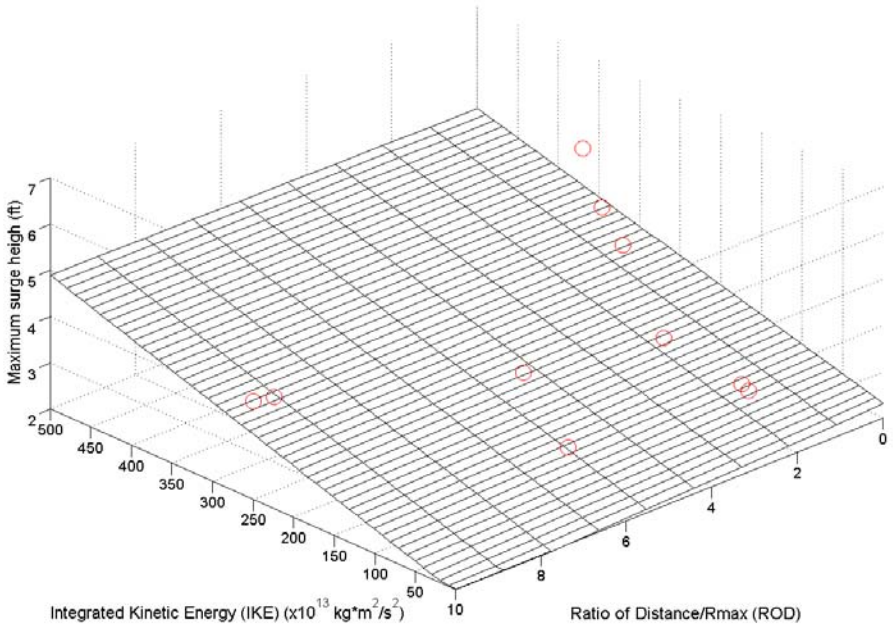

Figure 29: Median-fit response surface of maximum surge height for super cell #3 (SW Pass and Grand Isle area, LA

CHAPTER III

EVENT-BASED HAZARD CHARACTERIZATION FOR HURRICANES ALONG THE TEXAS COAST

Introduction

Typically, the hurricane hazard is described in terms of maximum wind speed V_{max} (i.e., at the eye-wall), since damage descriptors associated with the Saffir-Simpson Hurricane Scale and collateral hazards such as hurricane surge are related most often to maximum wind speed. However, the hurricane storm size (i.e., radius of maximum wind, R_{max}) also plays an important role in describing the hurricane wind field intensity and thus the spatial extent of damage. This may help to explain why hurricane Katrina, which was only a category 3 storm at the time-of-landfall, caused such extensive damage/losses. Prior to hurricane Katrina, few studies addressed storm size when evaluating hurricane damage. Irish et al. (2008) investigated the influence of storm size on hurricane surge for the coastal area around Corpus Christi, TX and showed that both maximum hurricane wind speed and storm size are important factors influencing hurricane surge and hence the damage impact on coastal infrastructure. For a given intensity, they found that storm surge varied by as much as 30% over a range of storm sizes. In order to properly characterize hurricane events for purpose of regional damage estimation and spatial impact analyses, it is therefore necessary to properly model storm size (e.g., R_{max}) as well as intensity. For performance-based engineering application, it would be useful to develop parameter combinations (e.g., V_{max} and R_{max}) that define

"characteristic" risk-consistent hurricane events (e.g., 2%/50 yrs, 10%/50 yrs, 50%/50 yrs). Some recent studies have focused on risk-consistent hurricane hazard characterization and these are described below.

Legg et al. (2010) suggested one way to identify a set of hurricanes to develop hazard-consistent probabilistic scenarios for the state of North Carolina. A set of hurricanes with different return periods was first developed by running HAZUS-MH (FEMA 2003) probabilistic analysis for each county in North Carolina and then recording the maximum gust wind speed for each county. An optimization program was then used to select a reduced set of hurricanes and determine the corresponding risk-consistent annual exceedance probabilities for each hurricane. Once the data pairs of annual exceedance probabilities (or return periods) and the maximum gust wind speeds for each county were generated, the hazard curve (wind speed vs. annual exceedance probability or return period) for a given county was able to be fit. Although this approach successfully characterized the hurricane hazard in a consistent probabilistic manner, the maximum wind speed (i.e., a point-measure of intensity with no spatial descriptor included) was the only hazard metric considered.

Phan and Simiu (2008) proposed a multi-hazard risk assessment approach to develop design criteria for structures subjected to hurricane wind and storm surge. The joint histogram and joint distribution of correlated wind speed/storm surge height was developed for the area around Tampa Bay, FL. This general approach to fitting the joint distribution of two hazard variables (i.e., wind speed and surge height) could also be used to determine the joint distribution of two hurricane variables (e.g., V_{max} and R_{max}).

However, the maximum storm surge was generated by the SLOSH model (Jelesnianski et al., 1992) and generally did not occur at the same time as maximum hurricane wind speed occurred. In the approach suggested by Phan and Simiu, the maximum storm surge and the maximum hurricane wind speed for one event are assumed to occur simultaneously and therefore any design criteria developed using their approach would be conservative.

In this paper, more accurate state-of-the-art hurricane prediction models are introduced to better simulate hazard events. Using the hurricane tracking models developed by Vickery et al. (2000a,b), Lee and Rosowsky (2007) developed a framework for the simulation of hurricane events. Using the Texas coastline as an example, all of the information (intensity, size and direction) needed to describe 10,000 years of hurricane events is completely developed in the synthetic wind speed database developed in part I, Chapter II. Using this information, the dominant variables (e.g., V_{max}, R_{max}, etc.) can be jointly characterized statistically and the characteristic hazard events can be defined.

Proposed Methodology

The approach developed in this study to defining risk-consistent characteristic hurricane events is described in the following four steps. First, the information (intensity, size and direction parameters) for each hurricane at time-of-landfall on the Texas coast is extracted from the 10,000 year synthetic wind speed record (Wang and Rosowsky, 2009) developed using state-of-the-art hurricane wind field and tracking models, and simulation techniques. Specifically, Georgiu's wind field model (Georgiu, 1985) and

Vickery's tracking model (Vickery et al., 2000a,b) are used herein and a set of simulated hurricane events are generated (Wang and Rosowsky, 2009). Hurricane information (descriptors) from the closest time (6-hour interval) prior to landfall are used. It would be a simple matter to decay the hurricane as a function of distance travelled inland using an appropriate decay model. The focus here is on characterizing (probabilistically) the hurricane at landfall only. Georgiu's and Vickery's models and simulation procedure are described in the Chapter II, part I.

Second, the critical parameters to fully describe the hurricanes are selected. State-of-the-art parametric hurricane wind field models such as the one used to create the 10,000 year synthetic hurricane wind speed database include multiple event parameters. However, the work by Vickery et al. (2000) reveals that the maximum wind speed V_{max} (i.e., at the eye-wall), and radius of maximum wind, R_{max}, are the two key parameters describing the hurricane wind field and therefore only these two critical parameters are considered in this study. With these two parameters, the vortex shape of gradient wind-field is fully defined as will be explained in a later section.

Third, the joint histogram of selected variables is constructed. Specifically, the histogram of V_{max} and R_{max} is generated for hurricane events simulated to make landfall along the Texas coast. Note that, other than the previous work by Phan and Simiu (2008) in which the maximum wind speed and corresponding maximum surge height generated by the SLOSH model (Jelesnianski et al., 1992) may not occur simultaneously, each data pair of V_{max} and R_{max} is presumed simultaneous herein. Once the joint histogram is generated, the joint exceedance probability "surface" of V_{max} and R_{max} can be developed.

The annual exceedance probability of each variable can then be determined knowing the mean annual occurrence rate. The marginal distributions of V_{max} and R_{max} also can be fitted separately for the landfalling hurricane events.

Fourth and finally, characteristic events are selected/identified. Once the joint annual exceedance probability of V_{max} and R_{max} is known, the corresponding Mean Recurrence Interval (MRI) and hazard curve (contour loop) for a given annual exceedance probability m in Y years (e.g., 2%/50 yrs) can be generated. Risk-consistent high (2%/50 yrs), medium (10%/50 yrs) and low (50%/50 yrs) events can then be defined by selecting the desired V_{max} and R_{max} combinations.

Probabilistic Description of Bivariate Hurricane Event

In Chapter II, part I, a total of 10,000 years of simulated hurricane events were generated using state-of-the-art hurricane wind-field and tracking models. Then, the time histories of hurricane wind speed and radius of maximum wind speed can be recorded to develop the joint histogram and estimate the probability of exceedance and mean recurrence interval of the joint events. A "cluster" of risk-consistent hazard events can thereby be defined by selecting the appropriate combinations of V_{max} and R_{max}.

In total, 4776 hurricanes during a period of 10,000 years were simulated along the Texas coast, which is assumed to have more or less equal event strike probability along its length, and the data pairs of V_{max} and R_{max} at time-of-landfall for each simulated hurricane were recorded. The equiprobably assumption is validated by looking at the landfalling positions for the simulated hurricane events. These are shown for simulation periods of 100, 1000 and 10,000 years in Figures 30(a)-(c), respectively. Paired value of

V_{max} and R_{max} are assumed to occur simultaneously. The 4776 data pairs were generated and a joint histogram was constructed as shown in Figure 31. As indicated in Figure 31, the Texas coast would be most frequently influenced by events with V_{max} of 50-100 mph and R_{max} of 20-40 miles at the time-of-landfall, which is normally within the range of tropical storm to hurricane category 2 according to the Saffir–Simpson Hurricane Scale.

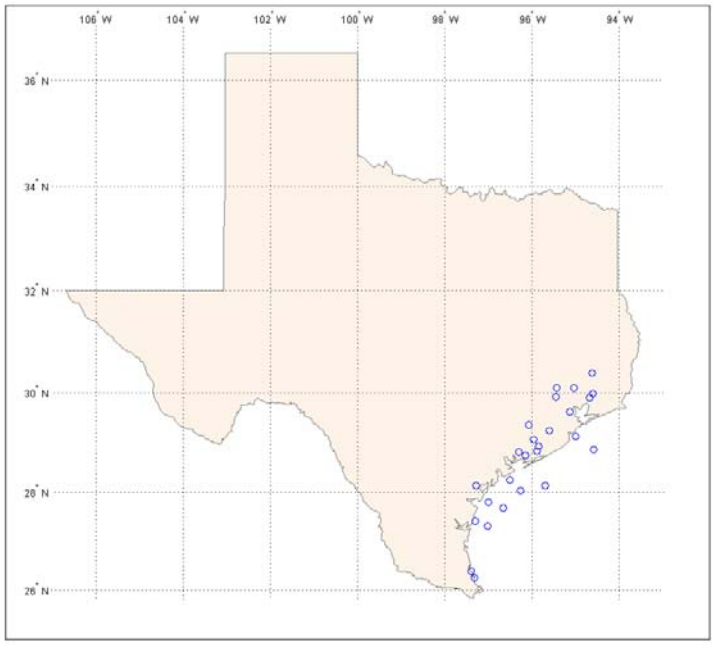

Figure 30(a): Landfalling positions during 100 years period

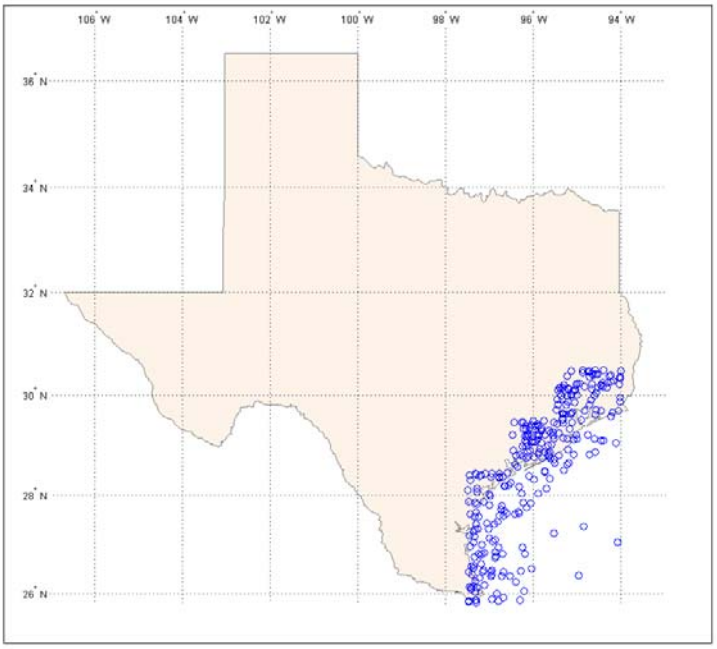

Figure 30(b): Landfalling positions during 1000 years period

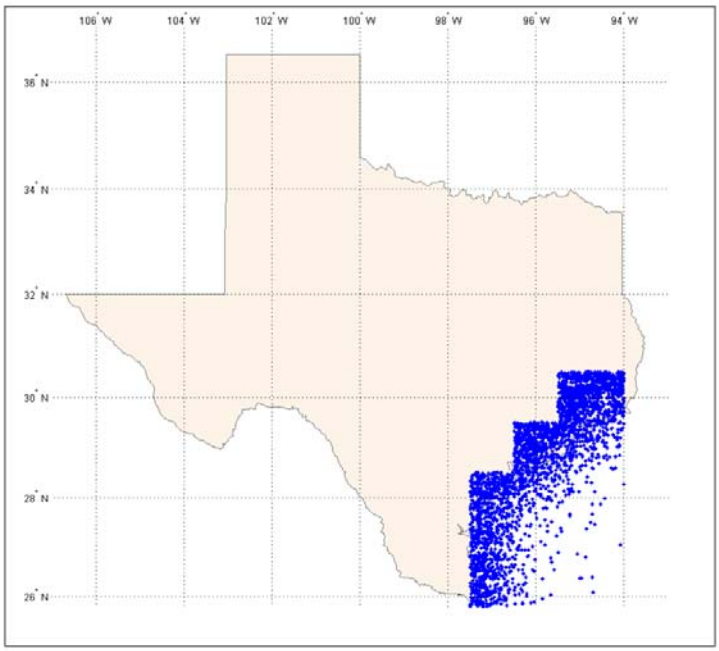

Figure 30(c): Landfalling positions during 10,000 years period

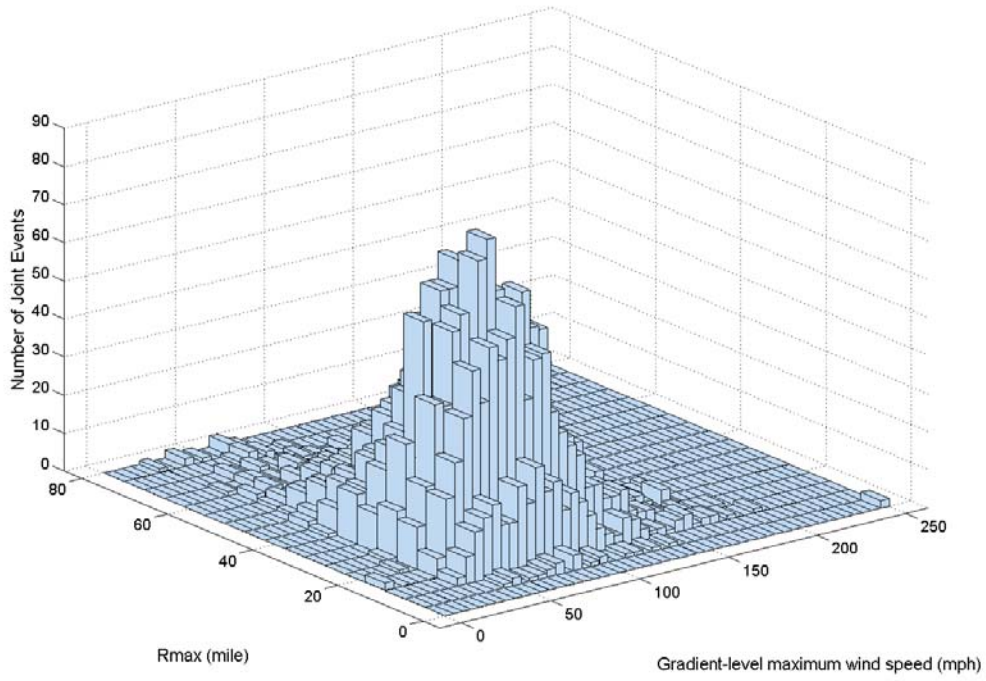

Figure 31: Joint histogram of V_{max} and R_{max}

From the histogram in Figure 31 (or its frequency-normalized equivalent joint PDF), the joint exceedance probability of V_{max} and R_{max}, denoted by $P(V_{max}>v, R_{max}>r)$, can be determined. Using the joint histogram (Figure 31), the number of data pairs having maximum wind speeds greater than v and radius of maximum wind speed greater than r would be divided by the total number n of data pairs (4776 here). Multiplying the joint exceedance probability by the mean annual hurricane rate of occurrence λ (λ = 4776/10000 = 0.4776 per year), one obtains the joint annual exceedance probability of V_{max} and R_{max}. This is shown in Figure 32.

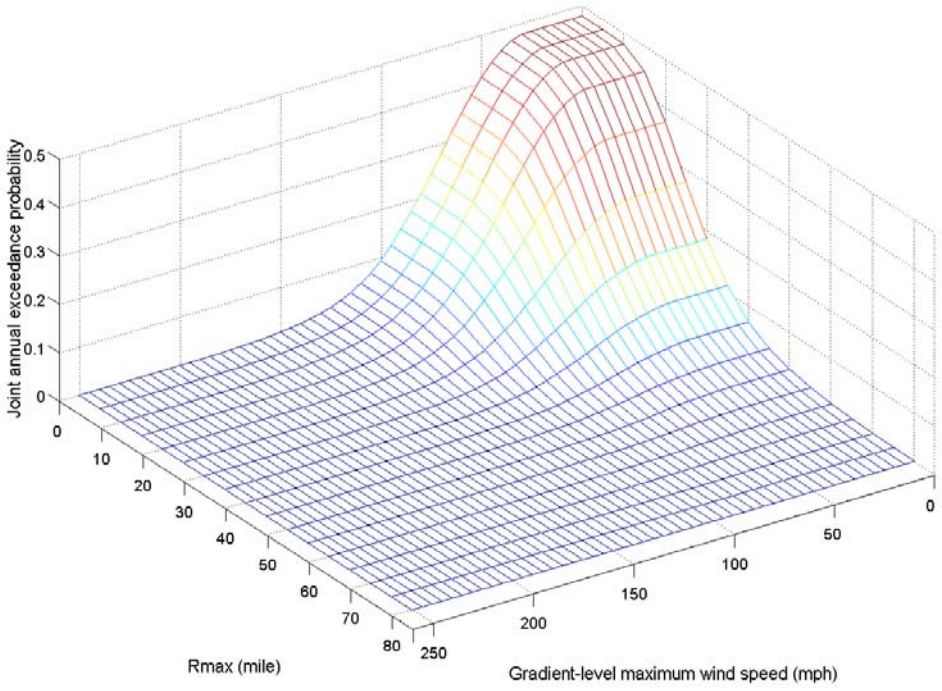

Figure 32: Joint annual exceedance probability of V_{max} and R_{max}

The marginal cumulative distribution functions (CDFs) for maximum wind speed (V_{max}) and for radius of maximum wind speed (R_{max}) also can be constructed using the synthetic records of V_{max} and R_{max} at the time-of-landfall, as shown in Figures 33 and 34, respectively. As shown in these figures, the Lognormal distribution provides an excellent fit to these marginal distributions.

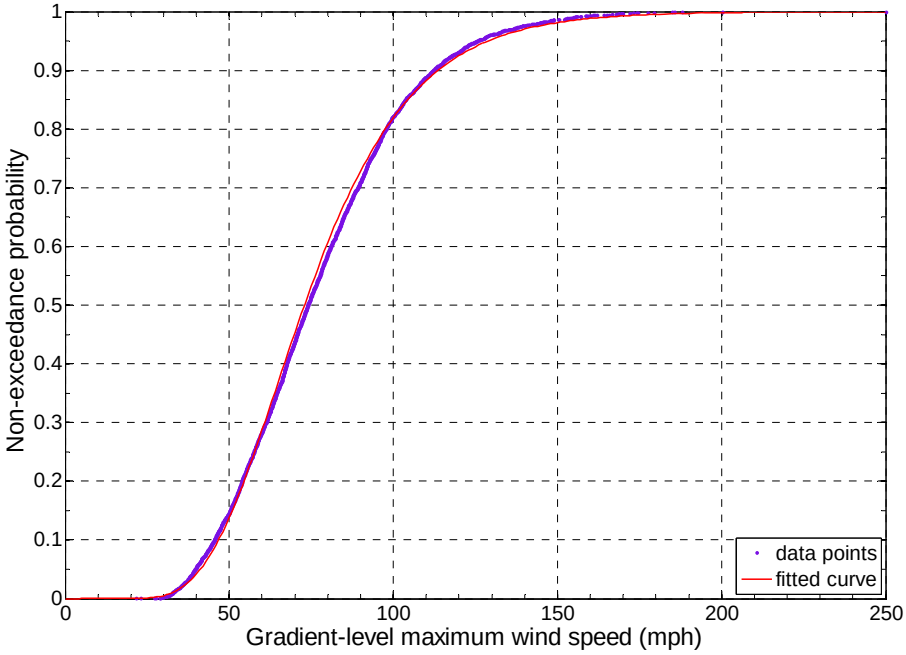

Figure 33: Marginal CDF for the gradient-level maximum wind speed V_{max}

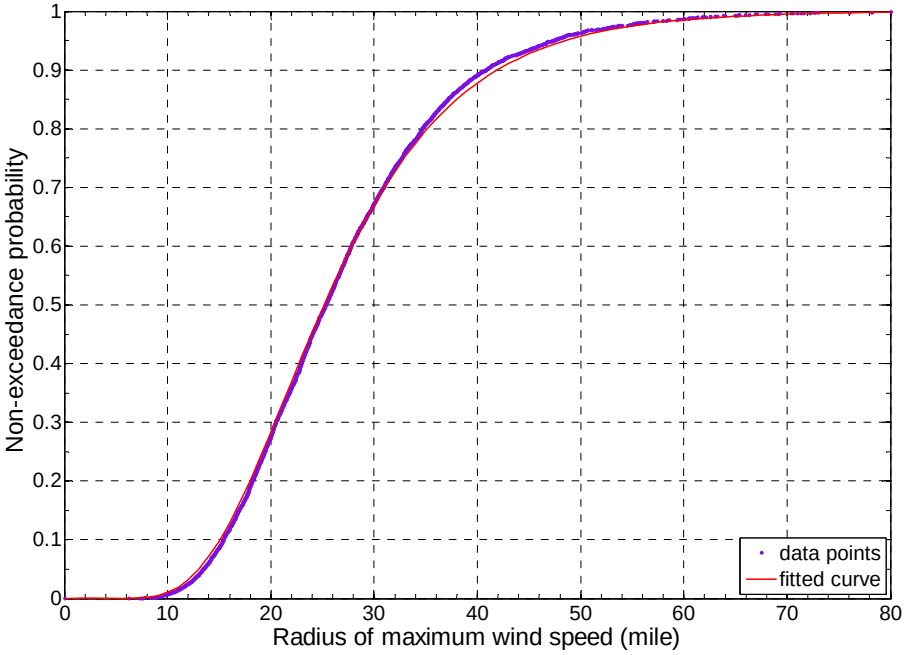

Figure 34: Marginal CDF for the radius of maximum wind speed R_{max}

Once the joint annual exceedance probability of V_{max} and R_{max} is developed, as shown in Figure 32, the contours of different hazard levels with given annual exceedance probabilities can be generated. Data pairs of V_{max} and R_{max} on (or near) the same contour have the same joint annual exceedance probability. The smoothed contour bands of bivariate annual exceedance probabilities corresponding to 0.04%, 0.2%, 1%, 1.4%, 2%, 5% and 10% are shown in Figure 35. The simulated V_{max} and R_{max} data points also are shown on this figure, indicating the density of data points (simulated land-falling hurricane events) in bivariate space. On Figure 36, the data pairs of actual historical hurricanes (dating back to 1851), tropical depressions and tropical storms, that made landfall along the Texas coast are also shown. This allows one to define the approximate hazard level of historical events. For design purposes, the hazard level is normally described as an exceedance probability in Y years (e.g., 2%/50 years). Table 3 presents hazard levels and corresponding values of annual exceedance probability and MRI (in years), where annual exceedance probability = 1/MRI and probability of exceedance (i.e., m% in Y years) given by MRI = $\frac{-Y}{\ln(1-m\%)}$. The MRI values for corresponding values of V_{max} and R_{max} are listed in Table 4. Note that this is simply another way to present the contours in Figure 35 and 36.

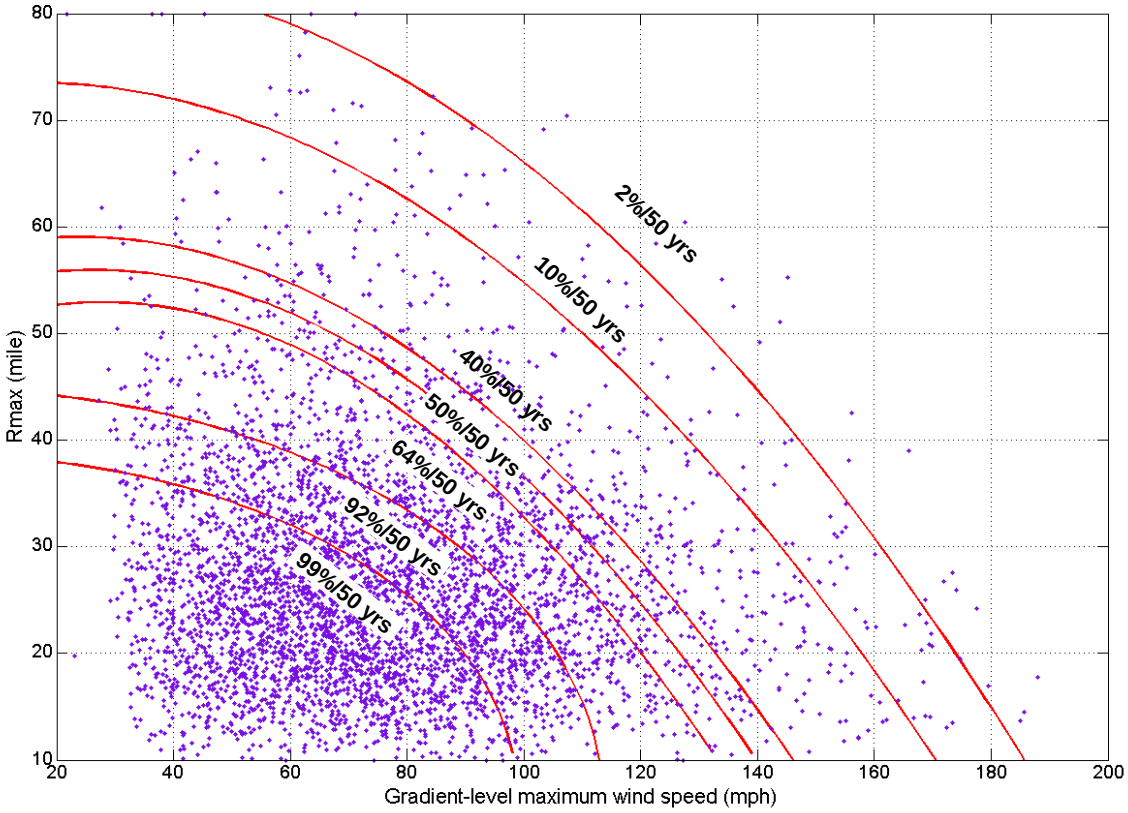

Figure 35: Hazard level contours

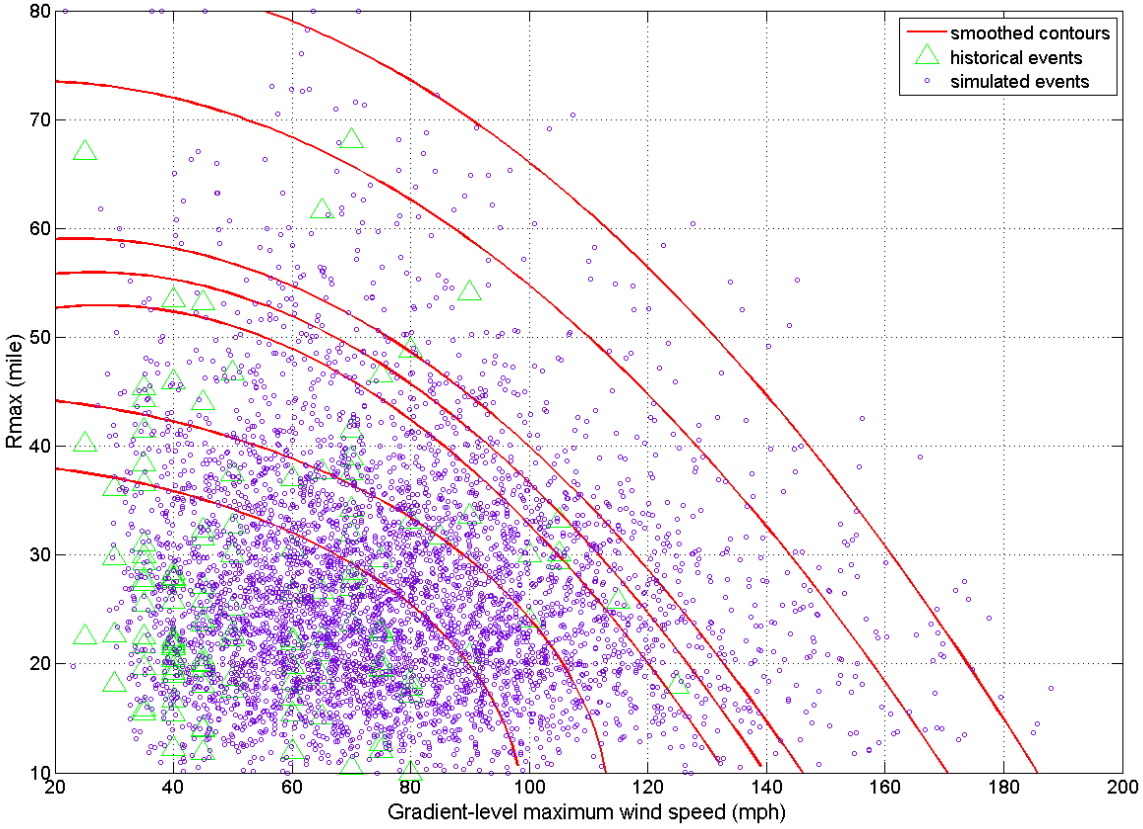

Figure 36: Hazard level contours showing both historical and simulated events

Table 3: Hazard levels and corresponding annual exceedance probabilities and MRI value

Hazard Level	Annual Probability of Exceedance (%)	MRI (years)
99%/50 yrs	10	10
92%/50 yrs	5	20
64%/50 yrs	2	50
50%/50 yrs	1.4	71
40%/50 yrs	1	100
10%/50 yrs	0.2	475
2%/50 yrs	0.04	2475

Table 4: Mean recurrence intervals for combinations of V_{max} and R_{max}. (Note: Inf = greater than 10,000 years)

V_{max} (mph)	R_{max} (mile)											
	20	25	30	35	40	45	50	55	60	65	70	75
75	5	8	12	20	36	59	105	182	333	625	1428	9996
80	6	9	13	23	43	71	132	227	416	714	1666	9996
85	7	11	16	28	53	88	167	286	500	909	2499	9996
90	9	13	20	35	68	112	208	400	625	1249	3332	Inf
95	11	16	25	46	93	156	256	526	909	2499	4998	Inf
100	14	21	33	61	123	208	345	625	1249	4998	4998	Inf
105	18	26	43	80	154	270	400	714	1666	4998	4998	Inf
110	23	32	53	104	192	333	526	833	2499	Inf	Inf	Inf
120	30	44	72	132	227	400	625	1111	4998	Inf	Inf	Inf
125	40	57	99	185	286	526	909	1428	4998	Inf	Inf	Inf
130	54	77	128	256	384	769	1249	1999	4998	Inf	Inf	Inf
135	69	105	175	322	476	1000	1666	2499	9996	Inf	Inf	Inf
140	90	139	250	500	714	1249	1999	3332	Inf	Inf	Inf	Inf
145	115	182	357	714	1000	2499	3332	9996	Inf	Inf	Inf	Inf
150	149	232	454	1000	1249	3332	4998	9996	Inf	Inf	Inf	Inf
155	208	357	769	2499	3332	9996	Inf	Inf	Inf	Inf	Inf	Inf
160	278	476	833	2499	3332	9996	Inf	Inf	Inf	Inf	Inf	Inf
165	555	1249	4998	9996	9996	Inf	Inf	Inf	Inf	Inf	Inf	Inf
170	714	1428	9996	9996	9996	Inf	Inf	Inf	Inf	Inf	Inf	Inf
175	833	1666	Inf	Inf	Inf	Inf	Inf	Inf	Inf	Inf	Inf	Inf

The information in Figure 35 or 36 or Table 4 can be used for regional loss estimation studies or other spatial risk analyses. The contour bands in Figure 35 can be used to select the desired combination of V_{max} and R_{max} corresponding to a given hazard level. For example, for the 10%/50 yrs hazard level, four combinations of V_{max} and R_{max} can be selected as (80, 63), (100, 55), (120, 45) and (140, 34). After the selection of desired combinations, a suite of risk-consistent candidate hurricanes can then be generated using Eq.(3)-Eq.(5) knowing the selected V_{max}, R_{max} and translational wind speed V_T of each candidate hurricane. Once the wind fields of these candidate hurricanes are developed, it is possible to estimate the total spatial damage losses of structures within the hurricane influencing area subjected to given hurricane hazard level and other subsequently induced hazards (e.g. surge or coastal flooding) by coupling with appropriate damage (loss) model. Thus, for each target location, once the losses resulting from each candidate hurricane corresponding to a certain hazard level (e.g., 2%/50yrs) are estimated using a damage model, a risk-based distribution of losses can be determined. Similarly, risk-consistent candidate hurricanes can be selected from Table 4 on the basis of MRI values rather than hazard level. However, Figure 35 and 36 are hazard level contours derived from all simulated hurricane events along entire Texas coast, which could not be used to specify the candidate hurricanes considering possible hurricane landfalling positions. Similar as the concept in the modified wind-surge model described in Chapter II, ROD can be introduced as a new random variable. A new axis of ROD can be added on to Figure 35 and 36 and the 3D surface of joint distribution of V_{max}, R_{max} and ROD can be generated for given location, which can be used to specify

the risk-consistent candidate hurricanes with information of the relative position of target location to the possible hurricane landfalling point.

Summary

A methodology to develop hazard-specific/risk-consistent characteristic hurricane events for regional loss estimation and other spatial risk analyses was presented, using the Texas coastline as a study region. Unlike previous studies, in which hurricane hazard level is related only to maximum wind speed, another critical parameter, radius of maximum wind speed, was introduced. Thus, the hurricane hazard definition explicitly takes into account both wind field intensity and spatial extent. Data pairs for V_{max} and R_{max} were extracted from a database of synthetic hurricanes making landfall on the Texas coast and the joint histogram was constructed. These joint descriptors (variables) were statistically characterized and characteristic hazard events corresponding to designated hazard levels were identified (i.e., combinations of V_{max} and R_{max}). The proposed methodology for event-based hurricane hazard characterization, when coupled with a hurricane damage model, can be used for regional loss estimation and other spatial impacts analyses. The proposed approach also can be used to develop characteristic hazard definitions for use in performance-based engineering applications.

CHAPTER IV

CREATING A RISK-CONSISTENT FRAMEWORK FOR DISPLACEMENT-BASED SEISMIC DESIGN OF ENGINEERED WOOD STRUCTURES*

Introduction

Wood-frame structures are the most common type of residential and light commercial buildings in North America. Besides the gravity loads, wood-frame structures built in regions of moderate and high seismicity must also be designed to resist earthquake loading. Using current force-based seismic design (FBD) procedures, such as those in the current International Building Code (International Code Council, 2006) and seismic design provisions of the ASCE 7 (2005), wood-frame buildings are currently designed to meet only one performance requirement, life safety. However, while casualties were low in recent severe earthquakes (e.g. Loma Prieta in 1989 and Northridge in 1994), the economic losses and social impact were substantial, largely due to extensive building damage. Thus, there has been a trend toward considering both life safety and damage limitation in evolving performance-based design procedures. Recent experimental studies have shown a correlation between displacement/drift and damage (Fischer, 2001; van de Lindt and Liu, 2006), and therefore inter-story drift is typically

---

*Note: Part of this Chapter is reprinted with permission from "Toward a Performance-Based Procedure for Direct Displacement Design of Engineered Wood-Frame Structures." by Yue Wang, David Rosowsky and Weichiang Pang, 2010, *Journal of Structural Engineering*, ASCE, to be published, Copyright [2010] by the American Society of Civil Engineers.

used as a rational metric for damage limitation. In order to meet multiple performance requirements, e.g., immediate occupancy, life safety and collapse prevention, the philosophy of performance-based seismic design (PBSD) has evolved with the intent of allowing engineers to specify performance expectations (drift limits) at different hazard levels.

Although existing FBD procedures are easy to use in design, there are many shortcomings/limitations in their application to wood-frame structures. These shortcomings, as identified by others (Filiatrault and Folz, 2002; Pang and Rosowsky, 2009) and discussed in a recent workshop on performance-based design of wood-frame structures (van de Lindt, 2006) are: (1) the use of an empirical equation to estimate a single elastic period to design mid-rise wood-frame structures is inappropriate since the force-displacement response of wood buildings is highly nonlinear; (2) the values of response modification factors (commonly known as the force reduction factor or R) assigned to the wood-frame systems are based primarily on experts' judgment and lack rigorous analytical basis; (3) story drift and stiffness are not directly addressed in FBD procedures, and therefore inter-story drift can not be properly assessed from the base shear obtained at the global level; and (4) the FBD procedure is a single-objective design procedure which focuses on achieving a target safety level (margin against collapse) for rare and severe earthquakes and, as such, does not ensure the structures meet other performance requirements (e.g., damage limitation under moderate earthquakes). In FBD, the equivalent static loads applied to wood-frame structures are planar loads and only a one dimensional wall line is designed at a time. Unlike FBD, a complete PBSD requires

modeling the entire structure and performing dynamic nonlinear time-history analyses (NLTHA) using suites of ground motions to determine displacement responses at different seismic hazard levels (e.g., Camelo et al., 2001; Pardoen et al., 2003; Filiatrault et al., 2007; Ellingwood et al., 2008). To be useful as a design tool, the PBSD design procedure should not require the engineer to perform fully dynamic modeling and analysis. One procedure, called displacement-based design, was originally proposed by Priestley (1998) and later adapted by Filiatrault and Folz (2002) for wood-frame structures. This design procedure was applied to a two-story wood-frame structure (Filiatrault et al., 2006) using nonlinear pushover analysis and estimating equivalent viscous damping at a target drift limit. More recently, Pang and Rosowsky (2009) developed a multi-objective direct displacement-based design (DDD) procedure for multistory wood-frame structures which allows the engineer to estimate the inter-story drift in multistory wood-frame structures without having to perform dynamic analyses. A simplified (spreadsheet-based) version of the DDD procedure (Pang et al., 2009) was used to design the six-story NEESWood Capstone Building. In order to design for additional performance requirements and non-exceedance (NE) probabilities other than 50% (median), an adjustment factor C_{NE} was introduced. This factor must be determined such that the structures designed using this procedure meet performance expectations in terms of both drifts and NE probabilities.

This paper presents the results from a study to determine the NE probability adjustment factors (C_{NE}) for different target NE probabilities and performance requirements (hazard levels/drift limits) for a portfolio of mid-rise wood-frame

structures. Selected ATC-63 multistory wood-frame structure archetypes (Applied Technology Council, 2008) were considered and re-designed using the simplified DDD procedure with different values of adjustment factor C_{NE}. NLTHA were performed on both the DDD and FBD structures using 22 bi-axial far-field ground motion records (also obtained from the ATC-63 project), and performance comparisons were made between the DDD and FBD structures. Finally, design charts were constructed which can be used to select the appropriate adjustment factor C_{NE} for use in the simplified DDD procedure.

Wood-Frame Archetype Buildings: Design Summary

A suite of archetype buildings was identified and analyzed herein to determine probability-based adjustment factors (C_{NE}). Two classes of multistory structures were considered, (1) multi-unit residential, and (2) commercial. The structural variables were assumed to include the number of stories, story height, wood shear wall pier aspect ratio (height/width), and presence of interior nonstructural (gypsum) walls. A total of 16 archetype buildings were found to be sufficient to represent the ranges of these structure-related design parameters and seismic hazard categories (high/low). In this study, only 3-5 story structures were considered and therefore only eight of the 16 ATC-63 archetypes (Applied Technology Council, 2008) were examined. These archetype buildings and the building elevations are shown in Figure 37. The multi-unit residential building plan dimensions are 12.2 m × 7.6 m (40 ft. × 25 ft.) and the commercial building plan dimensions are 12.2 m × 24.4 m (40 ft. × 80 ft). The story clear height is taken as 3.1 m (10 ft.) for all archetype buildings. The unit floor weight

for the archetype buildings is 1.44 kN/m^2 (30 lb/ft^2). Shear wall aspect ratios range from high (height/width ratios greater than 1.5) for commercial structures to low (height/width ratios of 1.5 or less) for residential structures. The maximum and minimum values of the short-period design spectral acceleration S_{DS} considered in the ATC-63 study were 1.00g and 0.5g. Specifically, high seismic hazard was defined by a value of S_{DS} = 1.00g (e.g., Southern California) while low seismic hazard was defined by a value of S_{DS} = 0.5g (e.g., the mid-America region). Both high and low seismic hazard categories were considered in selecting the representative archetype structures. The archetype structures with high pier length ratios (e.g., more shear wall piers), defined as the ratio of total length of sheathing piers to the total building length, for each of three building heights (3, 4 and 5 stories), reflect structures designed for high seismic hazard. Table 5 summarizes the properties of the eight design archetype structures considered herein. Using the simplified DDD procedure described later in this paper, the structures are re-designed for both high and low seismic hazard regions assuming the same shear wall pier configuration as the archetype FBD structures. For the high seismic hazard region designs, all buildings are assumed to be located in Southern California on soil class D and the design spectral acceleration is taken as 1.00g. For the low seismic hazard region, all buildings are assumed to be located in mid-America on soil class D and the short-period spectral acceleration parameter S_{DS} is taken as 0.50g. In the NLTHA, the corresponding short-period spectral accelerations for the Level 3 Maximum Considered Earthquake (MCE) S_{MS} in the high and low seismic hazard regions are 1.50g and 0.75g, respectively.

Table 5: Index building (archetype structure) configurations

Model	ATC-63 Model	Seismic Hazard S_{DS} (g)	Stories	Shear Wall Aspect Ratio	Type
1	Archetype 9	1	3	Low	Commercial
2	Archetype 11	0.50	3	Low	Commercial
3	Archetype 10	1	3	High	Multi-Family
4	Archetype 12	0.50	3	High	Multi-Family
5	Archetype 13	1	4	High	Multi-Family
6	Archetype 14	0.50	4	High	Multi-Family
7	Archetype 15	1	5	High	Multi-Family
8	Archetype 16	0.50	5	High	Multi-Family

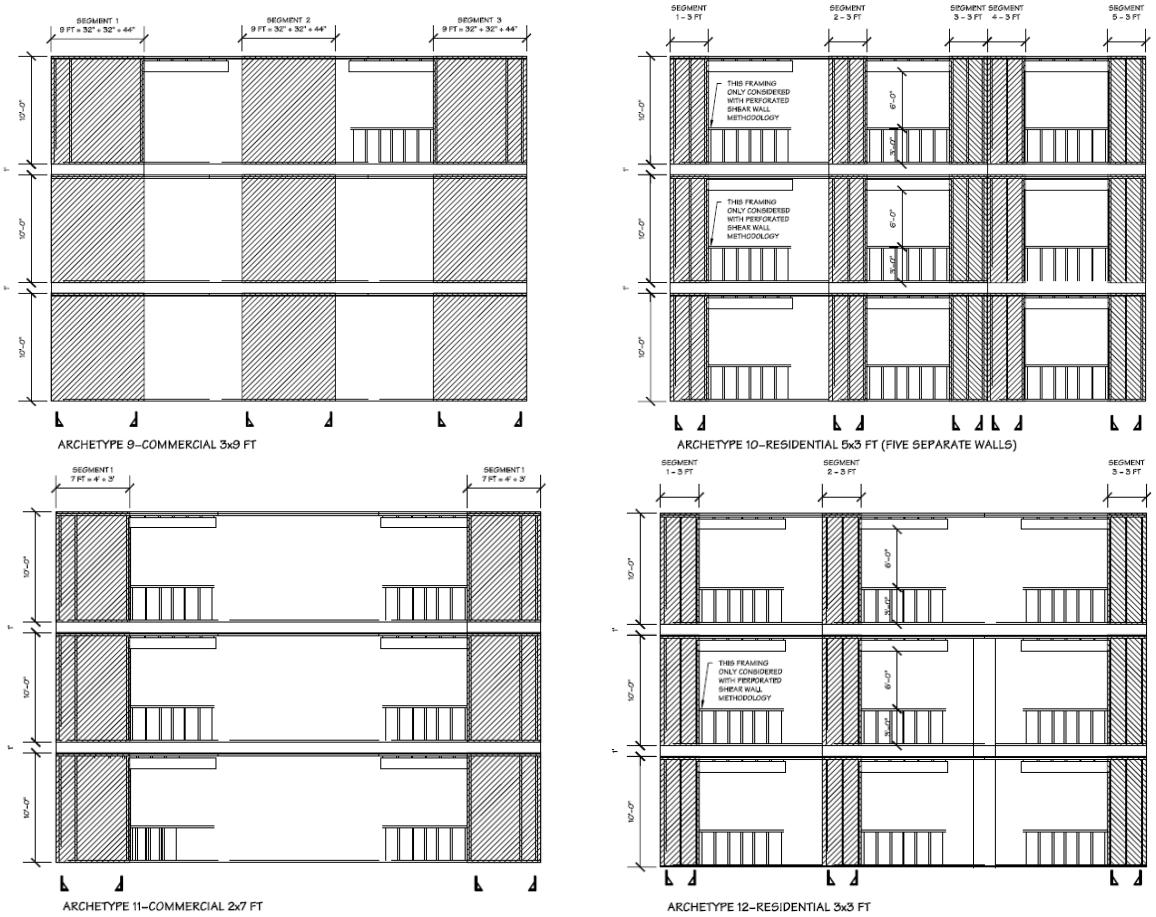

Figure 37 (a): Elevation of the design archetype structures

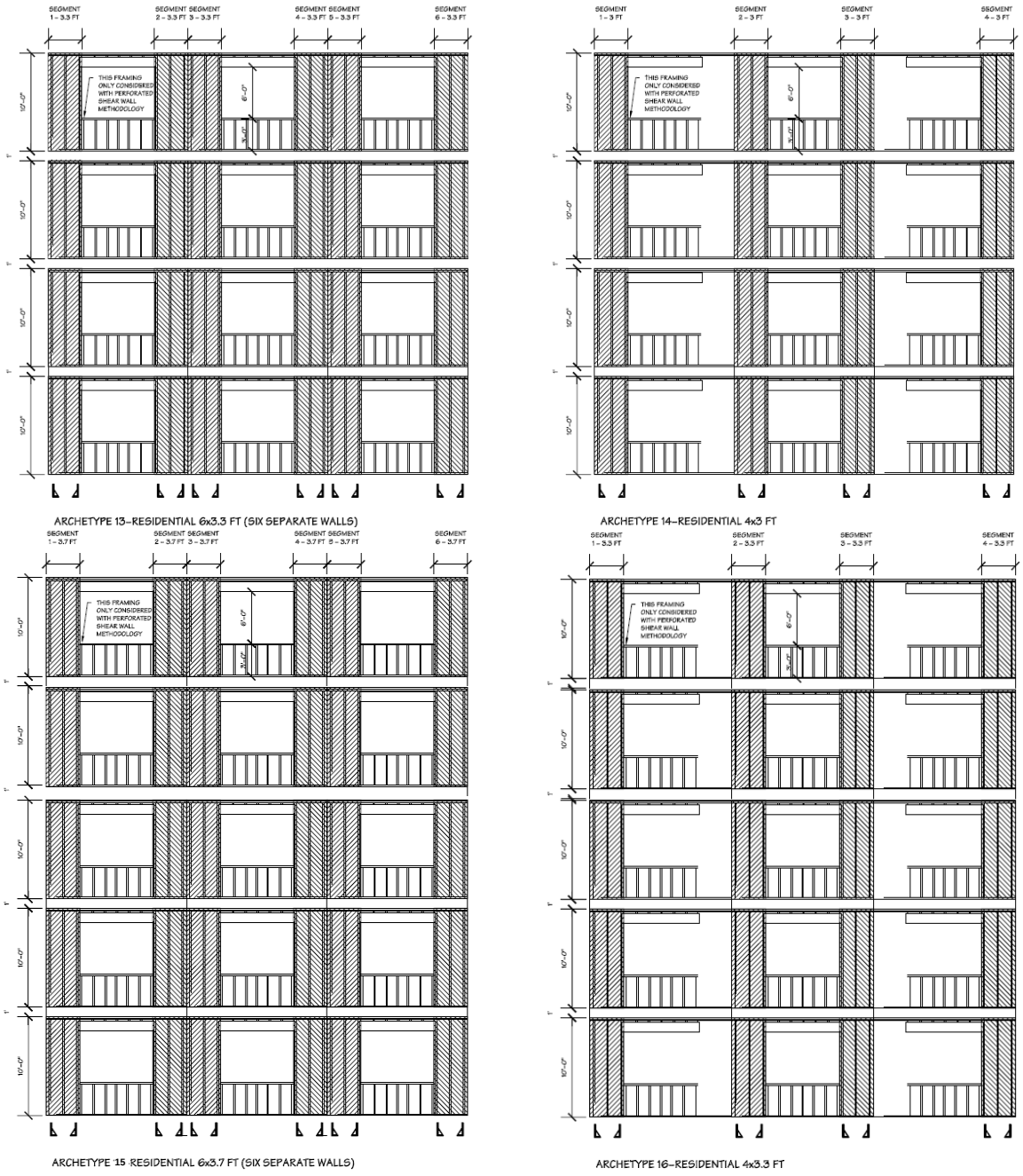

Figure 37 (b): Elevation of the design archetype structures (continued)

It should be noted that while only the shear wall nailing schedules are designed in this study using the DDD procedure, selection of hold-down or tie-down systems also

is part of the seismic design for wood-frame structures. However, no single design procedure can address the design requirements of all subassemblies (roof trusses, diaphragms, etc.) in wood-frame structures. Note that the proposed DDD procedure assumes that other components or subassemblies including the tie-down systems are properly designed. The inter-story shear values obtained from DDD procedure can be used to estimate the uplift forces required for tie-down design. The effects of uplift and second-order moment (P-delta) on shear wall performance are subjects worthy of further investigation and should be addressed in subsequent studies.

The shear walls are assumed to be constructed as follows: 3.1 m (10ft.) height sheathing panels attached to the framing members vertically with 11.1 mm (7/16 in.) thick oriented strandboard (OSB) attached with the 3.3 mm (0.131 in.) (8d common) nails, or 15.1 mm (19/32 in.) thick plywood (PLY) attached with 3.7 mm (0.148 in.) (10d common) nails at 51, 76, 102 or 152 mm (2, 3, 4 or 6 in.) edge spacing and 305 mm (12 in.) interior spacing; and 12.7 mm (1/2 in.) thick gypsum wallboard (GWB) attached using #6 drywall screws at 406 mm (16 in.) on-center. The shear wall backbone curves were obtained by nonlinear push-over analysis using the CASHEW program (Folz and Filiatrault, 2001), and the resulting backbone curves were normalized by dividing by the maximum force F_u in the backbone curve. The normalized backbone curves are shown in Figure 38, from which the design backbone force at different drift levels can be easily obtained. Finally, the design shear wall database was developed in terms of expected design inter-story drift and normalized required story shear force. This database is shown in Table 6. Note that the analytical results shown in Figure 38 certainly suggest a single

normalized backbone curve could be estimated and used to further simplify the design process. In this paper, the design inter-story drift limit is taken as 4% and therefore the shear wall backbone forces are found in the "4% drift" column. The 4% drift limit was based on the shake table test results of a full-scale two-story wood frame building where a maximum inter-story drift of 3.5% was recorded under a MCE ground motion (Christovasilis et al. 2007). The test building did not exhibit any visible sign of incipient collapse at 3.5% drift. Therefore, a higher drift limit (i.e., 4%) was selected as the design drift at the MCE level. In generating this design shear wall database, only the exterior sheathing panel was considered; i.e., the presence of GWB on the interior of the shear wall was not considered when modeling the walls. Information from the design shear wall database for the 3.1m (10ft) clear height walls was used as input to the DDD procedure described later in this paper to design the archetype structures.

Table 6: Shear wall database for 4 ft. × 10 ft. walls

4 ft. × 10 ft. Wall		Backbone Force at Different Drift Levels (kip/ft)					
Nail Type	Edge Nail Spacing	Fu	0.5%	1.0%	2.0%	3.0%	4.0%
0.131" diam. (8d common) nail with 7/16" OSB	2	2.22	1.16	1.69	2.11	2.15	1.95
	3	1.53	0.88	1.21	1.46	1.46	1.32
	4	1.17	0.69	0.94	1.12	1.11	0.99
	6	0.79	0.51	0.65	0.76	0.75	0.66
0.148" diam. (10d common) nail with 19/32" PLY	2	2.48	1.36	1.91	2.32	2.39	1.90
	3	1.64	1.00	1.35	1.59	1.56	1.43
	4	1.25	0.78	1.04	1.21	1.18	1.08
	6	0.86	0.57	0.71	0.85	0.79	0.71

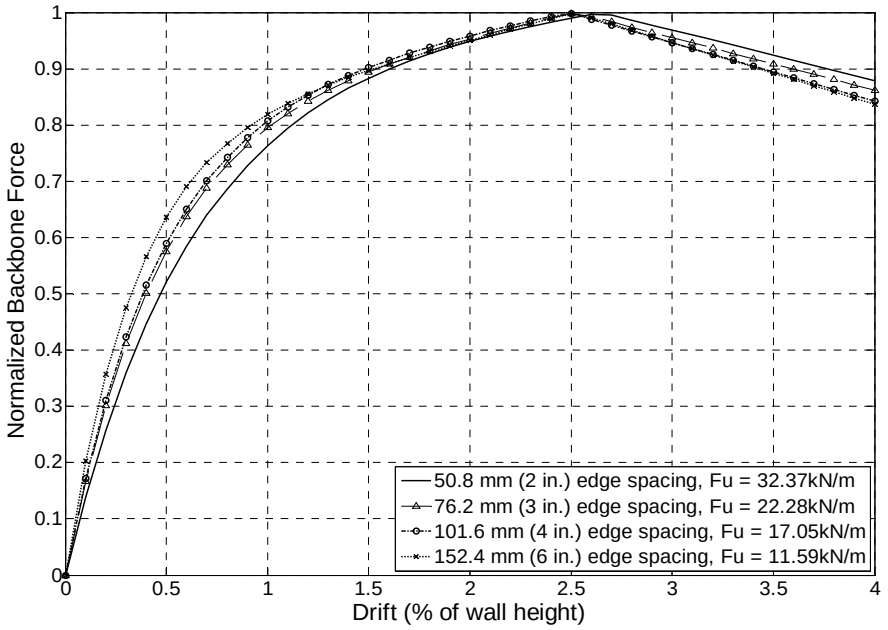

(a) 0.131 in. diameter (8d common) nails

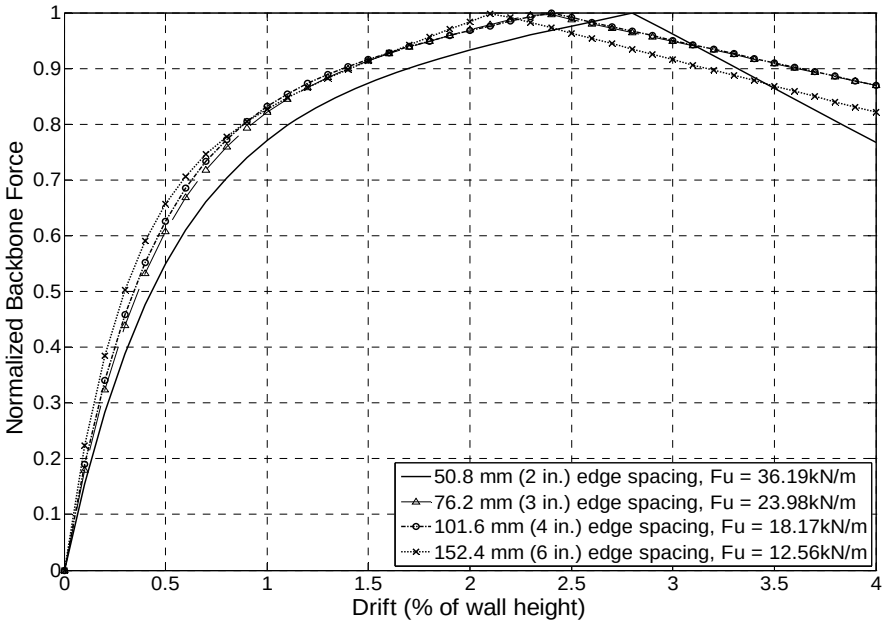

(b) 0.148 in. diameter (10d common) nails

Figure 38: Normalized design backbone curves of 4ft. × 10ft. shear walls

The three performance levels specified in ASCE/SEI 41 (2006) are considered in this study: Level 1-immediate occupancy (IO), Level 2-life safety (LS) and Level 3-collapse prevention (CP). For wood-frame buildings, the corresponding hazard level/drift limit pairs are: 50%/50 years and 1% drift, 10%/50 years and 2% drift, and 2%/50 years and 3% drift respectively. In the originally proposed DDD procedure (Pang and Rosowsky, 2009), design is pegged to the median drift (i.e. 50% non-exceedance probability). For example, the LS performance requirement ensures that the probability of exceeding 2% drift under a 10%/50 years seismic hazard event does not exceed 50%. Although intended as code-specified minimum requirements, informed building owners and/or engineers may specify additional performance levels to maximize the return of their investment or to provide protection to occupants beyond the code requirement (Krawinkler, 1999). Additionally, engineers may specify higher non-exceedance probabilities for more critical performance requirements. As an example, the seismic hazard level/drift limit pairs with corresponding NE probabilities proposed by the NEESWood project are shown in Table 7 (Pang et al., 2009). Note the higher drift limit for the Level 3 (CP) performance requirement of 4%, but also the higher non-exceedance probability of 80%. These performance levels are adopted herein. The Level 3 performance requirement was expected to be the governing requirement for most mid-rise wood-frame buildings and this was confirmed by Pang et al. (2009). Hence, in this study, the structures are only designed for the Level 3 performance requirement using the corresponding design spectral acceleration.

Table 7: Performance requirements and design spectral accelerations

Seismic Hazard		Performance Expectations		Spectral Acceleration	
		Inter-story Drift Limit	Non-exceedance Probability	Short-period S_{XS} (g)	1-Second S_{X1} (g)
Level 1	50%/50 yrs	1%	50%	0.44	0.26
Level 2	10%/50 yrs	2%	50%	1.00	0.60
Level 3	2%/50 yrs	4%	80%	1.50	0.90

Simplified Direct Displacement Design (DDD) Procedures

Pang and Rosowsky (2009) developed a multi-objective DDD procedure for mid-rise wood-frame buildings which allows engineers to estimate the inter-story drift without having to perform finite element or nonlinear dynamic analyses. Their proposed DDD procedure was intended to meet specified drift limits with a 50% non-exceedance probability (median) and inter-story drifts are estimated using a normalized modal analysis which includes all vibration modes. In the present study, a simplified version of the DDD procedure (Pang et al., 2009) was used in which (1) only the first-mode response is considered and, (2) consideration of drift limit non-exceedance probabilities other than 50% are able to be considered. The design steps for the simplified DDD procedure are summarized as follows:

Step 1. Calculate the vertical distribution factors for base shear, C_v:

$$C_{v_i} = \frac{W_i \Delta_{oi}}{\sum_{j=1}^{N} W_j \Delta_{oj}} \tag{12}$$

where N is the number of stories, W is the lumped seismic weight of the floor or the roof diaphragm and Δ_o is the design story displacement relative to the ground (Figure 39).

Eq.(12) is modified from the Eq.(12.8-12) in ASCE7-05, which is used to determined the vertical distribution factor of seismic forces. The C_v in the ASCE 7-05 is proportional to the story height whereas the C_v in Eq. (12) is proportional to the design story displacement. The parameter k is an exponent related to the structure period and lower values are associated with stiffer structures. The archetype structures considered in this study have a first period less than 1s and most are around 0.5s. According to Eq. (12.8-12), the range of k value would be 1~1.25 by interpolation and the Eq.(12) is for the case of k=1 here.

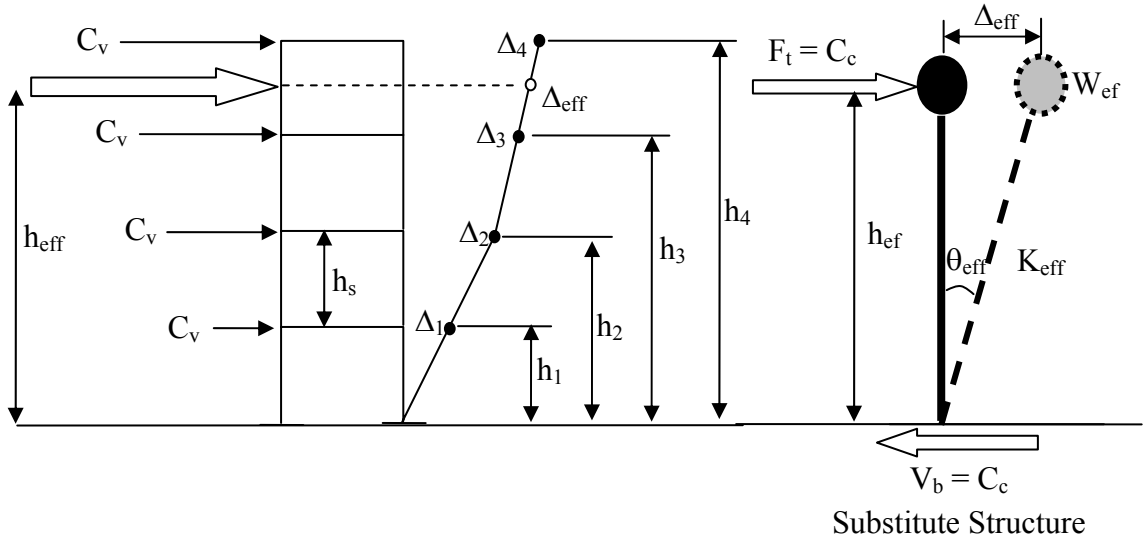

Figure 39: Example 4-story building and substitute structure for DDD procedure

Step 2. Compute the normalized story shear factors, β_v:

$$\beta_{v_i} = \sum_{j=i}^{N} C_{v_j} \tag{13}$$

Note that the shear factors are normalized with respect to the shear in the first-story (i.e., β_v=1 for the first floor).

Step 3. Calculate the effective height, $\boldsymbol{h_{eff}}$, for the *substitute structure* modeled as a single-degree-of-freedom (SDOF) system. The effective height is located at the centroid of the assumed lateral force distribution and is calculated as:

$$h_{eff} = \frac{\sum_{j=1}^{N} C_{v_j} h_{o_j}}{\sum_{j=1}^{N} C_{v_j} = 1} = \sum_{j=1}^{N} C_{v_j} h_{o_j} \tag{14}$$

where h_{oj} is the j^{th} story height relative to the ground. For typical multi-story buildings with approximately equal story heights and seismic weights at each story, the ratio of effective-to-roof height is generally about 0.7.

Step 4. Calculate the target displacement. Using interpolation, the target displacement at the effective height, Δ_{eff}, or target drift at effective height, θ_{eff}, can be determined (See Figure 39).

Step 5. Calculate the effective seismic weight, $\boldsymbol{W_{eff}}$, of the substitute structure:

$$W_{eff} = \frac{\left(\sum_{j=1}^{N} W_j \Delta_{o_j}\right)^2}{\sum_{j=1}^{N} W_j \Delta_{o_j}^{\ 2}} \tag{15}$$

For most mid-rise buildings of regular plan, the effective seismic weight is usually about 80% of the total seismic weight.

Step 6. Determine the damping reduction factor, $\boldsymbol{B_\zeta}$, per ASCE 41-06 section 1.6.1.5 as:

$$B_\zeta = \frac{4}{5.6 - \ln(100\zeta_{eff})} \tag{16}$$

where ζ_{eff} is the effective viscous damping as a fraction of the critical damping, calculated as the sum of the hysteretic damping, ζ_{hyst}, and the intrinsic damping, ζ_{int},

$$\zeta_{eff} = \zeta_{\text{int}} + \zeta_{hyst} \tag{17}$$

According to ASCE-41 section 1.6.1.5.3, a default damping of 5% can be assumed when using the FBD procedure. In order to compare to the FBD procedure, intrinsic damping of 5% was also assumed for this study. The hysteretic damping equation for wood shearwalls as a function of the secant-to-initial stiffness ratio (k_s/k_o) is given by the following equation (Pang et al., 2009).

$$\zeta_{hyst} = 0.32e^{-1.38\frac{k_S}{k_O}} \tag{18}$$

The secant-to-initial stiffness ratio as a function of wall drift can be determined from the shearwall database (e.g., Table 6). For example, the secant stiffness of the 51 mm (2 in.) perimeter nail spacing wall sheathed with OSB is 0.24 kN/mm/m (0.41 kip/in/ft) at 4% drift (28.4 kN/m ÷ 0.12m (1.95 kip/ft ÷ 4.8 in. or 4% drift)). The k_s/k_o ratio is about 0.15 (0.24 kN/mm/m ÷ 1.60 kN/mm/m (0.41 kip/in/ft ÷ 2.78 kip/in/ft)). Substituting k_s/k_o of 0.15 into equation (18) gives an estimated hysteretic damping of 0.26. The total equivalent viscous damping, including the intrinsic damping, is therefore 0.31. Using equation (16), the damping reduction factor is therefore 1.85.

Step 7. Determine the design base shear coefficient, C_c, using the capacity spectrum approach as:

$$C_c = \min \begin{cases} \dfrac{C_{NE} S_{XS}}{B_\zeta} \\ \dfrac{g}{4\pi^2 \Delta_{eff}} \left(\dfrac{C_{NE} S_{X1}}{B_\zeta} \right)^2 \end{cases} \tag{19}$$

where C_{NE} is the adjustment factor for different target non-exceedance probabilities. Equation (20) is the solution for the intersection between the demand and the capacity spectra (see Figure 40). For the high seismic hazard category Level 3, the spectral design values for short-period, S_{XS}, and 1-second period, S_{X1}, are 1.5 and 0.9 g, respectively (see Table 7). The first term of equation (20) is for structures having a secant period (at the design displacement, Δ_{eff}) less than or equal to the short-period, T_s, defined in Section 11.4 of ASCE 7-05. For most mid-rise buildings, where the secant periods are generally greater than T_s but less than T_L, the second term usually governs the design. The long-period transition period, T_L, can be obtained from ASCE 7-05.

Step 8. Calculate design forces. Once the base shear coefficient is obtained, the base shear, lateral forces, story shears, overturning moments and the required story secant stiffnesses are calculated as follows:

Base shear, V_b

$$V_b = C_c W_{eff} \tag{20}$$

Lateral forces, F_j

$$F_j = C_{v_j} C_c W_{eff} = C_{v_j} V_b \tag{21}$$

Story shears, V_{s_j}

$$V_{s_j} = \beta_{v_j} V_b \tag{22}$$

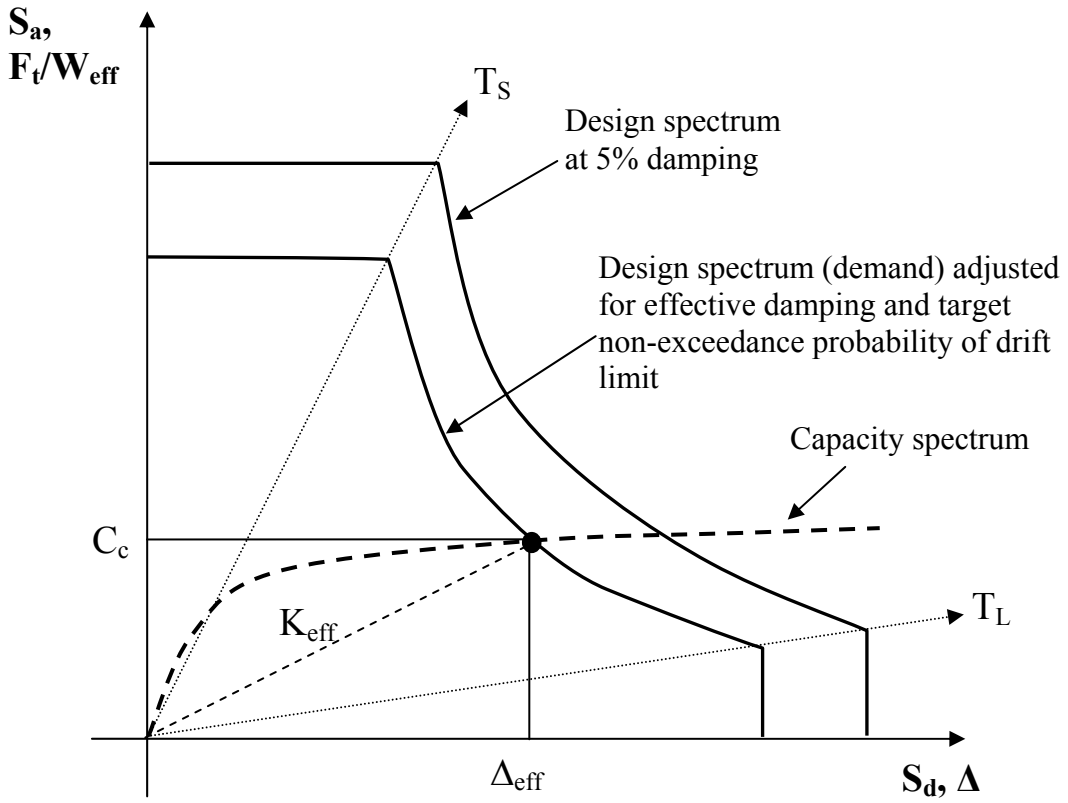

Figure 40: Determination of the design base shear coefficient using capacity spectrum approach

Step 9. Select shear walls. Once the story shears are determined using equation (23), the shearwall database (e.g., Table 6) is used to select shearwall nailing schedules that will meet or exceed the required story shear forces.

Table 8 summarizes the information used to determine the design shear forces for archetype structure 12 (high seismic hazard). In Table 8, h_s is the story height and h_0 is the story height relative to the ground; Δ_{it} is the inter-story displacement and Δ_0 is the displacement relative to the ground; θ is the design drift limit (4% in this case) and B_ζ is the damping reduction factor in equation (16); K_s is the required secant stiffness and the

V_s/L is the unit length story shear force. Note that the designs shown in Table 8 are just one example for archetype structure 12. The designs for all other archetype structures also were completed but are not presented due to length limitations.

Table 8: Design inter-story shear forces and shearwall edge nail spacings for archetype structure 12 (high seismic hazard)

Story	h_s (ft)	h_0 (ft)	θ (%)	W (kip)	Δ_{it} (in)	Δ_0 (in)	$W*\Delta_0$ (kip-in)	C_v	$W*\Delta_0^2$ (kip-in^2)
1	11	11	4	27.3	5.28	5.28	144.14	0.229	761.08
2	10	21	4	27.3	4.80	10.08	275.19	0.438	2772.86
3	11	32	4	13.65	5.28	15.36	209.66	0.333	3220.44
Sum				68.25		10.74	628.99	1	6755.38

B_ξ	S_{xs}	S_{xl}	h_{eff} (ft)	Δ_{eff} (in)	W_{eff} (kip)	C_{NE}	C_{c_s}	C_{c_l}	V_b (kip)
1.917	1.5	0.9	22.38	10.74	58.57	1.0	0.783	0.201	11.755
1.917	1.5	0.9	22.38	10.74	58.57	1.2	0.939	0.289	16.927
1.917	1.5	0.9	22.38	10.74	58.57	1.5	1.174	0.452	26.448

Story	C_{NE}	F_j (kip)	V_s (kip)	V_s/L (kip/ft)	Design nailing	FBD nailing	Demand/ Capacity
1	1.0	2.69	11.76	1.306	8dc @ 3”	8dc @ 2”	0.992
2		5.14	9.06	1.007	8dc @ 4”	8dc @ 3”	1.021
3		3.91	3.92	0.435	8dc @ 6”	8dc @ 6”	0.654
Sum		11.8	24.74				
1	1.2	3.88	16.93	1.881	8dc @ 2”	8dc @ 2”	0.964
2		7.41	13.05	1.450	8dc @ 2”	8dc @ 3”	0.744
3		5.64	5.64	0.627	8dc @ 6”	8dc @ 6”	0.943
Sum		16.9	35.62				
1	1.5	6.06	26.45	2.939	8dc @ 2”[(a)]	8dc @ 2”	0.753
2		11.6	20.39	2.265	8dc @ 3”[(a)]	8dc @ 3”	0.860
3		8.82	8.82	0.980	8dc @ 4”	8dc @ 6”	0.994
Sum		26.5	55.65				

(a): Double sheathing panels are required.

Nonlinear Time-History Analysis

NLTHA was performed both to verify that buildings designed using the DDD procedure met the specified performance requirements and to build the database of results from which appropriate adjustment factors (C_{NE}) could be selected. The analyses were performed using the SAWS (Seismic Analysis of Wood-frame Structures) program, developed by Folz and Filiatrault (2004a,b). The SAWS program uses nonlinear springs with stiffness and strength degradation to model the hysteretic behavior of the shear walls and assumes rigid diaphragms. More information about the SAWS program can be found in (Folz and Filiatrault, 2004a,b).

The archetype structures were analyzed using NLTHA and 22 bi-axial far-field ground motions records. The ground motions, which were used in the ATC-63 project, came from the PEER Strong Motion Database (PEER, 2000), and were scaled according to the ATC-63 procedure. Specifically, the median response spectrum of the ground motion ensemble was scaled to each of the three hazard levels using a single scaling factor to match the design spectral acceleration at the fundamental period of the building. The scaling procedure is further described in the ATC-63 90% draft report (Applied Technology Council, 2008). This paper reports on analyses considering only the 4% drift limit under high seismic hazard Level 3 (2%/50% years) and therefore only the ground motions scaled to this hazard level are considered. The bi-axial ground motions were applied at 0 and 90 degrees; thus, the structures were analyzed twice for each ground motion. As a result, for each DDD archetype structure, a total of 44 analyses were performed (considering values of C_{NE} of 1.0, 1.2, 1.5, 1.8 and 2.0) and 44 peak

inter-story drifts were recorded. For comparison, NLTHA also was performed on the corresponding FBD archetype structure. In order to investigate the effect of including GWB interior partition walls, the residential archetype structures also were analyzed with an assumed layout of interior walls.

While not considered in the design process, the presence of GWB was considered in the NLTHA (by modeling it as an additional nonlinear spring element). In CASHEW, it is possible to model the gypsum wallboard (assumed here as 12.7 mm (1/2 in.) thick gypsum wallboard and #6 drywall screws at 406 mm (16 in.) on-center) using the same procedure used for the structural sheathing panels. However, full-scale wall tests would be required to validate this modeling approach. As an alternative, and a simpler approach for modeling walls of any length, one could use the unit length GWB parameters obtained from a typical 1.2 m × 2.4 m (4 ft. × 8 ft.) panel and scale them up to the total GWB pier length. The time-history of inter-story drifts obtained using these two modeling approaches are compared in Figure 41. The results shown are for archetype building 12, for the controlling wall pier at each of the three stories. The results obtained using the two different approaches for modeling the GWB match well; thus, the unit length scaling method, which has the advantage of being simpler to include in SAWS, is used subsequently.

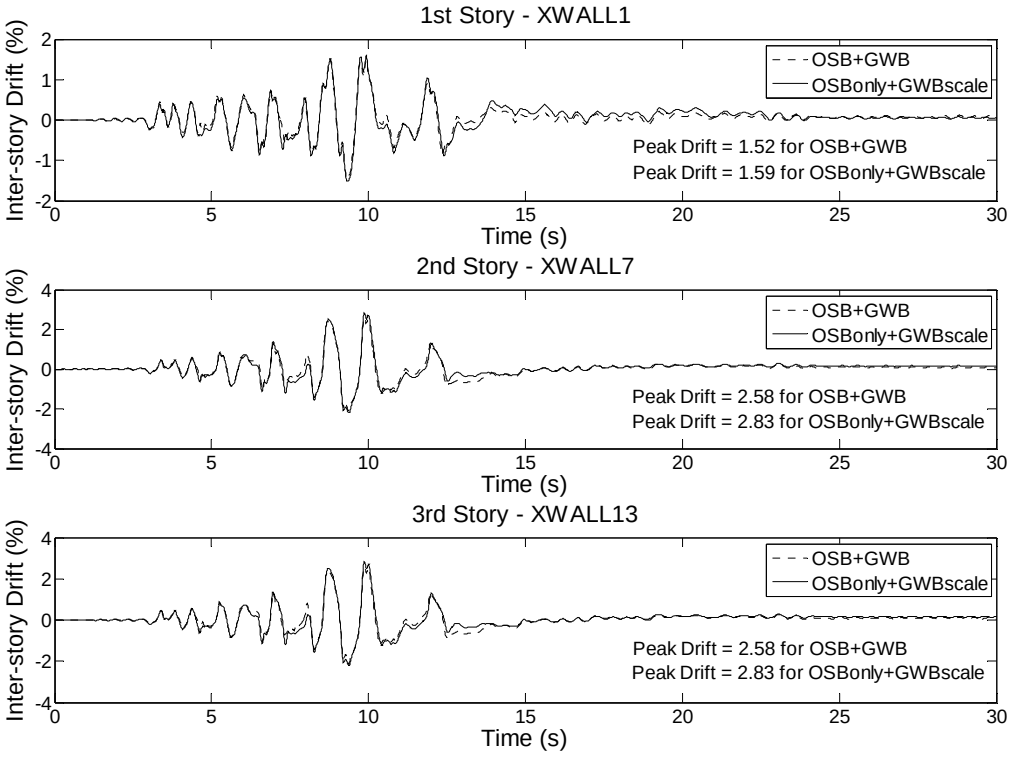

Figure 41: Comparison of time-history results using CASHEW modeling method and the unit length scaling method

The empirical cumulative distribution functions (CDF's) of the peak inter-story drifts for each DDD archetype structure and each different value of C_{NE} (as well as the FBD structure) were next constructed. The lognormal distribution was generally found to provide the best-fit. According to the results of incremental dynamic analyses performed by Christovasilis et al. (2009), numerical instability in the SAWS model occurred at inter-story drifts greater than about 7% and this drift limit has been used in the ATC-63 project to evaluate the collapse probability of wood buildings (ATC 2008). In this study, 8% is taken as the maximum inter-story drift beyond which collapse is

assumed to occur. Peak inter-story drifts were therefore truncated at 8%. As an example, the peak inter-story drift distributions for the three-story archetype 10 structure (2%/50 years, 4% drift limit) without partition walls are presented in Figure 42(a). Under hazard level 3 (2%/50 years), the NE probability of the 4% drift limit for the structure designed with C_{NE} = 1.0 is close to 50%. The NE probability increases with higher values of C_{NE}. For this structure designed with C_{NE} = 1.5, the NE probability is close to 80%, the proposed target NE probability in Table 7. The peak inter-story drift distributions for this same archetype 10 structure (2%/50 years, 4% drift limit), *including* partition walls are shown in Figure 42(b). The NE probability of the structure (with partition walls) designed with C_{NE} = 1.0 is 64%, which is higher than 50% but still lower than the target 80%. The NE probability of the structure (with partition walls) designed with C_{NE} = 1.5 at 4% drift limit is still close to 80% and almost the same as the NE probability of the same structure without partition walls. The presence of nonstructural GWB partition walls appears to significantly improve the performance of structures designed with lower C_{NE} values, but has little effect on structures designed with higher C_{NE} values. The NE probabilities at the design drift limit (4%) and the drifts at the possible target NE probabilities (50%, 80% and 90%) under high seismic hazard are summarized in the Tables 9 and 10 (without and with partition walls, respectively).

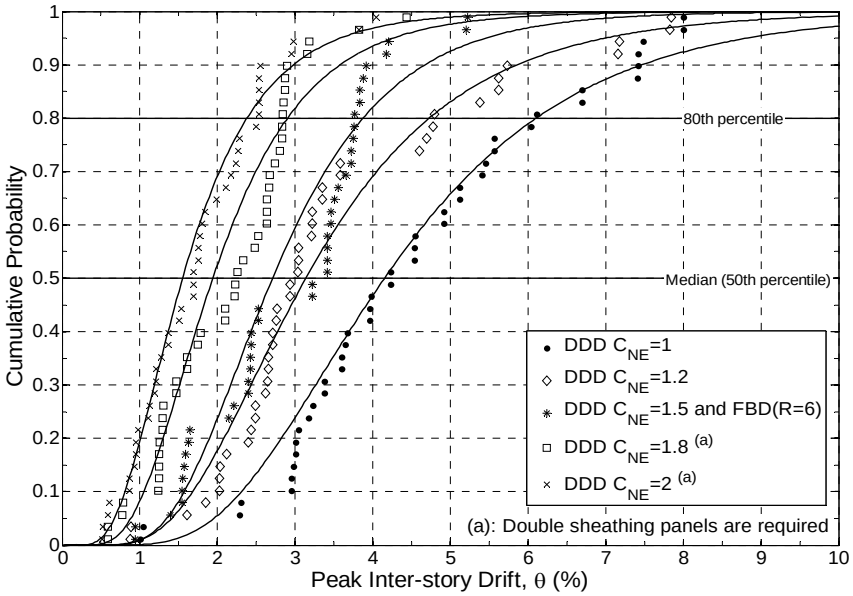

(a) Without partition walls

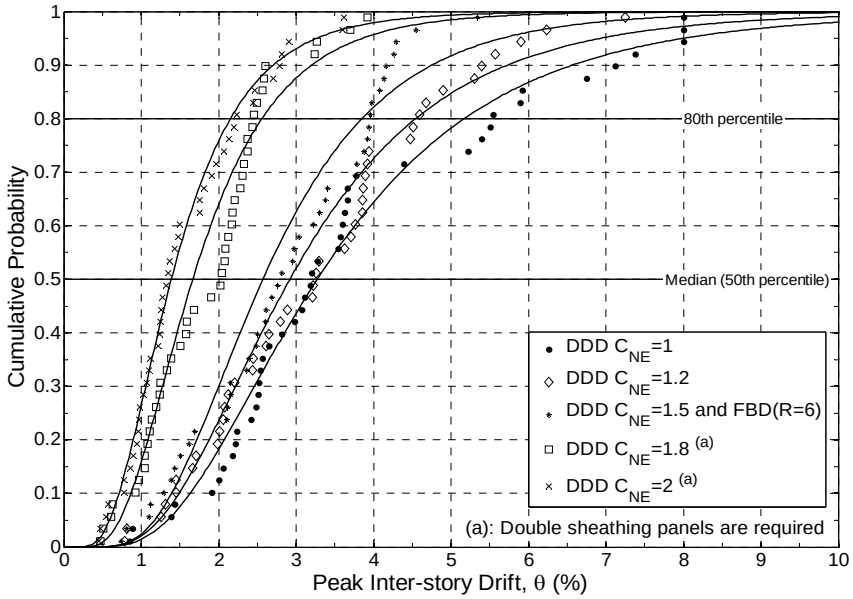

(b) With partition walls

Figure 42: Peak inter-story drift distributions for the 3-story ATC-63 archetype 10 structure under high seismic hazard (2%/50 years)

Table 9: Non-exceedance (NE) probabilities at the design drift limit (4%) and drifts corresponding to different NE probabilities (50%, 80% and 90%) (actual drifts values from NLTHA, not from fitted distribution); without partition walls

Archetype	DDD (Without partition walls)						FBD
	Results	C_{NE}					
		1.0	1.2	1.5	1.8	2.0	
Archetype 9 3 stories	NE probability @ 4% drift	0.35	0.46	0.65	N/A	N/A	0.46
	Drift (%) @ 50% NE prob.	4.76	4.31	3.32	N/A	N/A	4.31
	Drift (%) @ 80% NE prob.	6.87	6.13	4.92	N/A	N/A	6.13
	Drift (%) @ 90% NE prob.	7.57	8.00	6.08	N/A	N/A	8.00
Archetype 10 3 stories	NE probability @ 4% drift	0.47	0.69	0.82	0.93	0.97	0.82
	Drift (%) @ 50% NE prob.	4.23	2.98	3.32	2.24	1.69	3.32
	Drift (%) @ 80% NE prob.	6.09	4.79	3.77	2.84	2.52	3.77
	Drift (%) @ 90% NE prob.	7.42	5.88	3.94	2.92	2.59	3.94
Archetype 11 3 stories	NE probability @ 4% drift	0.35	0.51	0.61	0.89	N/A	0.17
	Drift (%) @ 50% NE prob.	4.82	4.32	3.75	2.44	N/A	6.23
	Drift (%) @ 80% NE prob.	6.20	5.36	5.40	3.40	N/A	8.00
	Drift (%) @ 90% NE prob.	8.00	6.46	5.79	3.74	N/A	8.00
Archetype 12 3 stories	NE probability @ 4% drift	0.37	0.52	0.84	N/A	N/A	0.42
	Drift (%) @ 50% NE prob.	4.39	3.80	2.78	N/A	N/A	4.80
	Drift (%) @ 80% NE prob.	6.41	5.96	3.51	N/A	N/A	5.74
	Drift (%) @ 90% NE prob.	7.52	7.25	4.17	N/A	N/A	7.86
Archetype 13 4 stories	NE probability @ 4% drift	0.07	0.25	0.47	0.68	0.87	0.61
	Drift (%) @ 50% NE prob.	7.39	6.17	4.54	2.94	2.74	3.40
	Drift (%) @ 80% NE prob.	8.00	8.00	5.79	5.63	3.19	5.71
	Drift (%) @ 90% NE prob.	8.00	8.00	8.00	8.00	3.48	8.00
Archetype 14 4 stories	NE probability @ 4% drift	0.22	0.31	0.39	0.60	N/A	0.31
	Drift (%) @ 50% NE prob.	4.61	4.98	4.54	4.54	N/A	4.98
	Drift (%) @ 80% NE prob.	8.00	8.00	7.33	5.56	N/A	8.00
	Drift (%) @ 90% NE prob.	8.00	8.00	8.00	6.85	N/A	8.00
Archetype 15 5 stories	NE probability @ 4% drift	0.05	0.18	0.40	0.57	0.73	0.57
	Drift (%) @ 50% NE prob.	7.13	6.82	4.36	3.33	2.58	3.33
	Drift (%) @ 80% NE prob.	8.00	8.00	8.00	8.00	5.11	8.00
	Drift (%) @ 90% NE prob.	8.00	8.00	8.00	8.00	6.73	8.00
Archetype 16 5 stories	NE probability @ 4% drift	0.20	0.38	0.55	0.70	N/A	0.38
	Drift (%) @ 50% NE prob.	5.28	4.24	3.56	3.19	N/A	4.24
	Drift (%) @ 80% NE prob.	8.00	8.00	5.76	4.80	N/A	8.00
	Drift (%) @ 90% NE prob.	8.00	8.00	6.44	5.79	N/A	8.00

N/A: Design not possible without additional shearwall piers

Table 10: Non-exceedance (NE) probabilities at the design drift limit (4%) and drifts corresponding to different NE probabilities (50%, 80% and 90%) (actual drifts values from NLTHA, not from fitted distribution); residential only, with partition walls

Archetype	DDD (With partition walls)						FBD
	Results	C_{NE}					
		1.0	1.2	1.5	1.8	2.0	
Archetype 10 3 stories	NE probability @ 4% drift	0.64	0.73	0.82	0.96	0.98	0.82
	Drift (%) @ 50% NE prob.	3.20	3.24	2.79	2.03	1.33	2.79
	Drift (%) @ 80% NE prob.	5.53	4.57	3.95	2.45	2.23	3.95
	Drift (%) @ 90% NE prob.	7.15	5.42	4.17	2.67	2.79	4.17
Archetype 12 3 stories	NE probability @ 4% drift	0.52	0.59	0.99	N/A	N/A	0.68
	Drift (%) @ 50% NE prob.	4.17	3.68	0.97	N/A	N/A	3.07
	Drift (%) @ 80% NE prob.	5.60	5.56	1.59	N/A	N/A	5.68
	Drift (%) @ 90% NE prob.	7.48	7.97	1.98	N/A	N/A	6.17
Archetype 13 4 stories	NE probability @ 4% drift	0.14	0.33	0.49	0.70	0.90	0.66
	Drift (%) @ 50% NE prob.	7.03	5.70	3.90	3.33	2.39	3.64
	Drift (%) @ 80% NE prob.	8.00	8.00	8.00	5.16	2.95	4.52
	Drift (%) @ 90% NE prob.	8.00	8.00	8.00	5.98	3.28	6.68
Archetype 14 4 stories	NE probability @ 4% drift	0.37	0.42	0.58	0.76	N/A	0.42
	Drift (%) @ 50% NE prob.	4.84	4.26	3.46	2.94	N/A	4.26
	Drift (%) @ 80% NE prob.	7.24	7.52	6.10	4.37	N/A	7.52
	Drift (%) @ 90% NE prob.	8.00	8.00	8.00	4.96	N/A	8.00
Archetype 15 5 stories	NE probability @ 4% drift	0.13	0.29	0.51	0.59	0.82	0.59
	Drift (%) @ 50% NE prob.	6.75	5.68	3.94	2.97	2.46	2.94
	Drift (%) @ 80% NE prob.	8.00	8.00	8.00	8.00	4.14	8.00
	Drift (%) @ 90% NE prob.	8.00	8.00	8.00	8.00	5.39	8.00
Archetype 16 5 stories	NE probability @ 4% drift	0.23	0.41	0.68	0.75	N/A	0.41
	Drift (%) @ 50% NE prob.	5.29	4.46	3.19	2.78	N/A	4.46
	Drift (%) @ 80% NE prob.	8.00	7.25	5.05	4.21	N/A	7.25
	Drift (%) @ 90% NE prob.	8.00	8.00	6.23	5.45	N/A	8.00

N/A: Design not possible without additional shearwall piers

Performance-based Design Charts for Selecting C_{NE}

The results from the NLTHA of the archetype structures (designed using a range of C_{NE} values) can be summarized/presented a number of different ways. For example, one could look at non-exceedance probabilities of target drifts (in this case 4%) as a

function of building height, building period, shear wall length as a percent of total wall length (or, conversely, percent openings), or other structural parameters. In this study, we first looked at the relationship between non-exceedance probability (p_{NE}) and building fundamental period, since this is a function of building height, opening, presence of interior partition walls, and so forth. Figures 43 and 44 present p_{NE} versus fundamental period, with and without consideration of interior partition walls, respectively. The actual results from the NLTHA are shown along with best-fit linear regressions for value of C_{NE} varying from 1.2 to 2. Also shown are the results from the FBD of the archetype structures as designed in ATC-63. The red boxes in these figures indicate the effective design space encompassing the archetype buildings specifically considered in the study. These figures illustrate the degree to which C_{NE} influences displacement performance across the period range considered. Comparing Figures 43 and 44 also provides some indication of the effect of partition walls on displacement performance. Finally, these figures suggest that current FBD procedures become less conservative as fundamental period increases. For example, in the case of structures without partition walls (Figure 43), FBD building performance would be equivalent to a DDD structure with C_{NE}=1.8 for a period of 0.4 seconds, and equivalent to a DDD structure with C_{NE}=1.2 for a period of 0.8 seconds. Thus, it appears that the proposed DDD procedure with the performance-based scaling factors C_{NE} has the potential to provide more risk-consistent designs across the period range. This would be an advantage in a performance-based seismic design framework.

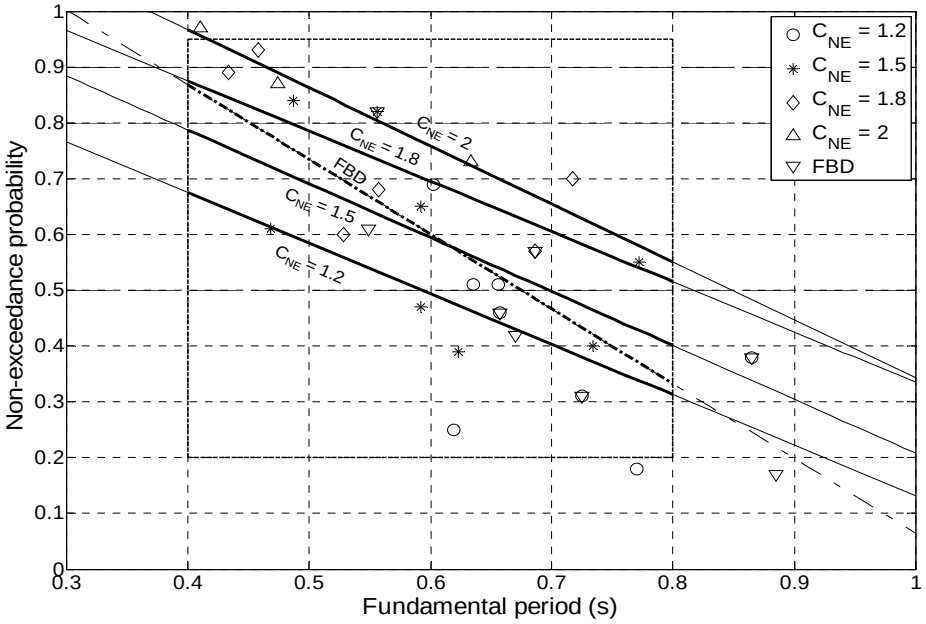

Figure 43: Non-exceedance probability vs. fundamental period, residential + commercial, without partition walls under high seismic hazard

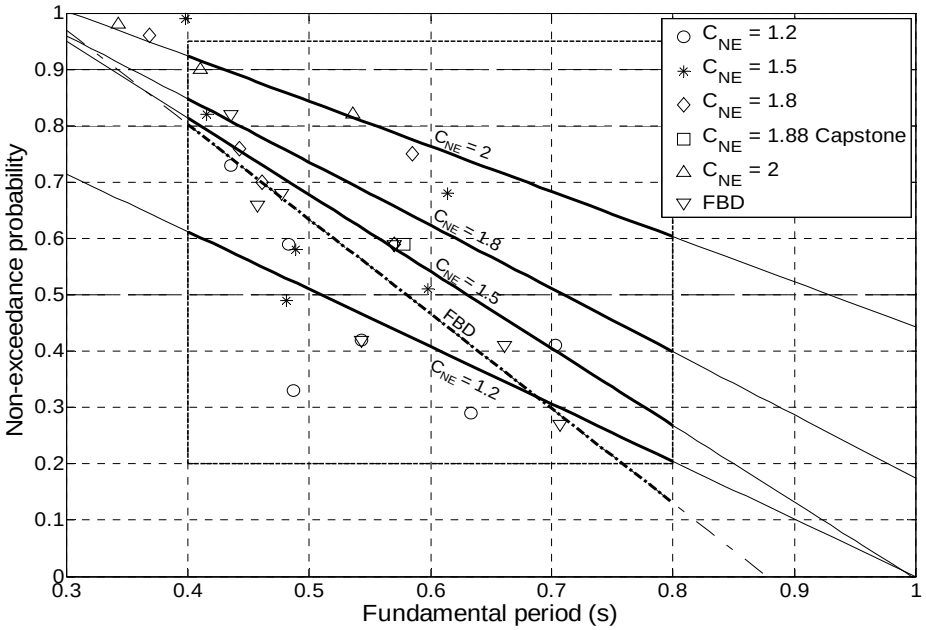

Figure 44: Non-exceedance probability vs. fundamental period, residential only, with partition walls under high seismic hazard

While presentation of the results as a function of building fundamental period is informative, it is not particularly useful as a design tool since one cannot estimate the fundamental period until an initial design is completed. One could, for example, estimate the period, design the structure, revise the estimate of the period, and re-design the structure using these figures in an iterative design procedure until the period converges. Estimating the period of wood-frame structures is not simple and is complicated by issues of period elongation through the displacement regime. As such, this likely would not be practical as a design tool for most engineers. As an alternative, the results from the NLTHA can be plotted versus building height (which varied from about 9.2 m (30 ft.) to 16.8 m (55 ft.) in this study). Figures 45 and 46 present the results from the NLTHA of the residential archetypes (numbers 10, 12-16) without and with the inclusion of partition walls, respectively. This allows one to assess the effect of including partition walls in the NLTHA analysis. Also shown on Figure 46 is the DDD of the NEESWood capstone building design (with C_{NE} =1.88; Pang et al., 2009). Figure 47 presents the results for all of the archetypes (both residential and commercial), without partition walls. (Recall that partition walls were only considered in the residential archetypes in this study. Commercial structures were assumed to have more open floor plans.) In addition to the actual NLTHA results, linear and exponential regression curves are shown in Figures 45-47. The results for the FBD structure also are shown in Figures 45-47. As can be seen, over the height range for which results were obtained, both regressions appear to provide about the same goodness of fit. If one were to extrapolate beyond the height range of 9.2 m-18.3 m (30-60 ft.), the exponential curves are probably more reasonable

as they ensure proper asymptotic behavior. As was seen in the presentation of p_{NE} versus fundamental period, the FBD results suggest decreasing conservatism as building height increases.

With an estimate of the building height, the engineer can use Figures 45-47 to select the value of C_{NE} to meet the target performance expectation and can then calculate the design base shear coefficient C_C and the design story shear forces V_{Sj} using Table 8. For example, with the desired NE probability and the target drift (4% in this case), the engineer uses Figures 45 or 46 for residential structures (depending on whether interior partition walls are included), or Figure 47 for commercial structures with more open floor plans, to select the minimum value of C_{NE} to ensure that the target NE probability of the target drift limit is not exceeded. In this paper, only the 4% drift limit under seismic hazard Level 3 (see Table 7) is considered. However, design charts for other drift limits and hazard levels can be generated easily using the same procedures with appropriately scaled ground motions. Some consideration also was given to structures designed/built in low seismic hazard regions, specifically in the mid-America region on soil class D (design spectral acceleration of 0.5g). It was found that wood-frame structures located in low seismic hazard regions and designed using current FBD procedures were very conservative (in terms of displacement performance) relative to those design using DDD and were more or less invariant with building height. Values of the minimum required C_{NE} to meet the performance requirements in the DDD procedure typically exceeded 2.0. Thus, while it might be possible to use DDD for wood-frame structures in low seismic hazard regions, it is clear that the greatest applicability (and

potential for more risk-consistent designs) would be for structures in high seismic hazard regions.

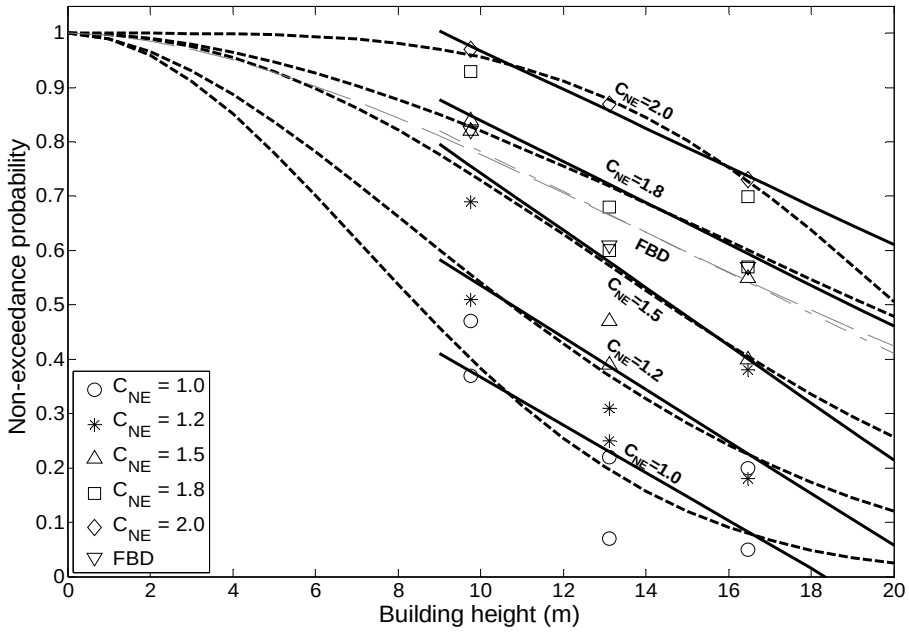

Figure 45: Non-exceedance probability vs. building height, residential only, without partition walls under high seismic hazard

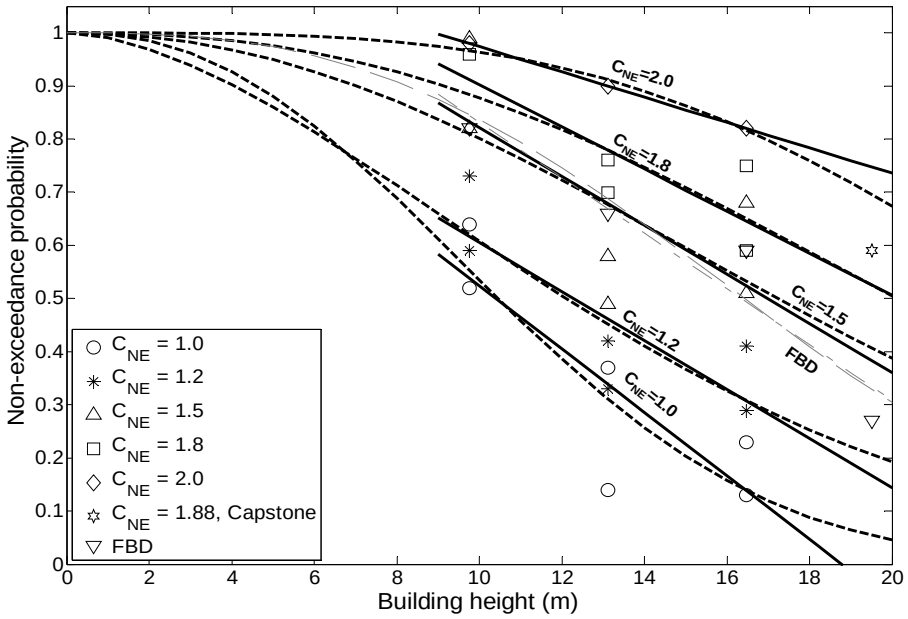

Figure 46: Non-exceedance probability vs. building height, residential only, with partition walls under high seismic hazard

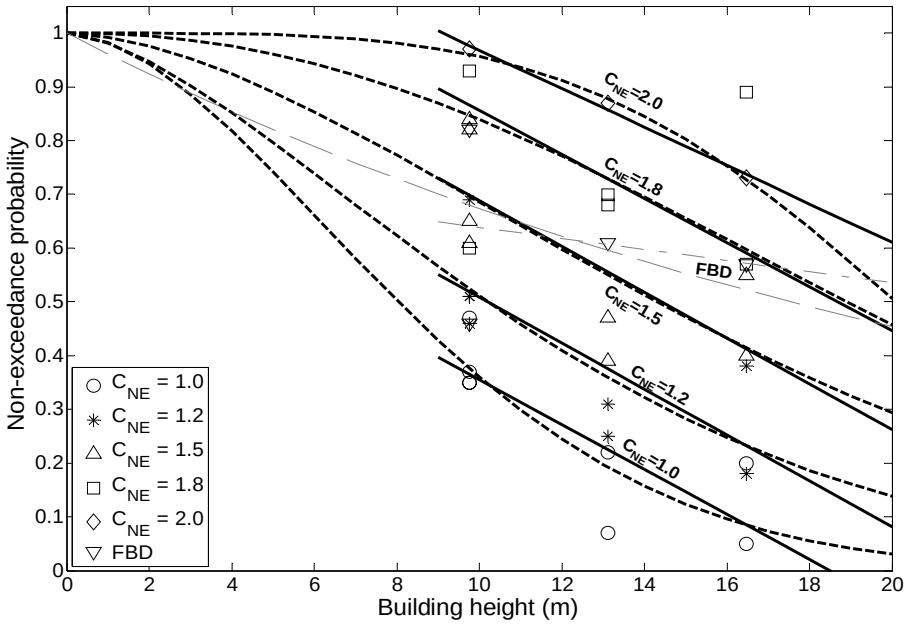

Figure 47: Non-exceedance probability vs. building height, residential + commercial, without partition walls under high seismic hazard

Summary

A probabilistic extension to a recently proposed DDD procedure for multistory wood-frame structures was presented, providing the engineer more flexibility when specifying performance requirements. Specifically, probability-based scale factors are proposed for use in the DDD procedure to ensure specified non-exceedance probabilities of target drift limits. The scale factor C_{NE} is used to determine the design base shear coefficient (step 7 of the design procedure). A database of scale factors was created by performing NLTHA on a portfolio of representative archetype wood-frame structures ranging in height from three to five stories. Each archetype structure was designed using values of C_{NE} ranging from 1.0-2.0 and analyzed using a set of 22 biaxial ground motion records scaled to the appropriate seismic hazard level. The performance requirements (i.e., seismic hazard level and corresponding inter-story drift limit, along with suggested non-exceedance probability) were based on these specified in the NEESWood project. The results were then plotted in terms of (1) fundamental period and (2) building height, the latter being more useful for design. Consideration was given to residential vs. commercial structures as well as the inclusion of non-structural (gypsum) partition walls. The present analysis only considered structures built in a high hazard region (Southern California). Comparisons were also made to results from analysis of the archetype structures designed using current force-based procedures. It was shown that current FBD procedures become less conservative (in terms of displacement performance) as fundamental period or building height increases. Thus, the proposed DDD procedure with the performance-based scale factors is able to provide more risk-consistent designs

across the period range considered. This would be an advantage in a performance-based seismic design framework.

Only the results for the 2%/50 years high seismic hazard level (and the corresponding drift limit of 4%) are presented in this paper. This was the controlling performance requirement for the design of most of archetype structures considered herein. However, in order to extend the flexibility of the proposed DDD framework, other combinations of hazard level and drift limits could be considered. The resulting database of probability-based scale factors will allow engineers to select factors for their specific performance objectives (drift limits and non-exceedance probabilities at given hazard levels). The results will be applicable to the design of wood-frame structures that fall within the range of archetype buildings and configurations considered.

CHAPTER V

SUMMARY AND CONCLUSION

This research examined and extended the state-of-the-art in hazard characterization for performance-based structural engineering. Hazard characterization, structural modeling, and nonlinear analysis techniques are required to fully and efficiently develop the fragility expressions that underpin performance-based engineering (PBE) concepts and related procedures. Note that PBE is assumed herein to include design, analysis, and assessment/evaluation. State-of-the-art hurricane models (including wind field, tracking and decay models) and event-based simulation techniques were used to characterize the hurricane wind hazard along the Texas coast. Actual recorded wind and surge data, the hurricane wind field model, hurricane size parameters and a measure of storm kinetic energy were used to develop wind-surge and wind-surge-energy models which can be used to characterize the wind-surge hazard at a level of accuracy suitable for PBE applications. In considering seismic hazard, a risk-consistent framework for displacement-based seismic design of engineered multistory woodframe structures was developed. Specifically, a database of probability-based scale factors which can be used in a direct displacement design procedure for woodframe buildings was created using nonlinear time-history analyses with suitably scaled ground motions records.

The availability of simulation tools, wind field, tracking and other models, as well as historical data make it possible to statistically characterize the hurricane wind

climate. In this study, a tracking model developed using regression analyses of the most up-to-date HURDAT data and a new decay model for Texas were developed and incorporated into a simulation framework. The simulation procedure was used to develop 10,000 years of synthetic hurricane wind speed records for each zip-code in Texas. Best-fit distributions were then determined for wind speeds at each zip-code location and design wind speed contour maps were constructed for coastal areas where the extreme wind climate is controlled by the hurricane hazard. In the future, data on non-hurricane winds, including extra-tropical storms, thunderstorms and tornados, can be statistically analyzed in order to characterize the extreme wind climate at inland (non-hurricane) locations. Thus, the mixed wind climate in Texas can be characterized for purposes of design, assessment, loss prediction or risk analysis.

Storm size is an important factor in defining risk-consistent characteristic hurricane events and for regional loss estimation. The simulation tools, wind field models and statistical analyses make it possible to characterize the risk-consistent hurricane events considering both hurricane intensity and size. These risk-consistent hurricane events are more robust and informative than those based only on maximum wind speed and are better suited for application considering collateral hazards, e.g., hurricane surge. The proposed methodology for event-based hurricane hazard characterization, when coupled with a hurricane damage model, can also be used for regional loss estimation and other spatial impact analyses.

The availability and ease of access of surge measurement data is the key factor making it possible to develop a simplified joint wind-surge model. Since historical

records are not complete at all locations throughout every hurricane season, and some records may have gaps resulting from power loss during the storm passage, the sparse nature of the measured surge data at specific sites may not be adequate. Therefore, a "super-cell" approach is used to group together data from contiguous measurement stations assumed to have similar topography/exposure. This approach enables the regression analysis needed to develop the simplified joint wind-surge model. The hurricanes surge hazard varies by location along the Texas coast. The most vulnerable regions are the Galveston area and TX/LA border area. Although the simplified joint wind-surge model has limitations, the predictions generally compare well with these from complex numerical models (e.g., the SLOSH model). Further refinements could be made as additional surge measurement data become available. The simulated wind speed data also were used to develop the simplified joint wind-surge model. However, due to the inherent modeling error in the wind field model, which increases at sites further away from hurricane eye, and due to differences between the actual landfall time and the time at which the simulated hurricane wind field makes landfall, the simulated wind/measured surge model is believed to be less accurate than measured wind/measured surge model. The simplified wind-surge model also has the limitation of not being able to properly account for the "direct-hit" situation (e.g., hurricane Ike on Galveston) and therefore a modified joint wind-surge model was developed in this study. Hurricane surge is affected by not only hurricane intensity but also spatial extent and the relative position of the location of interest to the hurricane eye, which were inherently considered in the modified joint wind-surge model. The wind-surge model is sufficiently

accurate to be used for real-time surge estimates (e.g., expected surge depth given best predictions of surface wind speed) as a hurricane approaches the coast and to characterize the distribution of maximum surge height for a given coastal location.

The modified joint wind-surge model was further enhanced to include a measure of hurricane energy using the Integrated Kinetic Energy (IKE) concept. The availability of wind field models, the IKE concept and historical data make it possible to characterize the joint wind-surge-energy model. The surge generation is an evolving process caused by hurricane wind time histories. The IKE definition implicitly accounts for both hurricane intensity and the effect of storm size and therefore the wind-surge-energy model can explain why hurricane Ike generated very high surge heights in the Galveston area, for example. Therefore, the wind-surge-energy model is believed to be more accurate than the wind-surge model and can provide improved rapid prediction of the maximum surge height during an approaching hurricane. In its current form, the wind-surge-energy model is limited to the prediction of the median value of maximum surge height. With additional surge data, it should be possible to generate confidence intervals ("surfaces") or other statistical bounds on predicted surge values.

In the study to develop a risk-consistent framework for displacement-based seismic design of woodframe structures, a portfolio of mid-rise engineered woodframe archetype structures was identified and re-designed using the deterministic direct displacement-based design (DDD) procedure. The portfolio of structures was analyzed using nonlinear time-history analyses to develop a database of scale (adjustment) factors. Finally, performance-based design charts was developed to enable the selection of

probability-based scale factors. Such charts could be used by engineers/designers to select the appropriate minimum adjustment factor given the building height and desired drift non-exceedance probability. This approach therefore extends the deterministic DDD procedure to include the probabilistic factors for adjustment of design spectral acceleration corresponding to target non-exceedance probabilities of inter-story drift. The resulting risk-based DDD procedure takes into account the uncertainty in the seismic hazard (ground motions) and variations in the type of structures (e.g., number of stories, story height and presence of interior nonstructural walls). The new risk-based DDD procedure allows the engineer/designer the flexibility of specifying their own performance requirements (target drifts and non-exceedance probabilities). This represents an improvement over existing force-based design (FBD) procedure since it results in more risk-consistent designs. Existing FBD procedures become less conservative (in terms of drift performance) as the fundamental period or building height increases, and does not ensure consistent levels of risk (again, considering drift) in both high and low hazard regions.

The multiple studies comprising this dissertation have advanced the state-of-the-art in hazard characterization for purposes of performance-based engineering of structures subjected to natural hazards. There are four major contributions: the joint wind-surge model based on historical measured data; the modified wind-surge model considering the storm size and ROD concept; the extended wind-surge-energy model with the introduction of hurricane wind energy concept; and the framework of risk-based DDD procedures for designers to specify their desired combinations of

performance requirements and non-exceedance probabilities in seismic design of multistory woodframe structures. The combination of advanced simulation techniques, wind field models, and easily accessible hurricane wind measurements allowed for the advances in hurricane wind hazard characterization. Available surge measurement data and both measured and simulated wind records were utilized to develop joint wind-surge models and to characterize the hurricane surge hazard. A measure of kinetic energy of a hurricane was used to extend the wind-surge model to a wind-surge-energy model. The framework developed to characterize the hurricane wind and surge hazards is modular and is easily updatable with new data and/or models. In consideration of seismic hazard, a deterministic DDD approach (Pang and Rosowsky, 2009) was extended into a risk-consistent procedure for displacement-based seismic design of multistory woodframe structures. This was accomplished through the development of a set of scale factors intended to ensure that the designed structures meet specified drift performance levels with certain target probabilities. These seismic scale (adjustment) factors take into account the dominant uncertainty source (i.e., uncertainty in the seismic hazard or ground motions) and make it possible to design for different combinations of performance requirements and non-exceedance probabilities. This resulting DDD procedure results in more risk-consistent designs and therefore advances the state-of-the-art in displacement-based seismic design of woodframe structures.

REFERENCES

Applied Technology Council (2008). *Quantification of Building Seismic Performance Factors*, ATC-63 Project Report, FEMA P695. Washington, DC, in preparation.

American Society of Civil Engineers (ASCE) (2005). *Minimum Design Loads for Buildings and Other Structures* (ASCE/SEI 7-05), American Society of Civil Engineers, Reston, VA.

American Society of Civil Engineers (ASCE) (2006). *Seismic Rehabilitation of Existing Buildings* (ASCE/SEI 41-06), American Society of Civil Engineers, Reston, VA.

Atlantic Basin Hurricane Database (HURDAT), http://www.aoml.noaa.gov/hrd/hurdat/, Atlantic Oceanographic and Meteorological Laboratory (AOML), National Oceanic and Atmospheric Administration (NOAA), accessed October 1, 2008.

Batts, M.E., Cordes, M.R., Russell, L.R., Shaver, J.R., and Simiu, E. (1980), *Hurricane Wind Speeds in the United States, NBS Building Science Series 124*, U.S. Department of Commerce, National Bureau of Standards, Washington, DC.

Bell, G.D., Halpert, M.S., and Schnell, R.C. (2000), "Climate assessment for 1999," *Bulletin of American Meteorological Society*, 81(6):1328-1378.

Businger, S., and Businger J.A. (2001), "Viscous dissipation of turbulence kinetic energy in storms," *Journal of Atmospheric Science*, 58(24):3793-3796.

Camelo, V., Beck, J., and Hall, J. (2001). *Dynamic Characterization of Woodframe Structures*, CUREE Report W-11, Task 1.3.3, Consortium of Universities for Research in Earthquake Engineering, Richmond, CA.

Caton, P.G.F. (1975), "Standardized map of hourly mean wind speed over the United Kingdom and some implication regarding wind speed profiles," *Proceedings: 4th International Conference on Wind Effects on Buildings and Structures*, London, UK, 7-21.

Center for Operational Oceanographic Products and Services (CO-OPS), http://tidesonline.nos.noaa.gov/geographic.html, National Ocean Service (NOS), National Oceanic and Atmospheric Administration (NOAA), accessed October 1, 2008.

Darling, R.W.R. (1991), "Estimating probabilities of hurricane wind speeds using a large scale empirical model," *Journal of Climate*, 4 (10): 1035-1046.

Ellingwood, B.R., Rosowsky, D.V. and Pang, W.C. (2008). "Performance of light-frame wood residential construction subjected to earthquakes in regions of moderate seismicity," *ASCE Journal of Structural Engineering*, 134(8):1353-1363.

Emanuel, K. (2005), "Increasing destructiveness of tropical cyclones over the past 30 years," *Nature*, 436(7051):686-688.

Federal Emergency Management Agency (FEMA) (2003). *HAZUS_MH Multi-Hazard Loss Estimation Methodology: Hurricane Model Technical Manual*, FEMA, Washington, DC.

Filiatrault, A., and Folz, B. (2002). "Performance-based seismic design of wood framed buildings," *ASCE Journal of Structural Engineering*, 128(1): 39-47.

Filiatrault, A., Christovasilis, I., Wanitkorkul, A., and Folz, B. (2006). "Displacement-based seismic design of light-frame wood buildings," *Proceedings of the 9th World Conference on Timber Engineering*, Portland, OR.

Filiatrault, A., Wanitkorkul, A., Christovasilis, I.P., van de Lindt, J., Symans, M., Rosowsky, D., and Davidson, R. (2007). "Experimental seismic performance evaluation of a full-scale woodframe building," *Proceedings of the 2007 Structures Congress*, Long Beach, CA.

Fischer, D., Filiatrault, A., Folz, B., Uang, C-M, and Seible, F. (2001). *Shake Table Tests of a Two-Story Woodframe House*, CUREE Report W-06, Task 1.1.1, Consortium of Universities for Research in Earthquake Engineering, Richmond, CA.

Folz, B., and Filiatrault, A. (2001). "Cyclic analysis of wood shear walls," *ASCE Journal of Structural Engineering*, 127(4): 433-441.

Folz, B., and Filiatrault, A. (2004a), "Seismic analysis of woodframe structures I: model formulation," *ASCE Journal of Structural Engineering*, 130(9): 1353-1360.

Folz, B., and Filiatrault, A. (2004b). "Seismic analysis of woodframe structures II: model implementation and verification," *ASCE Journal of Structural Engineering*, 130(9): 1426-1434.

Georgiu, P.N. (1985), *Design Wind Speeds in Tropical Cyclone-Prone Regions*, Ph.D. Dissertation, Department of Civil Engineering, University of Western Ontario, Canada.

Heneka, P. (2008), "A damage model for the assessment of storm damage to buildings," *Engineering Structures*, 30(12):3603-3609.

Ho, F.P., Su, J.C., Hanevich, K.L., Smith, R.J., and Richards, F. (1987), *Hurricane Climatology for the Atlantic and Gulf Coasts of the United States*, NOAA Technical Report NWS 38.

Huang, Z., Rosowsky, D.V., and Sparks, P.R. (2001), "Hurricane simulation techniques for the evaluation of wind-speeds and expected insurance losses," *Journal of Wind Engineering and Industrial Aerodynamics*, 89(7-8):605-617.

International Code Council (ICC) (2006). *International Building Code*, Building Officials and Code International Code Council Inc., Country Club Hills, IL.

Irish, J.L., Resio, D.T., and Ratcliff, J.J. (2008), "The influence of storm size on hurricane surge," *Journal of Physical Oceanography*, 38(9):2003-2013.

Jelesnianski, C.P., Chen J., and Shaffer W.A. (1992), *SLOSH Sea, Lake, and Overland Surges from Hurricanes*, NOAA Technical Report NWS 48, Silverspring, Maryland.

Kantha, L. (2006), "Time to replace the Saffir-Simpson hurricane scale?," *Eos, Transaction of American Geophysical Union*, 87:3-6.

Khanduri, A.C., and Morrow G.C. (2003), "Vulnerability of buildings to windstorms and insurance loss estimation," *Journal of Wind Engineering and Industrial Aerodynamics*, 91(4):455 – 467.

Krawinkler, H. (1999). "Challenges and progress in performance-based earthquake engineering." *International Seminar on Seismic Engineering for Tomorrow*, Tokyo, Japan.

Lee, K.H., and Rosowsky, D.V. (2007), "Synthetic hurricane wind speed records: development of a database for hazard analysis and risk studies," *ASCE Natural Hazards Review* 8(2):23-34.

Legg, M.R., Nozick, L.K., and Davidson, R.A. (2010), "Optimizing the selection of hazard-consistent probabilistic scenarios for long-term regional hurricane loss estimation," *ASCE Structural Safety*, 32(1): 90-100.

Luettich, R., and Westerink, J. (2004), "Formulation and numerical implementation of the 2D/3D ADCIRIC finite element model version 44.XX," http://www.adcirc.org, accessed March 1, 2008.

National Climatic Data Center (NCDC) (2008), http://cdo.ncdc.noaa.gov/CDO/cdo, accessed October 1, 2008.

Pacific Earthquake Engineering Research Center (PEER) (2000). "PEER Strong Motion Database," http://peer.berkeley.edu/smcat, accessed February 1, 2009.

Pang, W.C., and Rosowsky, D.V. (2009). "Direct displacement procedure for performance-based seismic design of mid-rise woodframe structures," *Earthquake Spectra*, 25(3):583-605.

Pang, W.C., Rosowsky, D.V., Ellingwood, B.R., and Wang, Y. (2009), "Seismic fragility analysis and retrofit of conventional residential wood frame structures in

the central United States," *ASCE Journal of Structural Engineering*, 135(3):262-271.

Pang, W.C., Rosowsky, D.V., van de Lindt, J.W., and Pei, S. (2009), "Simplified direct displacement design of six-story NEESWood capstone building and pre-test seismic performance assessment," NEESWood Report NW-05, Colorado State University, Fort Collins, CO.

Pardoen, G., Waltman, A., Kazanjv, R., Freund, E., and Hamilton, C. (2003). *Testing and Analysis of One-story and Two-story Shearwalls under Cyclic Loading*, CUREE Report W-25, Task 1.4.4, Consortium of Universities for Research in Earthquake Engineering, Richmond, CA.

Phan, L.T., and Simiu, E. (2008), "A Methodology for developing design criteria for structures subjected to combined effects of hurricane wind speed and storm surge," *Proceeding of the 4th International Conference on Structural Engineering and Mechanics (ASEM 08)*, Jeju, Korea, 1510-1524.

Powell, M.D., Houston S.H., Amat, L.R., and Morisseau-Leroy, N. (1998), "The HRD real-time hurricane wind analysis system," *Journal of Wind Engineering & Industrial Aerodynamics,* 77&78:53-64.

Powell, M.D., and Reinhold, T.A. (2007), "Tropical cyclone destructive potential by integrated kinetic energy," *Bulletin of American Meteorological Society*, 88(4):513-526.

Priestley, M.J.N. (1998). "Displacement-based approaches to rational limit states design of new structures," *Proceedings of the 11th European Conference on Earthquake Engineering*, Paris, France.

Probabilistic Hurricane Storm Surge (PHSS) (2008), http://www.weather.gov/mdl/psurge, NOAA / NWS's Meteorological Development Laboratory, accessed June 1, 2008.

Rosowsky, D.V. and B.R. Ellingwood (2002), "Performance-based Engineering of Wood Frame Housing: A Fragility Analysis Methodology," *ASCE Journal of Structural Engineering*, 128(1): 32-38.

Rosowsky, D.V., Sparks, P.R., and Huang, Z. (1999), *Wind Field Modeling and Hurricane Hazard Analysis*, Report to the South Carolina Sea Grant Consortium, Department of Civil Engineering, Clemson University, SC.

Saffir, H. (1975), "Low cost construction resistant to earthquakes and hurricanes," Working Paper, *ST/ESA/23*, United Nations, New York.

Simiu, E., and Scanlan R.H. (1996). *Wind Effects on Structures*. John Wiley & Sons, New York.

Simpson, R.H. (1974), "The hurricane disaster potential scale," *Weatherwise*, 27(4):169-186.

Sparks, P.R., and Huang, Z. (1999), "Wind speed characteristics in tropical cyclones," *Proceeding of the 10th International Conference on Wind Engineering*, Copenhagen, Denmark, 343-350.

Sparks, P.R. (2003), "Wind speeds in tropical cyclones and associated insurance losses," *Journal of Wind Engineering and Industrial Aerodynamics*, 91(12-15):1731-1751.

van de Lindt, J.W. (2006). "The next step for ASCE 16: performance-based design for woodframe structures," *e-Proceedings of the 1st Invitational Workshop on Performance-Based Design of Woodframe Structures*, http://www.engr.colostate.edu/pbd, Fort Collins, CO.

van de Lindt, J.W., and Liu, H. (2006). "Correlation of observed damage and FEMA 356 drift limits: results from one-story woodframe house shake table tests," *Proceedings of the 2006 Structures Congress,* St. Louis, MO.

Vickery, P.J., and Twisdale, L.A. (1995), "Wind-field and filling models for hurricane wind-speed prediction," *ASCE Journal of Structural Engineering*, 121 (11): 1700-1209.

Vickery, P.J., Skerlj, P.F., Steckley, A.C., and Twisdale, L.A. (2000a), "Hurricane wind field model for use in hurricane simulations," *ASCE Journal of Structural Engineering*, 126 (10): 1203-1221.

Vickery, P.J., Skerlj, P.F., and Twisdale, L.A. (2000b), "Simulation of hurricane risk in the U.S. using empirical track model," *ASCE Journal of Structural Engineering*, 126 (10): 1222-1237.

Wang**,** Y., and Rosowsky, D.V. (2009), "Hazard-specific hurricane event characterization for regional loss estimation and other spatial impact studies," *Paper in preparation*.

Wang**,** Y., Rosowsky, D.V., and Pang, W.C. (2009), "Toward a performance-based procedure for direct displacement design of engineered woodframe structures", *ASCE Journal of Structural Engineering*, accepted for publication.

Watson C., and Johnson M. (2004), "Hurricane loss estimation models: Opportunities for improving the state of art," *Bulletin of the American Meteorological Society*, 85:1713-1726.

APPENDIX A

ARCHETYPE STRUCTURES DESIGNED AND ANALYZED FOR LOW SEISMIC HAZARD

(CHAPTER IV)

Structures built in the low seismic hazard region are assumed to be located in the mid-America region on soil class D and the design spectral acceleration is taken as 0.50g. In the NLTHA, the corresponding spectral acceleration of the Level 2 Design Basis Earthquake (DBE) also is taken as 0.50g and the spectral design values of S_{XS} and S_{X1} in equation (20) are 0.75 and 0.3g, respectively. Table A1 summarizes the information used to estimate the design shear forces for archetype structure 12 under low seismic hazard. The peak inter-story drift distributions for the 3-story archetype 12 structure (designed with 4% drift limit) under (low) seismic hazard Level 3 (2%/50 years) without partition walls are presented in Figure A1. The design charts for the 4% drift limit under (low) seismic hazard Level 3 are presented in Figures A2-A4. These figures illustrate two things: (1) the structures built in the low hazard region and designed using current FBD procedures are very conservative (relative to the DDD structures) and are more or less invariant with building height, with all NE probabilities greater than 90%; and (2) C_{NE} values greater than or equal to 2.0 are possible while still meeting the performance objectives (drift limit and target NE probability). While design charts such as those proposed in Figures A2-A4 could be used for structures built in the low seismic hazard

region considered, the DDD procedure developed in this paper appears to have greater utility to design in high hazard regions (the focus of the paper).

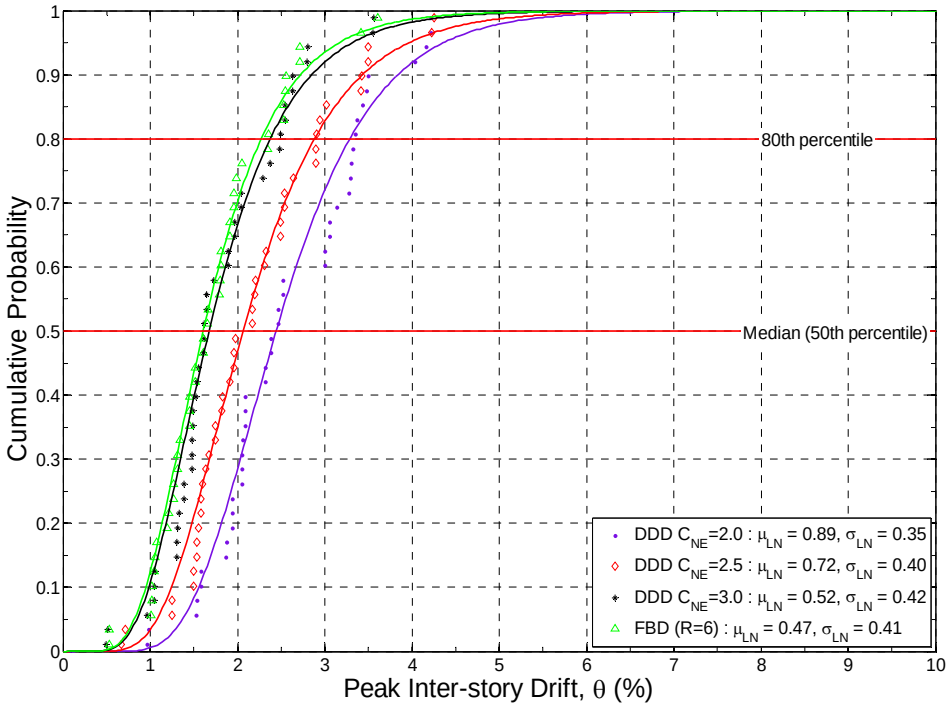

Figure A1: Peak inter-story drift distributions for the 3-story ATC-63 archetype 12 structure under low seismic hazard (2%/50 years)

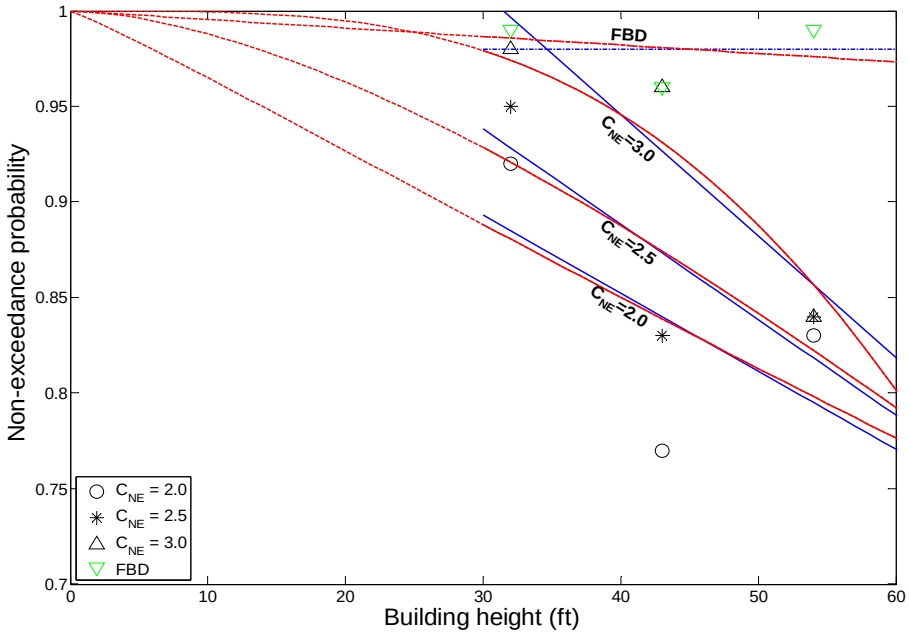

Figure A2: Non-exceedance probability vs. building height, residential only (without partition walls), under low seismic hazard

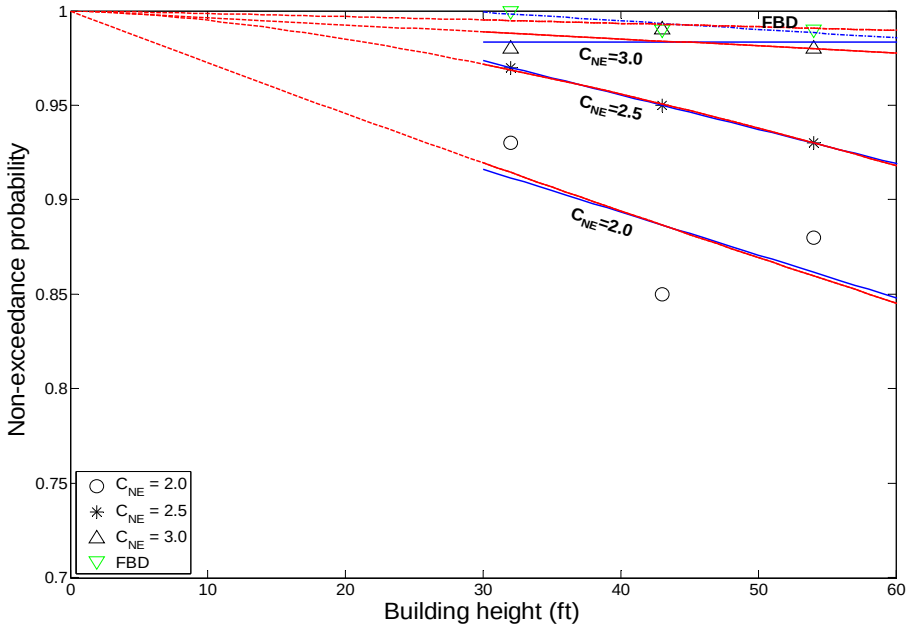

Figure A3: Non-exceedance probability vs. building height, residential only (with partition walls), under low seismic hazard

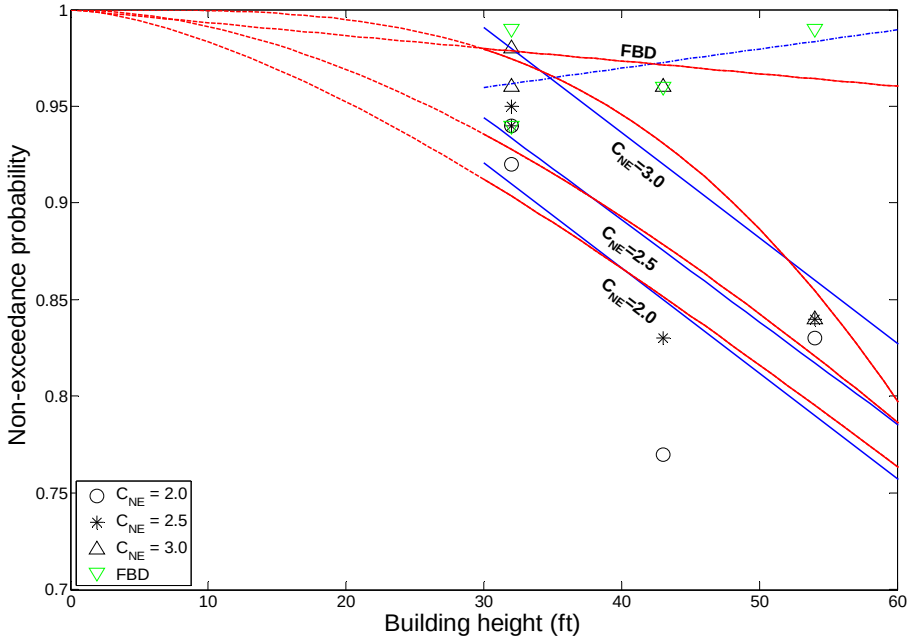

Figure A4: Non-exceedance probability vs. building height, residential + commercial (without partition walls), under low seismic hazard

Table A1: Design inter-story shear forces and shearwall edge nail spacings for archetype structure 12 (low seismic hazard)

Story	h_s (ft)	h_0 (ft)	θ (%)	W (kip)	Δ_{it} (in)	Δ_0 (in)	$W*\Delta_0$ (kip-in)	C_v	$W*\Delta_0^2$ (kip-in^2)
1	11	11	4	27.3	5.28	5.28	144.14	0.229	761.08
2	10	21	4	27.3	4.80	10.08	275.19	0.438	2772.86
3	11	32	4	13.65	5.28	15.36	209.66	0.333	3220.44
Sum				68.25		10.74	628.99	1	6755.38

B_ξ	S_{xs}	S_{xl}	h_{eff} (ft)	Δ_{eff} (in)	W_{eff} (kip)	C_{NE}	C_{c_s}	C_{c_l}	V_b (kip)
1.917	0.75	0.3	22.38	10.74	58.57	2.0	0.783	0.089	5.224
1.917	0.75	0.3	22.38	10.74	58.57	2.5	0.978	0.139	8.163
1.917	0.75	0.3	22.38	10.74	58.57	3.0	1.174	0.201	11.755

Story	C_{NE}	F_j (kip)	V_s (kip)	V_s/L (kip/ft)	Design nailing	Demand/ Capacity
1	2.0	1.20	5.23	0.581	8dc @ 6”	0.873
2		2.29	4.03	0.447	8dc @ 6”	0.673
3		1.74	1.74	0.193	8dc @ 6”	0.291
Sum		5.23	10.99			
1	2.5	1.87	8.16	0.907	8dc @ 4”	0.921
2		3.57	6.30	0.699	8dc @ 4”	0.710
3		2.72	2.72	0.302	8dc @ 6”	0.455
Sum		8.16	17.18			
1	3.0	2.69	11.76	1.306	8dc @ 3”	0.992
2		5.14	9.06	1.007	8dc @ 3”	0.765
3		3.92	3.92	0.435	8dc @ 4”	0.655
Sum		11.8	24.74			

APPENDIX B

ARCHETYPE STRUCTURES DESIGNED AND ANALYZED FOR OTHER PERFORMANCE REQUIREMENTS

(CHAPTER IV)

The seismic hazard level/drift limit pairs with corresponding NE probabilities proposed by the NEESWood project and adopted herein are shown in Chapter IV, Table 7. In the previous study, the structures were only designed for the Level 3 performance requirement using the corresponding design spectral acceleration. The Level 3 performance requirement was expected to be the governing requirement for most mid-rise woodframe buildings, although this was not yet confirmed. In the present analysis, the expectation that Level 3 controls the design is validated. Two archetypes, one residential and one commercial, were selected from ATC-63 archetypes and re-designed for the lower hazard levels (Level 1, 50%/50 years and Level 2, 10%/50 years) using the same simplified DDD procedure. These archetypes were still assumed to be located in a high seismic hazard area (e.g., Southern California). In the NLTHA, the spectral accelerations shown in Table 7 were adopted for Level 1 and Level 2 seismic hazards. The inter-story drift limits with corresponding NE probabilities in Table 7 also were adopted herein as the Level 1 and Level 2 performance expectations (i.e., 1% and 50% for Level 1; 2% and 50% for Level 2). The peak inter-story drift distributions for these two archetypes (without partition walls) with the minimum required C_{NE} factors for different performance requirements are presented in Figures B1 and B2, respectively.

From Figure B1, the minimum required C_{NE} factor value for hazard level 3 and a 4% drift limit with 80% NE probability is 1.8; the minimum required C_{NE} factor value for hazard level 2 and a 2% drift limit with 50% NE probability is 1.3, and the minimum required C_{NE} factor value for hazard level 1 and a 1% drift limit with 50% NE probability is 1.5. Similarly from Figure B2, the minimum required C_{NE} factor value for hazard level 3 and a 4% drift limit with 80% NE probability is 1.5; the minimum required C_{NE} factor value for hazard level 2 and a 2% drift limit with 50% NE probability is 1.3, and the minimum required C_{NE} factor value for hazard level 1 and 1% drift limit with 50% NE probability is 1.5. These figures illustrate that minimum design C_{NE} factors vary with the different hazard levels and corresponding performance expectations; however, the controlling C_{NE} factors (1.8 for archetype 11 and 1.5 for archetype 12), defined as the largest value of the minimum required C_{NE} factors for different hazard levels and performance expectations, are those for the Level 3 (2%/50 years) hazard level and performance expectation. On this basis, it is concluded that the Level 3 performance requirement can be assumed to be the controlling requirement for the mid-rise woodframe buildings considered in this study, and that therefore only the Level 3 performance requirement needs to be considered in the design.

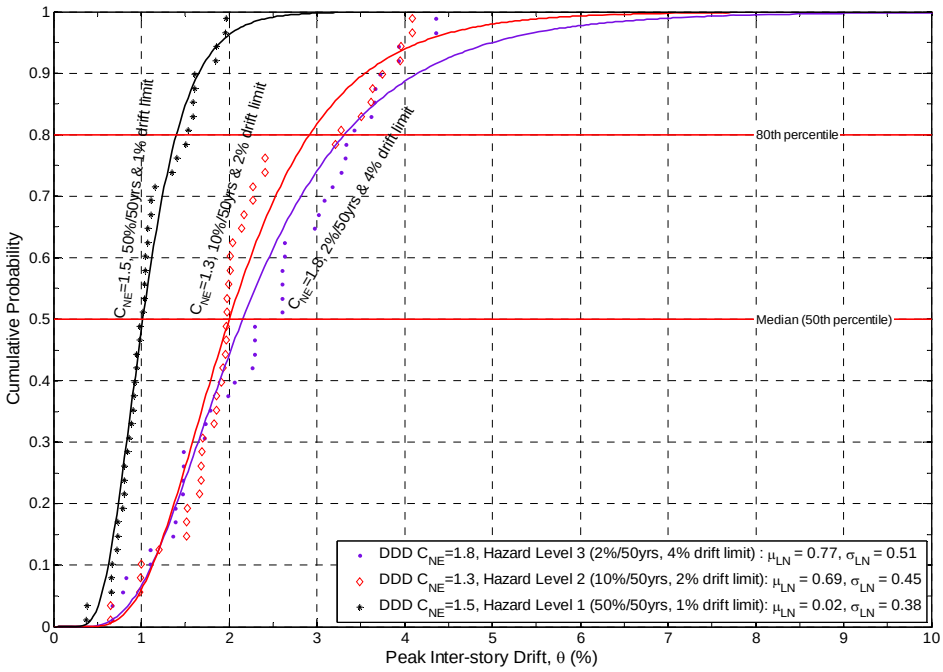

Figure B1: Peak inter-story drift distributions for the ATC-63 archetype 11 under different hazard levels and drift limits with minimum required C_{NE} factors

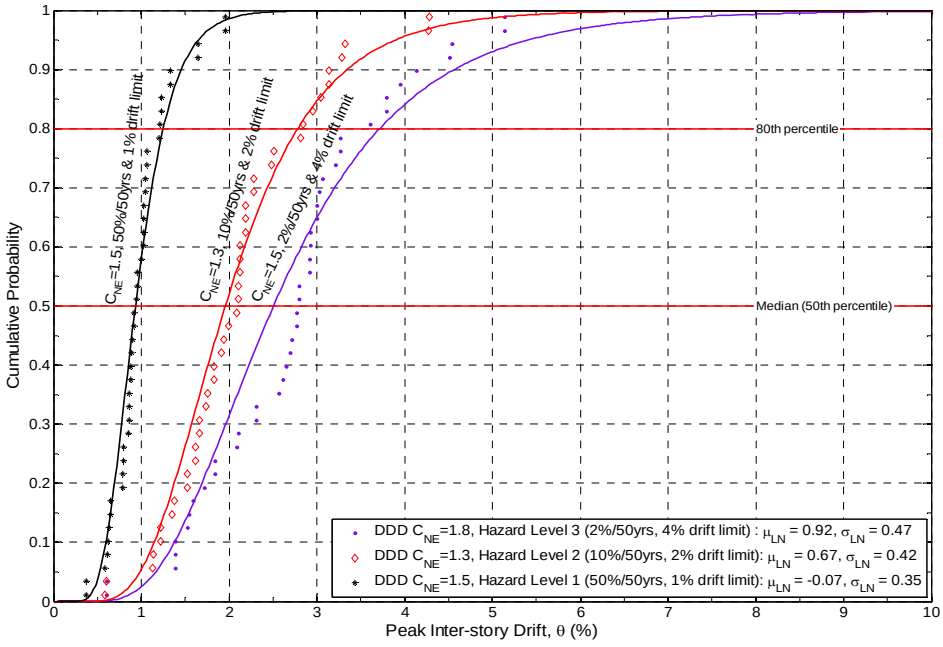

Figure B2: Peak inter-story drift distributions for the ATC-63 archetype 12 under different hazard levels and drift limits with minimum required C_{NE} factors

VITA

Yue Wang received his Bachelor of Science degree in civil engineering from Beijing Polytechnic University, Beijing, China in 2002. He then entered the Department of Civil Engineering in Tsinghua University, Beijing, China in September 2002 and received his Master of Science degree in 2005. He started his doctoral studies in May 2006 in the Zachry Department of Civil Engineering at Texas A&M University and graduated with his Ph.D. in May 2010. His research interests include natural hazard characterization and mapping, structural reliability, performance-based engineering, risk assessment and loss estimation.

Dr. Wang can be reached by email at: wangyue430@gmail.com. His permanent address is: Room 502, Unit 2, Building 6, Northwest Institute of Law and Politics, Xi'an, China, 710063.